CRANFIELD UNIVERSITY

ZHUO LI

Gas Turbine Transient Performance Simulation, Control and Optimisation

School of Aerospace, Transport, and Manufacturing
Propulsion Engineering Centre
PhD

PhD
Academic Year: 2012 -2016

Supervisor: Dr. Theoklis Nikolaidis, Dr. Pavlos Zachos
April 2016

CRANFIELD UNIVERSITY

School of Aerospace, Transport, and Manufacturing
Propulsion Engineering Centre

PhD

Academic Year 2012 -2016

ZHUO LI

Gas Turbine Transient Performance Simulation, Control and Optimisation

Supervisor: Dr. Theoklis Nikolaidis, Dr. Pavlos Zachos
April 2016

ABSTRACT

A gas turbine engine is a complex and non-linear system. Its dynamic response changes at different operating points. The exogenous inputs: atmospheric conditions and Mach number, also add disturbances and uncertainty to the dynamic. To satisfy the transient time response as well as safety requirements for its entire operating range is a challenge for control system design in the gas turbine industry. Although the recent design of engine control units includes some advanced control techniques to increase its control robustness and adaptability to the changing environment, the classic scheduling technique still plays the decisive role in determining the control values due to its better reliability under normal circumstances. Producing the schedules requires iterative experiments or simulations in all possible circumstances for obtaining the optimal engine performance. The techniques, such as scheduling method or linear control methods, are still lack of development for control of transient performance on most commercial simulation tools. Repetitive simulations are required to adjust the control values in order to obtain the optimal transient performance. In this project, a generalised model predictive controller was developed to achieve an online transient performance optimisation for the entire operating range. The optimal transient performance is produced by the controller according to the predictions of engine dynamics with consideration of constraints. The validation was conducted by the application of the control system on the simulated engines. The engines are modelled to component-level by the inter-component volume method. The results show that the model predictive controller introduced in this project is capable of providing the optimal transient time response as well as operating the engine within the safety margins under constant or varying environmental conditions. In addition, the dynamic performance can be improved by introducing additional constraints to engine parameters for the specification of smooth power transition as well as fuel economy.

Keywords:

Transient Performance Optimisation, Inter-Component Volume (ICV) Method, Online System Identification, Recursive Least Squares (RLS), Constrained Model Predictive Control (MPC), Gas Turbine Simulation

ACKNOWLEDGEMENTS

I would like to express my sincere gratitude to my supervisors: Dr P Zachos and Dr. T Nikolaidis for providing valuable support and guidance throughout my research.

I also would like to express my appreciation to Mr S Floyd for providing me with knowledge and experience on the research of engine controls.

Finally, I would like to thank my parents who supported me throughout my three years Ph.D. study.

TABLE OF CONTENTS

LIST OF FIGURES

LIST OF TABLES

LIST OF EQUATIONS

NOMENCLATURE

a, b, c, d	Constant
A, B, C, D, E, F	Coefficient matrix
A_{con_in}, B_{con_in}, C_{con_in}	Constant matrix of engine constraints in the increment engine constraint state space model
ALT	Altitude (m)
A_{max}, A_{min}	Constant state variable matrix of maximum, minimum constraints
B_{max}, B_{min}	Constant input variable matrix of maximum, minimum constraints
CN	Corrected relative rotational speed
COT	Combustor outlet temperature (K)
C_p	Heat capacity at constant pressure (J/kg·K)
CW	Compressor work (J)
e, ε	Error
EPR	Engine pressure ratio
G	Transfer function
GT	Gross thrust (N)
$\dot{h}$	Climb rate
H	Control function
H	Flight altitude
H, h	Enthalpy (J/kg)
ΔH	Change of enthalpy
I	Identity matrix
J	Objective function
k	Sampling interval; discrete time
K	Control gain
K_d	Derivative control gain from PID
Ki	Integral control gain from PID
K_p	Proportional control gain from PID
M	Mach number
$\dot{m}$	Mass rate (kg/s)
m	Mass (kg)
M, γ	Constraint matrix in MPC
M_{max}, M_{min}	Constant value matrix of engine constraints
N	Rotational speed (RPM)
n	System noise or total number of elements in the matrix
N_c	Control horizon
N_p	Prediction horizon
N_{DP}	Design point rotational speed
NDMF	Non-dimensional mass flow
$\dot{P}$	pressure rate dP/dt
P	Pressure (kPa) for engine model; covariance matrix for identification process
p	Static pressure (kPa)
P_{AMB}	Ambient pressure (kPa)
P_c	Controllability matrix
PCN	Relative rotational speed
P_o	Obervability matrix

PR	Pressure Ratio
ΔQ	Torque change (N·m)
R	Gas constant (J/kg·K)
Ref	Control reference
s	Continuous function at frequency domain
S, s	Entropy (J/K)
SFC	Specific fuel consumption (kg/kN·s)
ss	Steady state
ΔT	Torque produced by imbalance of turbine and compressor power (W)
$\dot{T}$	Temperature rate dT/dt
T	Temperature (K)
t	Static temperature for engine model (K); time for identification algorithm and controller (s)
T_{AMB}	Ambient temperature (K)
TET	Turbine entry temperature (K)
TR	Temperature ratio
T_s	Sampling time
TW	Turbine work (J)
U	Input
U_{max}, U_{min}	Maximum, minimum control input matrix
V	Measurement noise in the identification process/ volume in the gas turbine model
Vol	Volume
W	System or state noise
W	Mass flow (kg/s)
w, ω, λ	Weighting factor in constrained MPC
W_{ff}	Fuel flow (kg/s)
ΔW_{ff}	Change of fuel flow at time interval (kg/s)
X	State
X_{con}	State variable matrix of engine constraints
X_{con_in}	State matrix of constrained engine variables in the increment constraints state space models
$\hat{Y}$	Estimated output
Y	Output
Y_{con}	Output matrix of engine constraints
Y_{con_in}	Output matrix of constrained engine variables in the increment constraints state space models
z	Discrete function
γ	Gas constant ratio
η_{is}	Isentropic efficiency
θ	Objective parameter
λ	Eigenvalue
μ, ρ	Adjustable parameters in RLS-SI and RLS-SV
φ	Parametric matrix
ψ	Inverse eigenvector
$\dot{\omega}$	Angular acceleration

LIST OF ABBREVIATIONS

AGR	Air gas ratio
ARE	Algebraic Riccati Equation
ASVM/SVM	Augmented State variable model
CMF	Constant mass flow method
CPR	Compressor pressure ratio
DTA	Digital to analogue
ECU	Engine control unit
EEC	Electronic engine controller
FADEC	Full authority digital electronic control system
FGR	Fuel Gas Ratio
GTR	Gross thrust ratio; the ratio of gross thrust to the gross thrust at design point
FMU	Fuel metering unit
GT	Gross thrust (N)
HPC	High pressure compressor
HPC-PR	High pressure compressor, pressure ratio
HPT	High pressure turbine
ICV	Inter-component volume method
IPC	Intermediate pressure compressor
IPC-PR	Intermediate pressure compressor, pressure ratio
IPT	Intermediate pressure turbine
LPC	Low pressure compressor
LPC-PR	Low pressure compressor, pressure ratio
LPT	Lowe pressure turbine
LPV	Linear parameter varying
LQR	Linear quadratic regulation
LS	Least squares
Max	Maximum
MIMO	Multi-input Multi-output
Min	Minimum
MPC	Model predictive controller
NDMF	Non-dimensional mass flow
NN	Neural networks
PID	Proportional-integral-derivative control
PLA	Power lever angle
RLS	Recursive least squares
RLS-DF	RLS with direction forgetting factor
RLS-SI	RLS stabilised with invariant factors
RLS-SV	RLS stabilised with variable factors
RLS-VFF	RLS with robust variable forgetting factor
RPM	Revolution per minute
SISO	Single Input Single Output
SS	State space model
ZN	Ziegler Nichols tuning method

1 INTRODUCTION

In recent years, the technology for numerical simulation tools has been vastly improved in its functionality, accuracy and reliability for estimations of gas turbine performance. Improved computing techniques have allowed the transfer of experiments from test beds to simulations, resulting in the reduction of design costs and a shortened design cycle. In a gas turbine engine, some or most of the variables remain in their transient states and their performance can change over time while the engine is in operation. Transient states are so important that three-quarters of development effort are normally spent on the design and tuning control law in order to ensure the optimum transient performance could be the most efficient, fastest and safest for entire transient operation range [1]. However, most commercial simulation tools, such as GasTurb or GSP, only include the classic fuel scheduling and proportional-integral-derivative (PID) methods for control of engine transient performance. In addition to the prediction and assessment of the transient performance, proceeding simulations is also an important method to produce optimum fuel schedule or control law for control data of real engine control unit. The desired transient performance could be only obtained from iterative procedures by tuning each entry of the control schedule from the classic control designs. In this project, an advanced control algorithm has been developed to provide an intelligent control solution to solve the issues from design and simulation. This control algorithm includes a controller: constrained model predictive controller (MPC) with an engine dynamic identifier: least squares method with varying stabilised factor (RLS-SV). The new algorithm simplifies the classic process by eliminating the majority of iterative processes. The optimal performance within the safety margin can be produced while the engine is operating, and optimising process evolves adaptively to the change of engine dynamic. Generality feature of this design also increases the robustness of the controller, which allows this controller can be easily implemented to most engine configurations.

The application of the control algorithm is based on the concept of mechatronic system. The term of mechatronics was firstly introduced in Japan

in the 1970s[2,3]. Mechatronics is the integration of mechanical with electrical and electronic systems. A typical mechatronics system is shown in Figure 1-1. A gas turbine engine is a mechanical system in this cycle. Engine data is being measured by sensors. However, inaccuracy and noise are commonly present in these measurements, therefore, filtering is required. The signal processing module produces dynamic models or corrects the pre-defined models according to the measurements. The control signals are analysed from the mathematical models by the controller.

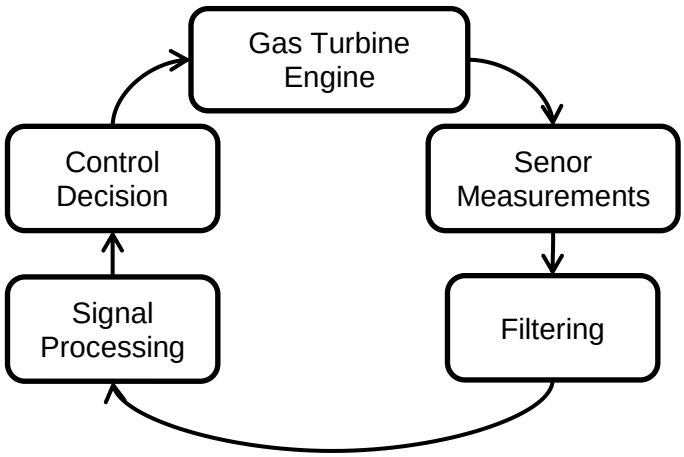

Figure 1-1 Mechatronics system

The computational engine model is considered as the real gas turbine engine of Figure 1-1in this project. Due to no exogenous disturbances existing in the virtual engine, the sensor measurement and filtering blocks are no longer required in the mechatronics system. The mechatronics system can be reduced to Figure 1-2.

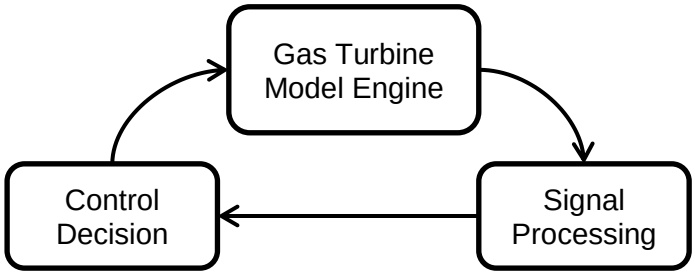

Figure 1-2 Reduced mechatronics system

The gas turbine engine is modeled to component level by the inter-component volume (ICV) method. This engine modeling technique allows engine components, such as compressor, combustor and turbine, to be developed individually. The dynamic model of individual components can be designed separately from the overall predictions of engine performance so that an iterative or mapping process can be directly applied to estimate the thermodynamic and aerodynamic parameters, and so future development of the components will not affect the estimation process of overall engine performance. A volume connects two consecutive engine components. The integral terms in the volume eliminate the iterations for matching flow continuity between inlet and outlet of the two consecutive components.

MPC is a model based controller and treats the engine as a dynamic system. A control-oriented model is required to supply to the MPC for analysis of the engine dynamic. A stabilised recursive least squares (RLS) method is executed to produce a reduced state space model from the online identification of the ICV model.

The MPC changes the conventional concept of process demand to target demand, in order to control engine transient performance. It is capable of searching for and obtaining the fastest transient route to reach the performance target, by manipulating the control inputs, because of the linear predictions on engine future performance based on the identified models. The constraints of the engine parameters can also be predicted through the control algorithm if their dynamic models are chosen to be identified by RLS. The optimum control solution produced by the MPC includes the consideration of both the constraints and performance requirements on the engine parameters. The constraints of corrected fuel flow, shaft speed, compressor pressure ratio, thrust delivery and specific fuel consumptions are designed to single, twin and three spool gas turbine engines. From the results of this research, the included constraints ensure the engine is always being operated within an allowable and safe operating envelope. Furthermore from the research, the performance of fuel economy and the smoothness of transient operation can be further improved by

implementing the constraints to engine parameters, i.e. SFC and percentage of overshoot.

The block diagram, Figure 1-3, shows the architecture of the engine system. The transient command is given by the user or pilot as a control reference. The controller (MPC) determines the optimal control signal (fuel flow) by minimising the error of command to engine output as well as ensuring the safety of operation. The identification process (RLS) keeps the control-orientated model updated. The closed loop process repeats until the simulation is terminated.

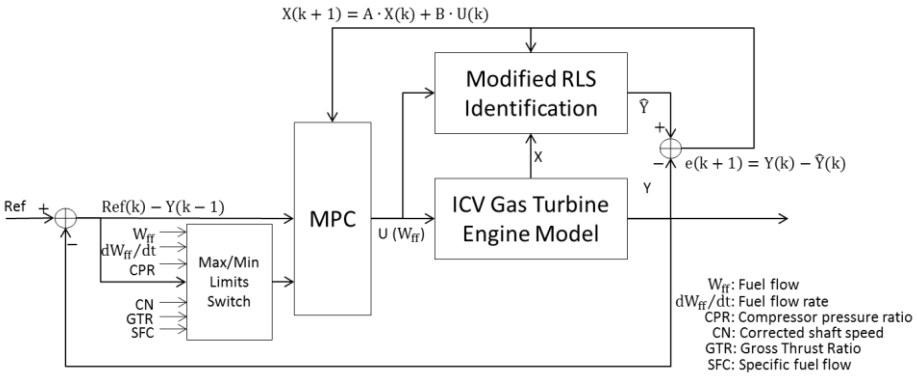

Figure 1-3 Block diagram of the engine system (Equations are explained in Chapter 4)

This project is also required to improve transient simulation capability of simulation tool – Turbomatch. Turbomatch is a gas turbine engine performance simulation tool developed by Cranfield University. This computational tool is used to simulate and prognosticate steady state and transient performance of gas turbine engine. The original design of control transient process in the Turbomatch used fuel scheduling technique, which requires the user to attempt repetitive simulations by manipulating individual value in the fuel schedule in order to obtain the satisfied transient results. The designed control and optimisation of transient process shown in Figure 1-3 could automatically search the best transient lines and simplifies the design process of producing the fastest transient response within the engine constraints for the entire operating range.

1.1 Aim

The project is aimed to develop a control process for the online transient performance optimisation of gas turbine engines.

1.2 Contributions to Knowledge

- The developed optimal control algorithm changes the descriptive to objective concept for improvement of the control capability and the adaptability to the transient operations and change of environmental conditions on gas turbine engines
- The development of optimal control method: constrained model predictive controller (MPC), with the adaptive identification algorithm: recursive least square with variable stabilised factor (RLS-SV), allows transient performance of gas turbine engines can be optimised online for the entire operating range.
- The automatic control process simplifies the process of developing the fuel schedules and is generalised techniques to most engine configurations.
- The awareness of performance boundaries allows the engine can be operated safely, effectively to the command and efficiently to the fuel consumption. This capability allows the MPC could be constrained by the design from any of engine parameters to satisfy the operation requirements.
- The constraints of corrected shaft speed, compressor pressure, turbine entry temperature, engine thrust delivery and specific fuel consumption are designed on model predicted controller for ensuring safety during gas turbine transient operation.

1.3 Contributions to Simulation Tool (Turbomatch)

- Introduced the design of closed-loop feedback system
- Implemented open/closed loop PID control method
- Implemented constrained model predictive control (MPC) algorithm for transient performance control and optimisation

2 LITERATURE REVIEW

2.1 Overview of Gas Turbine Engine System

Gas turbine engine is the propulsion module of an aircraft, which provides continuous thrust in order to maintain flight. The engine control system has a critical role, which is to ensure that the engine performs at maximum efficiency as well as safety in any given condition. Back in the 1930s, the world's first gas turbine engine patented by Sir Frank Whittle was only equipped with a simple throttle lever to control fuel injection to the combustor chamber [4]. The throttle lever angle or power lever angle (PLA) had to be adjusted to take into account the effects of altitude, intake pressure, and temperature as well as the flight speed. Therefore, the need to develop an automatic system was required for fuel decisions. Then, in the 1950s, a greater impact on the gas turbine technologies was brought due to higher demands being made on engine performance, the length of serving life and safety. As a result, the heavy and complex hydromechanical control system had been developed [5]. Later still, during the 1970s, higher thrust, and higher bypass ratio engines were being developed, and consequently, more frequent adjustment of power levels was required. As a result, the hydromechanical control components were quickly being replaced by electronic control systems. The digital system was preferred because of the development of computer technology, allowing complex performance estimation and control algorithms to be programmed and also because of its quick response time. The growth of digital computers enhanced the reliability and functionality of control systems. During sixty years development, the control system had been evolved to full authority digital electronic control (FADEC) where the engine is capable of managing the performance by itself from the commands given by the pilots [6].

Figure 2-1 shows a typical application of FADEC system to a gas turbine engine [7]. A typical FADEC system includes an electronic engine controller (EEC) (or engine control unit (ECU)), a fuel flow metering unit (FMU), speed sensors, temperature and pressure sensors and hydromechanical systems [8].The pilot applies command through the PLA. The angle of the thrust lever is

taken as a control input to the FADEC system. The system firstly converts the value of the lever angle to the control reference before the command is being imported to the downstream controller as shown in Figure 2-2. The control reference can be interpolated from a table of reference speed, compressor or engine pressure ratio because the thrust cannot be directly measured by sensors. The change of control input is determined by control logic through comparison between the control reference and the measurements from sensors. A lead-lag controller shown in Figure 2-1is a typical linear control design. Nowadays, more advanced and intelligent control techniques have been embedded to the FADEC. The acceleration and deceleration fuel schedules are added downstream of the controller, and the logic gates are used to switch the fuel schedule between acceleration and deceleration. During the accelerating process, the acceleration schedule is activated when the control input from the controller is smaller than the value from the schedule. The opposite action is applied during the deceleration operation. Figure 2-3 shows an example of the implementation of switching logics to the engine control unit. After the amount of fuel change has been determined by the control logic, the effect of the changed fuel on engine transient performance must be predicted. The predictions are then compared with the installed constraints of engine parameters in the limit logic module. This module draws the performance boundary for safe operation and longevity of components. If the fuel rate exceeds any maximum or minimum limits, the value will be limited to the predefined values by the constraints. The logic in the constraint module acts as a filter and follows the rules of a low pass during acceleration and high pass during deceleration. Then, the command fuel change, according to the pilot’s lever command, can be integrated and passed through a digital to analog (DTA) converter, through the fuel metering unit (FMU), and finally injected to the engine combustor. The engine performance responses to the disturbed fuel flow and the new performance is measured by the sensor and fed back to the control logic. The closed-loop is being repeated while the engine is in operation.

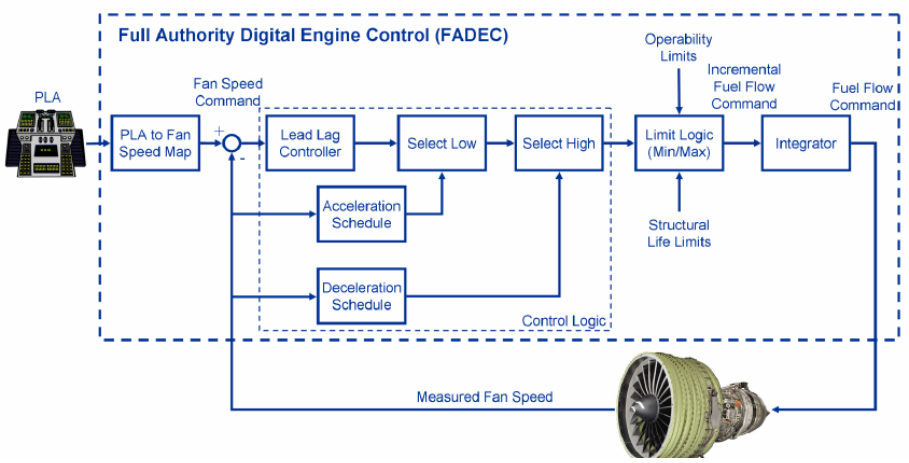

Figure 2-1 FADEC system for control of gas turbine engine [7]

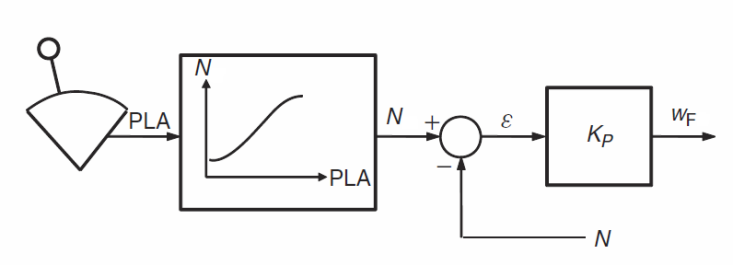

Figure 2-2 The schedule for PLA to shaft speed[9]

The conceptual design of the control logic is shown inFigure 2-3. The speed governor includes a lead-lag controller to determine the fuel flow.The estimated fuel flow is non-dimensionalised to adapt the variant ambient conditions.

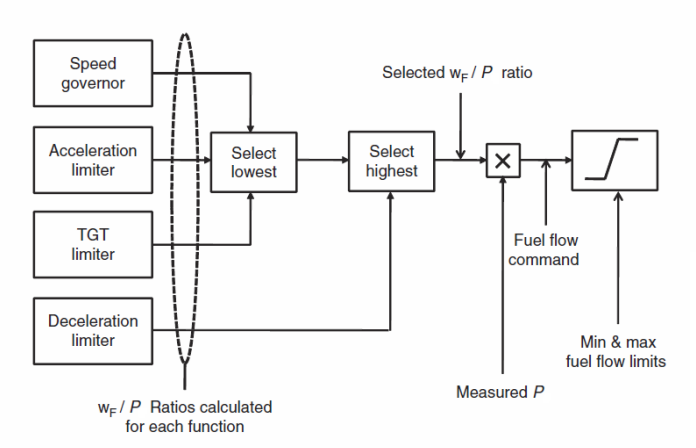

Figure 2-3 Conceptual design of fuel control logic[9]

A “min-max” structure is normally included as a limiter for the protection of critical engine variables as shown by the example of Figure 2-4[10]. The “min-max” design is implemented to limit the logic module in an engine system of Figure 2-1. The final fuel command is achieved by comparing the output from the controller with the selected engine constraints as well as with the value interpolated from the fuel schedules. The minimum fuel flow command is selected from the schedule of the constrained parameter which has the smallest safety margin.

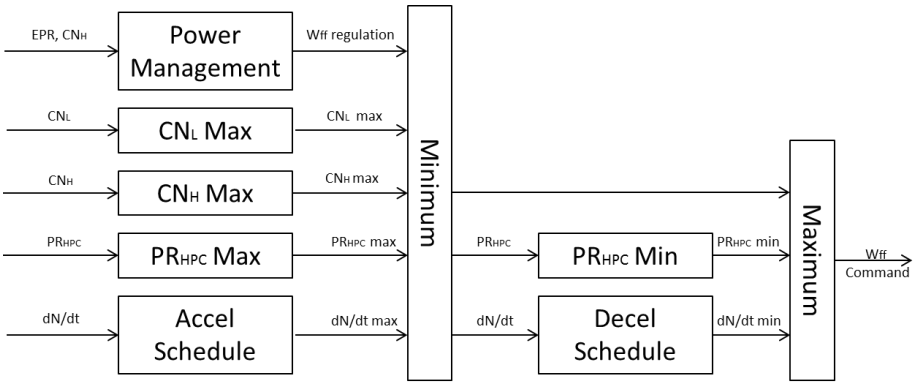

Figure 2-4 Conceptual design of control limits[10]

The engine system demonstrated from Figure 2-1 to Figure 2-4 shows a typical structure for achieving optimal performance as well as maintaining operations under safe criteria. However, the literature fails to demonstrate the procedures of processing the parameter constraints with the input command from the controller, so that the selected engine parameters can be protected. The problem inherent in the max-min constraint design is that it must deal with the delay of the engine response. This means that the command fuel input must be adjusted or constrained in advance before the constraints become significant enough to threaten safety. Therefore, each constraint module in Figure 2-4should be an algorithm rather than a simply constrained value. Each module should be capable of predicting the future behaviour about the parameter of the module and also analyse the effects of constrained fuel input to its future dynamics. Therefore, in order to successfully implement the control system of Figure 2-1, a performance prediction feature must be added to the controller so that the protection logic can successfully ensure the safety of operation.

2.2 Transient Performance of Gas Turbines

Transient performance considers the dynamic of engine performance parameters changing over time. If the constant fuel flow is supplied to the engine combustor, the engine performance will remain near or at a steady state point over time in a constant environmental condition. For any disturb of fuel flow given by either the control system or by the pilot's command, the transient operation starts because of an imbalance of power between compressors and turbines. The objective of control system design is to ensure a smooth, stable, and stall-free transient operation. Airworthiness also has strict regulations for the minimum requirements of engine transient performance. According to FAA's Federal Aviation Regulation, Part 33, Section 33.73, the rules for power and thrust response of aircraft engines indicate:[11]

(a) From minimum to take-off power or thrust rate with the maximum bleed air and power extraction without exceeding any performance limits, the thrust lever is required to move from idle to maximum power within in 1s.

(b) The time to reach the take-off power is required within 5sfrom the idling rated take-off power or thrust which is not more than 15% available, to 95% rated take-off power or thrust at a stabilised static condition.

The transient command is given by a slam increase or decrease of power lever angle (PLA). The control system responses to the command from the PLA regulate the fuel flow at a defined limit of rate. The rate of over-fuelling is typical between 20% and 100% of steady state for the current shaft speed[12].

The transient performance for compressors is shown in Figure 2-5 and Figure 2-6. The compressor transient running lines deviate from the steady state running lines. For the transient performance of a twin spool engine, the high pressure compressor follows the typical performance characteristic: so that where the operating point moves closer to the surge line, which is above the steady state running line during acceleration, as shown in Figure 2-5 (b), and moves below the steady state running line during deceleration, Figure 2-6 (b). The transient performance of a low-pressure compressor shows on the opposite side of the steady state running line to the transient performance of a high-

pressure compressor. During engine acceleration, the operating point moves below the steady state running line, shown in Figure 2-5 (a) due to the higher increment of shaft speed than the increment of pressure ratio. The low-pressure compressor is more likely to surge while the engine is decelerating, Figure 2-6 (a). Understanding the transient behaviour of compressors is essential when designing the constraints of compressor pressure ratio in the model predictive controller. For example, the upper limit can be applied to higher pressure compressor and lower limit can be designed for low or intermediate compressor on compressor pressure ratio rather than implementing all upper limits to all compressors during the operation of engine acceleration.

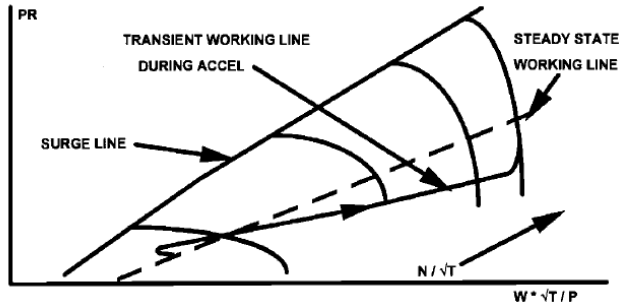

(a)

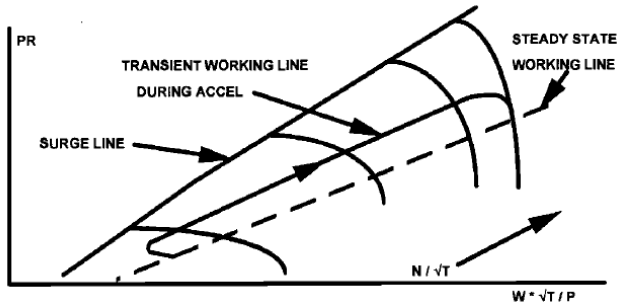

(b)

Figure 2-5 LPC or IPC (a); HPC (b) transient performance of engine acceleration[12]

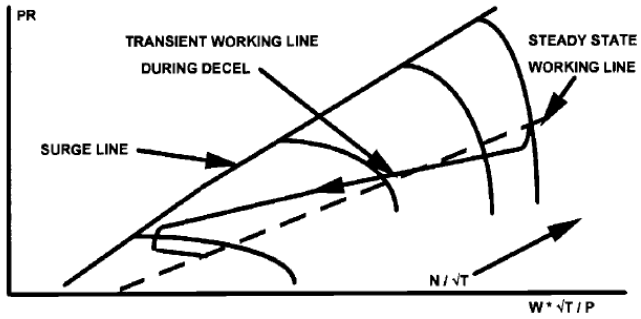

(a)

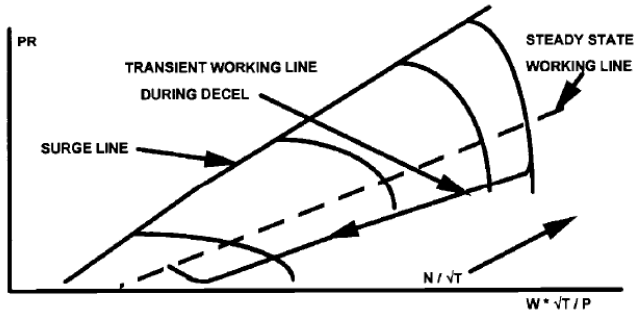

(b)

Figure 2-6 LPC or IPC (a); HPC (b) transient performance of engine deceleration[12]

The engine dynamics can also be observed from its frequency response. The frequency-domain analysis was conducted by Ceri Evans [13,14].A complex gas turbine engine was simplified into transfer functions with one zero and two poles. The nonlinearity is shown by the varying dynamics of a gas turbine within its operating range. A series of linear models were estimated for a set of operating points to demonstrate the non-linear dynamics. The data obtained from multi-sine testing with input: (2-1), were used to estimate the nonparametric and parametric (non-defined and defined structure/parameters) frequency-domain models.

$$u(t) = \sum_{k=1}^{F} a_k \cos\left(i_k \, 2\pi f_0 t + \varphi_k\right) \qquad \textbf{(2-1)}$$

where "a_k" is the input gain, "i_k" is the harmonic number, "f_0" is the sampling frequency and "φ_k" is the phase shift.

The frequency responses of low and high-pressure shafts on a twin-spool engine are shown by bode plots, Figure 2-7 and Figure 2-8, at three

operating points of the HP shaft: 65%, 75% and 85%. The results show the evolution of dynamics for both shafts with different shaft speeds. The analysis shows a decrease of steady-state gain and an increase of dynamics while shaft speed is being increased.

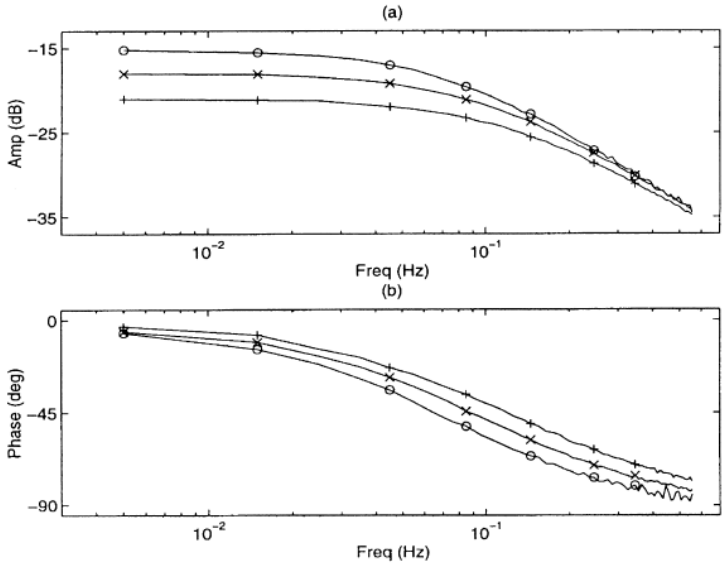

Figure 2-7 Frequency response for LP shaft response at relative HP shaft speed: 65% (∘), 75% (×), 85% (+), [14]

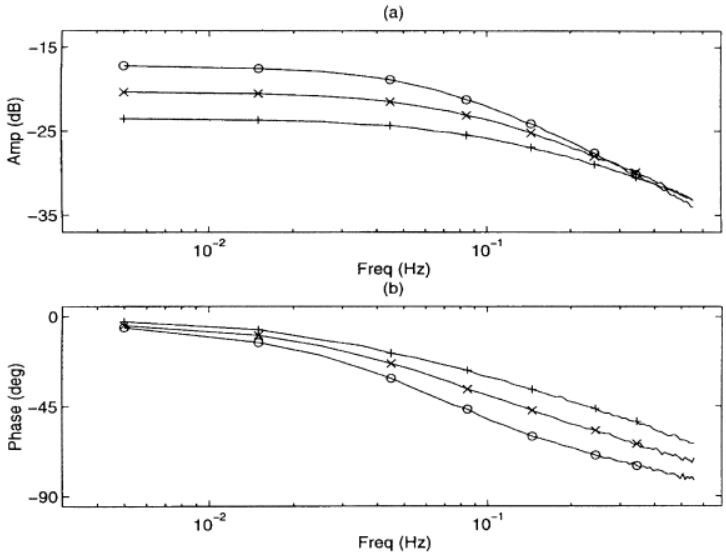

Figure 2-8 Frequency response for HP shaft response at relative HP shaft speed: 65% (∘), 75% (×), 85% (+), [14]

The values of poles and zeros (poles are the routes from denominator and zeros are the routes of numerator of transfer function) in Figure 2-9 from the research of Ceri Evans (1998) suggest that the dynamic of the HP shaft can be estimated to a 1st order model; and that 2nd order model is more suitable for modelling the dynamic of LP shaft at 65% and 75% of relative HP shaft speed. An additional pair of pole-zero was found at low frequencies for both HP and LP shafts due to the effect of heat soakage. In addition, the result also suggests that the dynamic of an HP shaft behaves as a 2nd order system at high rotational speeds (85% and 90%) due to the separation of zero and pole.

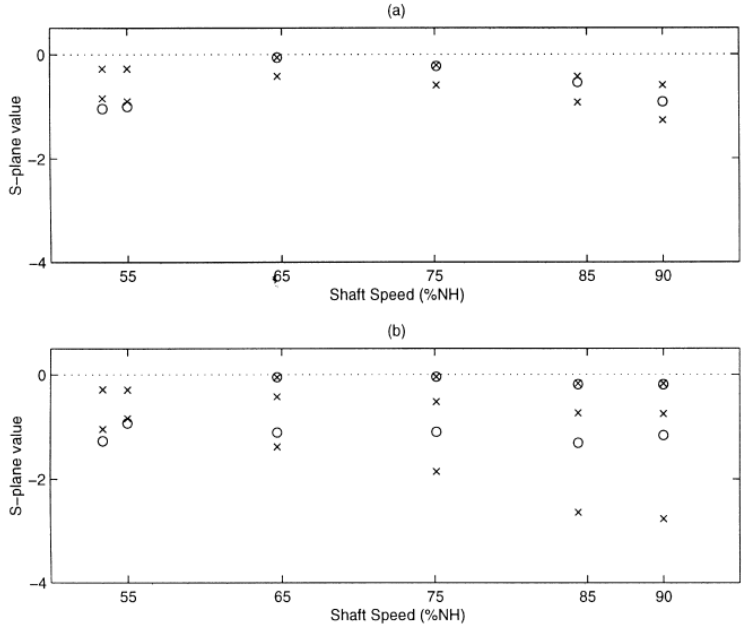

Figure 2-9 The poles (×), zeros (∘) for LP shaft (b), HP shaft (a) from estimated model

2.3 Engine Modelling Techniques

There are four common engine modeling techniques: component-level model, state variable model, adaptive model and intelligent model, to simulate the transient performance as shown in Figure 2-5 and Figure 2-6 [15]. The component-level techniques can be further divided into two common methods: constant mass flow (CMF) and inter-component volume (ICV), and the component-level simulation was implemented as early as 1975 by NASA Lewis

Research Centre to perform the computational performance prediction for gas turbine engines [16].

The CMF uses an iteration process to maintain the flow continuity through the engine component. The process is to match the non-dimensional flow between the inlet and outlet of two consecutive engine components. If a transient calculation of a single spool turbojet shown by Figure A-1is taken, the iterative process is shown in Figure A-2. The combustor outlet temperature can be calculated from the input of fuel flow. Iterations are applied matching the turbine pressure ratio and exit temperature by assuming choked turbine with constant inlet and outlet non-dimensional mass flow (NDMF). Because of constant turbine inlet NDMF, the turbine inlet pressure can be obtained from NDMF with available values of turbine entry temperature (TET) and gas flow from the last time step. If a constant combustor pressure drop is assumed, the compressor exit pressure for the next time step is the proportion of turbine inlet pressure. Other aerodynamic and thermodynamic parameters can be interpolated from the compressor map using inputs of pressure ratio and relative shaft speed from the previous time step. The change of shaft speed can be calculated from the imbalance of work between compressor and turbine. The process is repeated with each new input of fuel flow.

The ICV modeling technique introduces volumes between two consecutive engine components. The volumes allow the temporary imbalance of fluid continuity. The volume added downstream of the turbine module removes the iteration of outlet pressure matching by feeding forward the volume pressure [17]. The advantage of utilising the ICV method allows the algorithm of performance predictions to be developed individually for each engine component [18].

The difference in the simulation results between the CMF and ICV method are shown in Figure 2-10. Both methods yield similar results towards to the end of the transient line. During the initial transient step, an instant increase of compressor pressure ratio is calculated from the assumption of constant shaft speed by the CMF method. By incorporating mass storage, a gradual

increment of the transient line is produced by the ICV method for transient acceleration and the result is much closer to the actual transient performance. Furthermore, the volumes in the ICV method ensure a continuous engine system; hence a control system can be easily designed for a continuous system.In this project, the ICV method is developed for engine simulation in order to achieve a very high degree of accuracy of performance prediction, and the continuous characteristic of the model also allows for easier implementation of the control system.

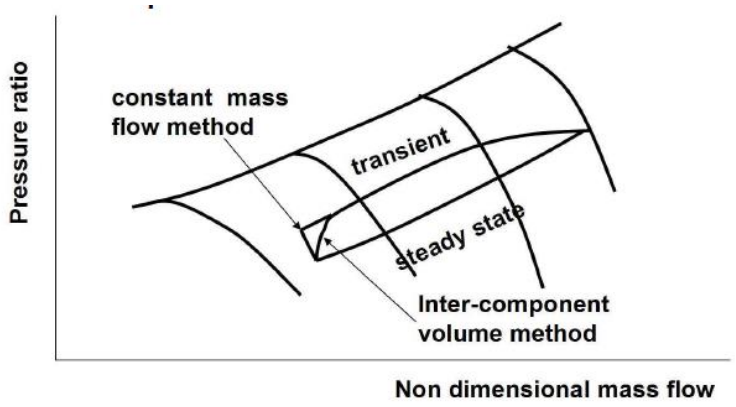

Figure 2-10 Comparison of CMF and ICV methods on transient performance simulation[19]

The adaptive and intelligent modeling techniques use dynamic functions, which are more suitable for the incorporation of advanced control algorithm and diagnosis. The model structures are much simpler than component-level models, and are commonly written to transfer functions or state variable models (SVM) for correlation to the dynamics of engine parameters [15].

The adaptive method uses an augmented state variable model (ASVM), (2-2). This particular adaptive modeling technique is especially powerful when the measurements from the plants have noises, uncertain or immeasurable engine variables existing in the plant.

$$\Delta\dot{X} = A\Delta X + B\Delta U + W \qquad \textbf{(2-2)}$$
$$\Delta Y = C\Delta X + D\Delta U + V$$

where “W” is the system or state noise, and “V” is observation or measurement noise. A Kalman Filter is commonly applied to state and sensor predictions by

minimising the error between values given by the hypothesis of (2-2) and the measurements from the engine. Therefore, the state variable model is capable of tracking the engine dynamics.

In the interests of increasing artificial intelligence, the intelligent technologies, such as neural networks (NN), fuzzy theory and generic algorithms, were originally developed for application to control systems, but they are also applicable for modeling of the controlled plants [15].

A neural network is a learning algorithm which simulates the processing procedures or problem-solving technique as found in the human brain, and it has been applied successfully to solve complex and uncertain control and modeling problems. The NN structure is illustrated in Figure 2-11, which contains neurons and synapses, plus an input layer, output layer, and a hidden layer. In the diagram, neurons are shown as circles, whilst synapses are illustrated by lines. Neural networks, which have been utilised in much published research, can approximate well to a nonlinear continuous function for a real engine system with only one internal hidden layer [20,21]. The schematic drawing of the neural network model is shown in Figure 2-11.Unlike the component-level modeling technique constructed by the engine components, the NN engine model only provides the dynamic model for specific engine parameters. However, the input and output parameters have to be normalised to the same value interval: $[0,1]$ so that a universal weighting factor can be obtained from training the networks.

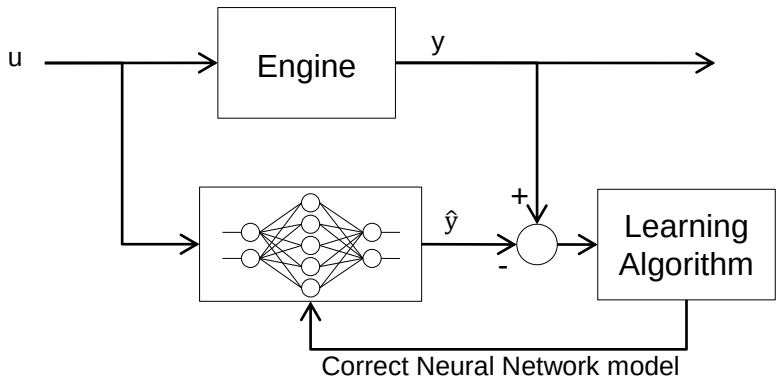

Figure 2-11 Modelling of neural networks

From the research conducted by J. Sun (1999), the NN method was introduced for simulation of a turboshaft gas turbine engine [22]. The input variables were chosen as engine fuel flow and load moment of the engine. The output variables were selected as rotational speed of the gas generator and power turbine, the total temperature of the gas turbine discharge and the static pressure of compressor discharge. The two control inputs and four outputs (a total of six variables) create a multi-input multi-output (MIMO) system. Three past steps of engine data are included in the input layer. Including the output parameters, the input layer consists of eighteen units. A sufficient number of hidden units are capable of providing accurate tracking results to the dynamics of the output parameters. The output layer has four units. A weighting factor of for each input unit is assigned onto the synapse. The combination of synapses creates a weighting matrix. As the diagram illustrated in Figure 2-11 shows, the sum of input units with a multiplication of weighing factors is imported to each hidden unit, so that each hidden unit indicates a unique combination of input parameters. The matrix created by the combination of hidden units in a layer defines the activity of the hidden layer and the activation function is applied to each hidden unit to give the propagation unit. The propagation from each hidden unit then multiplies the weighting factor on each synapse between the hidden layer and the output layer. The estimated outputs are the function of the sum to the multiplication of hidden units with weighting factors. The training process minimises the error between the engine's actual and the estimated outputs. This process is achieved by minimising the cost (quadratic) functions in order to find the most appropriate values of weighting factors.

For successful implementation, the NN requires a database of the engine at different operating points. In J. Sun's research, a 40 set of data is used for training the NN, which includes static and dynamic data at different operating points. The static data is used for modeling the performance near steady states, whilst the transient model is created by the dynamic data [15]. Choosing a sufficient length of input data and estimating the activation functions in the hidden layer determine the performance of NN, and require repetitive simulations to obtain the best design for tracking engine performance.

2.4 Performance Simulation Platforms for Gas Turbines

The simulation platforms, such as GasTurb, GSP and CMAPSS, are well-known tools for simulating both steady state and transient gas turbine performance.

Gas Turbine Simulation Program (GSP) is a component-based modeling tool developed by NLR for gas turbine engine performance analysis (NLR is the Netherlands Aerospace Centre for identifying, developing and applying advanced technological knowledge in the area of aerospace.). The earliest version can be traced back to DYNGEN in 1975 (A program for calculating steady-state and transient performance of turbojet and turbofan engines). The original design of DYNGEN for engine steady-state and transient performance simulation can be referenced in the NASA report [16]. The latest version of GSP allows steady-state and transient simulation of any gas turbine configuration. Nowadays, the simulation can be performed on an object-oriented design with much more advanced computing power. Its user-friendly interface allows for the designing of an engine by quick “drag & drop” of engine components. However, the transient simulation can only be conducted by the inputting of a fuel schedule. The fuel schedule can be designed on a user-friendly interface shown in Figure 2-12 [23].

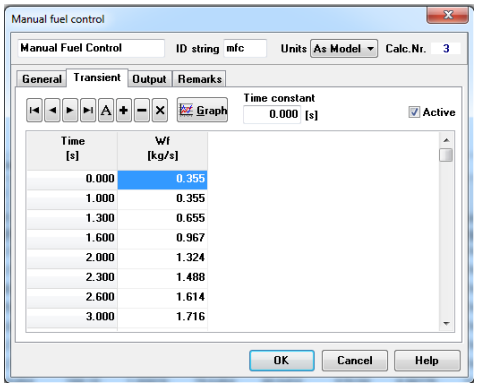

Figure 2-12 Manual fuel control for simulation of transient performance on GSP

GasTurb is another gas turbine performance simulation tool developed in Germany. The platform is devised in the interests of the overall engine performance from the design of component level models. GasTurb is designed

for the interpretation of engine test results and the diagnosis of performance; development and maintenance the overall performance model; and the provision of control system design with an estimation of engine dynamics. The software provides operators, airframe manufacturers and power station designers with mathematical models for searching for solutions to performance enhancement. The software was also developed for the purpose of providing teaching material for gas turbine performance [24].

In the interests of transient performance simulation, GasTurb provides more control options for transient performance estimation. The classic fuel schedule against time graph is shown in Figure 2-13. However, the fuel schedule only supports a maximum of 20 sets of inputs. The simulation time steps are limited to 300 maximum transient steps. As a result, details of schedule data must be compromised, and multiple transient cycles cannot be simulated.

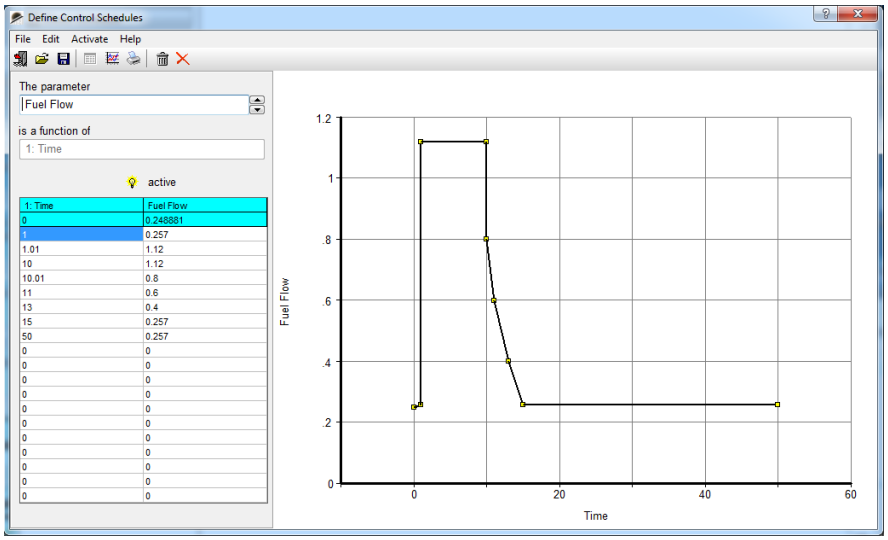

Figure 2-13 Fuel schedule for transient performance simulation on GasTurb

GasTurb provides possible methods of control to the transient performance. As shown in Figure 2-14, apart from the fuel schedule, the transient performance can be realised by the input of low and high-pressure shaft speed schedules and the pilot lever schedule. A step fuel change can also be simulated. The most distinctive feature of GasTurb is the manual control for transient simulation. The manual control allows the user manually adjust a slider

in order to provide the demand of the percentage engine output thrust. The fuel flow is estimated from the PID controller, which is defined at the steady state design stage, according to the differences between model output and user command.

Unlike GSP, GasTurb allows user defined compressor and turbine maps. The Turbomatch compressor map was implemented to GasTurb for transient simulation as shown in the compressor transient performance in Figure 2-14.In the transient performance validation of a single spool turbojet engine in Section 6.1.2 in Chapter 6, the estimated engine performance by GasTurb provides similar results as the results from Turbomatch.

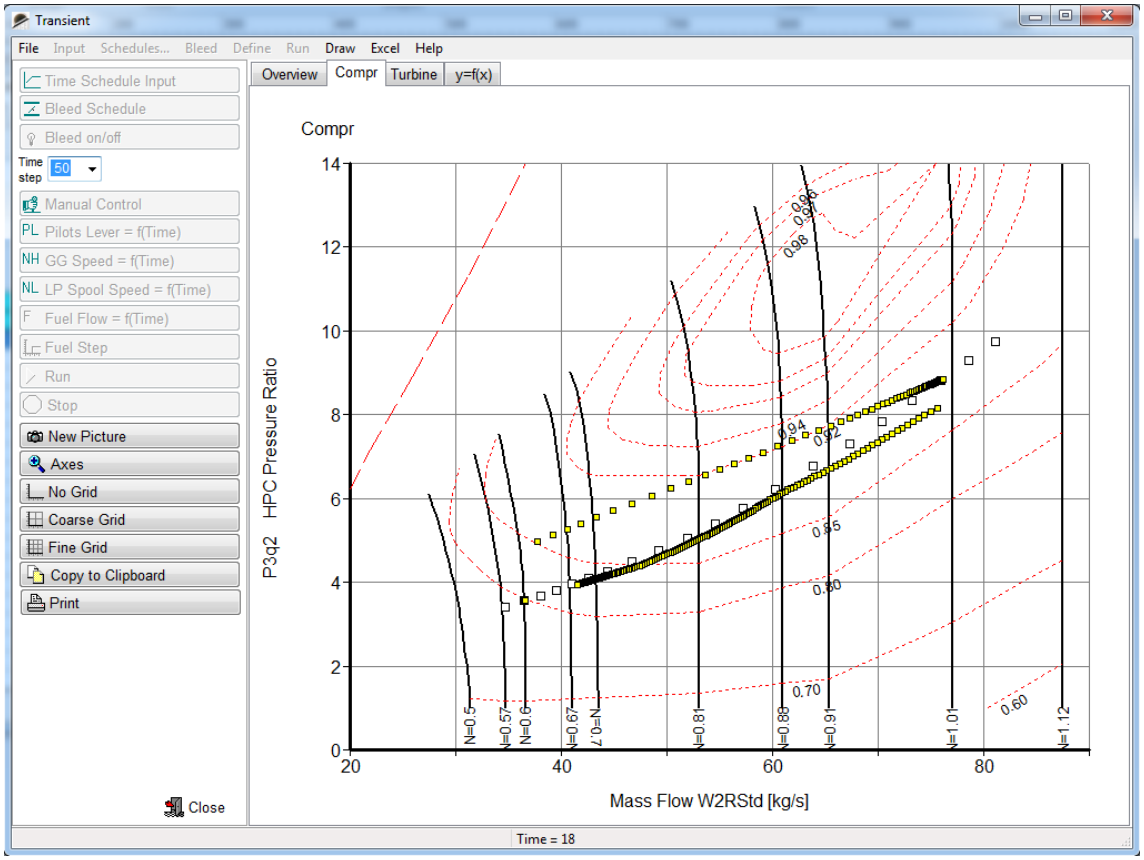

Figure 2-14 The interface of transient simulation on GasTurb

CMAPSS is also a software simulation engine performance developed by NASA. The textbook, “Advanced Control of Turbofan Engines” by Hanz Richter (2012) demonstrates that the CMAPSS is not only capable of using a lead-lag controller to simulate engine performance, but that more advanced and

nonlinear control techniques, such as Linear Quadratic Regular (LQR) and H-infinity, are also applied to optimise transient performance.[25]

From the review of commercial simulation tools, most available platforms still keep the classic control designs for transient performance estimation. The new Turbomatch, improved by this project has been incorporated into the advanced control algorithm (MPC) for optimisation of engine transient performance. This design provides a competitive feature on the performance prediction capability to the NASA CMAPSS. Turbomatch is engine performance simulation tool developed by Cranfield University. The simulation capability and accuracy of the platform was continuously being enhanced since 1974. Turbomatch was originally developed for design and off-design performance analysis of all kind of engine configuration. The capability of transient performance simulation was introduced in 2010 by JánJanikovič [26].In this project, the advanced control technique allows Turbomatch to carry out the transient performance optimisation along with simulation, which has reduced further the time needed for gas turbine developments. The classic control schedule and the PID controller are also included in Turbomatch so that Turbomatch has much functionality as GSP and GasTurb. Unlike GSP and GasTurb, however, the control or feedback variables are defined by users in the new Turbomatch. This means that all engine variables are able to be fed back as a control reference, which greatly enhances the design flexibility.

2.5 Classic Control of Engine Transient Performance

As per the performance regulations mentioned in the previous section, the design of the controller is developed to provide the required performance for the entire operating range in any operating conditions. The conventional fuel scheduling method is shown in Figure 2-15. In this design, the fuel schedules have to compensate for the effect of various flight conditions.

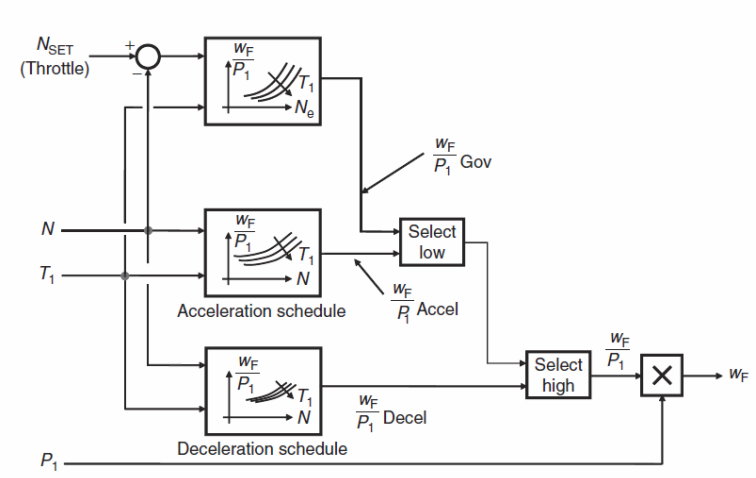

Figure 2-15 Scheduling speed governing control[9]

The gain scheduling techniques of PID control demonstrated by Hanz Richter also required being compensated for varying flight conditions [27].The classic gain scheduling control assumes the concept of a fixed-structure compensator. The control gains are chosen to reflect the changes in environmental conditions: altitude, Mach number and temperature deviation. The scheduling tables, Figure 2-16, are built for the selected engine parameters. In the gas turbine engine, the parameters, such as atmospheric pressure and temperature and flight Mach number, have a stronger influence on the numerical values of the linearized system. The engine experiments must be repeated at various combinations of the influence parameters. The control gains are then included in lookup tables until an optimal engine performance is achieved. The PI structure can then be used in the closed-loop control for fan speed, core speed and engine pressure ratio.

Any scheduling techniques are the most efficient and safe way to achieve the required specifications for the entire operating range under normal flight conditions. However, the main disadvantage of this design is its lack of flexibility and adaptability to the unpredictable operating circumstances. If the engine performance changes in a way that has not been accounted for in the control schedules, loss of control stability may occur. Besides, engine aging and deterioration are also required to be taken into account. As a result, more complex look-up tables are developed and a scheduled maintenance is required

to adapt to the change of performance. Therefore, there is an increased demand of application of intelligent control technologies adapting the control characteristics to the changing engine performance.

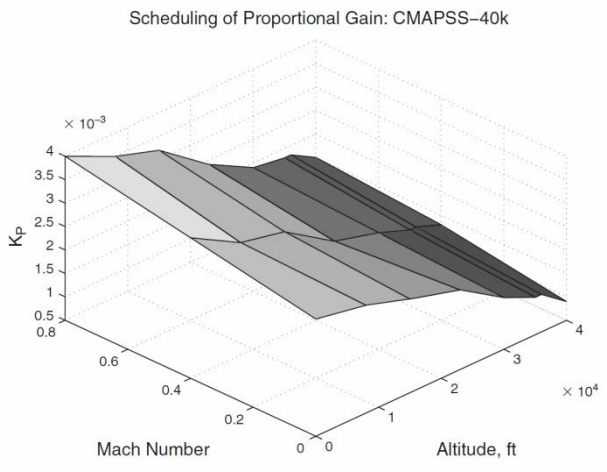

(a)

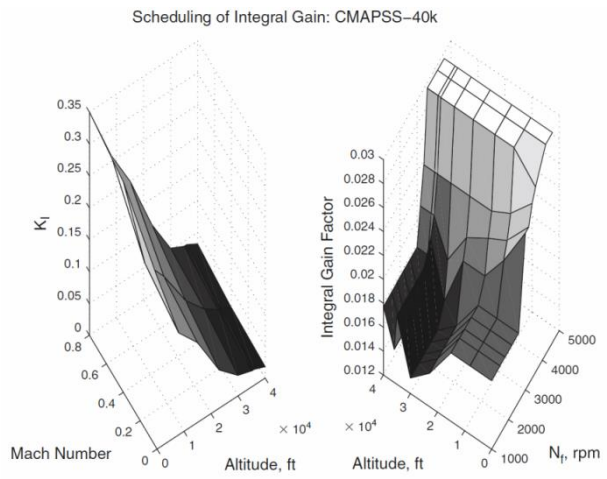

(b)

Figure 2-16 Scheduling of proportional and integral gains[27]

2.6 Identification for Dynamic Systems

The Model identification process has been commonly used in the industry and a reduced system model has been produced from this process. The purpose of implementing model identification techniques is that either a simplified dynamic model is required to reduce the complexity of the original system for the model based control requirement or the system is treated as a

black box where a certain dynamic model does not exist. The estimated model from a dynamic system can be identified through either an off-line or on-line identification process. MATLAB provides algorithms for both on-line and off-line system identification, known as Toolbox. For off-line identification methods, the methods can be chosen from nonlinear autoregressive exogenous (AR/ARX/NARX) methods, prediction error estimation (PEM), estimation of state space model from time or frequency domain (SSEST) and transfer function estimation (TFEST).The online estimation methods are recursive least squares (RLS), and a recursive polynomial model estimator, such as the recursive format of AR, ARX, and ARMA.

The difference between the off-line and the on-line methods is the requirement of knowledge of all input and output data. Because data is complete, the off-line methods can generally provide a more accurate model if a sufficient order of the function has been selected, and system characteristics can be obtained, such as natural frequency and time delay. In contrast, with on-line methods, the time delay sometimes is impossible to estimate.

The identified engine model is only used by the controller for prediction of the engine's dynamic response. Based on these predictions, the fuel input is be given by the controller to reach the performance demand. The off-line methods require the available data of engine inputs and outputs to estimate the discrete model. The iterations on the simulation are required until the same outputs are provided by the ICV engine model and the identified model under the same fuel inputs from the controller. The off-line identification algorithms are thus suitable for off-line controller design. However, the on-line algorithms are more suitable as a supplementary of an optimal model based controller on a time varying system.

2.6.1 Least Squares Identification Algorithms

For the identification processes, Isermann (1974) compared six methods which are commonly used in the industry and most of the online methods are based on the theory of least squares (LS) and likelihood [28]. These six methods are all linear methods for application to nonlinear systems. The

advantages of linear methods are favoured for online identification, particularly for their simplicity and computing efficiency. They do not require iterations and training such as Neural Networks or NARAX, but it sometimes compromises the estimating accuracy.

The classic least squares (LS) method is designed for off-line linear system identification. For example, if there are number of inputs (n) and number of outputs (m), where $\mathrm{m} > n$, the LS method is capable of estimating both static and dynamic models of a given structure from the reading of input and output data, as shown in Figure 2-17 [29,30].

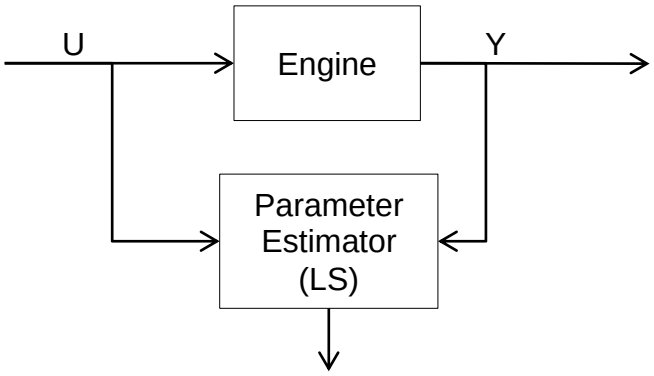

Figure 2-17 Parameter estimation from time series of input and output variables

The parameter coefficients are the objective to be identified by LS. The estimated function should be:

$$\underbrace{\begin{bmatrix} y_1 \\ \vdots \\ y_m \end{bmatrix}}_{Y} = \underbrace{\begin{bmatrix} u_{11} & \cdots & u_{1n} \\ \vdots & \ddots & \vdots \\ u_{m1} & \cdots & u_{mn} \end{bmatrix}}_{U} \underbrace{\begin{bmatrix} \theta_1 \\ \vdots \\ \theta_n \end{bmatrix}}_{\hat{\theta}} \quad \textbf{(2-3)}$$

The solution of coefficients is obtained from the minimisation of the normal equation [29]:

$$\frac{\partial J}{\partial \theta} = 2U^{T}U\hat{\theta} - 2U^{T}Y = 0 \quad \textbf{(2-4)}$$

or

$$U^T U\hat{\theta} = U^T Y \quad \textbf{(2-5)}$$

LS-solution is obtained by pre-multiplying the inverse of input terms on the right-side of (2-5):

$$\theta_{LS} = \left(U^T U\right)^{-1} U^T Y \quad \textbf{(2-6)}$$

where a full rank is required for input matrix (U).

This simplification is the key advantage of the LS method and is preferred by the industry to estimate the dynamic functions for the complex system. However, the disadvantage of matrix operations in (2-6) makes itself difficult to be implemented to a real-time identification process due to the expansion of the data set. Therefore, recursive methods are much preferred for the application of online system identification.

The recursive least squares (RLS) method is a typical form of AR system and it is a modification from LS theory. The RLS and its extensions will be discussed in more detail in the model identification chapter. The application of an RLS algorithm is well known for tracking time-varying systems. It is mainly used in signal processing for system monitoring and as a supplementary on adaptive control systems, such as health monitoring on infrastructures [31], manoeuvre control of heavy-duty road vehicles [32] and control of spacecraft thrust [33]. It had also been attempted off-line to identify the dynamic of gas turbine engines mainly at steady states with stochastic signals by Torres [34]. Because of the computational advantage of the RLS method, Arkov (2000) focused on real-time identification for transient operations, and concluded that an engine system would be averaged to a time-invariant first or second-order transfer functions by the extended RLS [35]. The tracking speed and accuracy for RLS had been improved by introducing different uses of forgetting factors. The effect of using forgetting factor is to shift the estimating average towards the most updated data, such as the research from Constant in Paleologu [36].

2.6.2 Linear Parameter Varying System Identification

Apart from the RLS algorithms, the linear parameter varying method is another dynamic estimation technique allowing online performance tracking for enhanced adaptivity. A linear parameter varying (LPV) system represents a linear system. This system can be written to a state space model whose dynamic varies with the relationship of certain time-varying parameters. The LPV system can be represented on a grid-based model as shown in Figure 2-18 [37]. Figure 2-18 is a two-dimensional model. Each point on the grid is assigned to a linear time-invariant time (LTI) system, and it represents the local dynamics of that point; furthermore, the dynamic at the location in between the points is interpolated between the LTI systems from its neighbouring grids. The coordinates: “α” and “V”, from each local LTI system in **Error! Reference source not found.** could be combined to produce the general direction on horizontal and vertical axis where the overall dynamics should change by looking at the gradients. The gas turbine engine is a parameter-dependent system. Gary J. Balas (2002) has obtained modeling of a turbofan engine by an LPV model constructed from state-space descriptions [38].

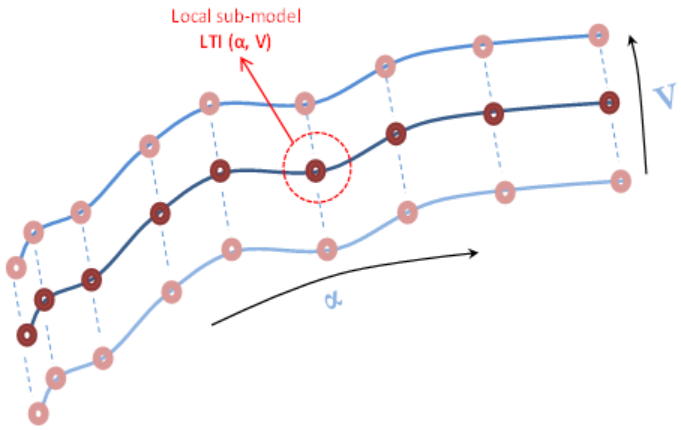

Figure 2-18 LPV grid-based model

2.7 Advanced Control Techniques

The built-in control system is essential to provide the correct and accurate command to the aero engine in order to deliver the required thrust, thus allowing the aircraft to complete the flight manoeuvre. An advanced control design with a certain degree of flexibility is developed to adapt the various dynamics of the gas turbine engines due to the requirement of wide operating range as well as varying working conditions. Therefore, the features of the controller must have:

- Robust to cope with the uncertainty of system dynamics
- A low coupling between the control channels

The implementation of advanced control techniques has become a developing trend to improve the performance of classic scheduling technique.

2.7.1 Linear Quadratic Regulator

A linear quadratic regular (LQR) is a typical control optimisation technique. This method minimises quadratic or cost functions, (2-7), to find the best solution for control signals. The idea is to achieve the performance target from the current operating point as fast as possible by searching for the optimal solution of input “u” by using the Algebraic Riccati Equation (ARE).

$$J = \int_0^\infty x^T Q x + u^T R u dt \quad \textbf{(2-7)}$$

For a continuous system as:

$$\dot{x} = Ax + Bu \quad \textbf{(2-8)}$$
$$u = -Kx$$

where the input term in (2-8) is called the linear quadratic regulator. However, the LQR method is sometimes not practically achievable. One reason is that the dynamic response associated with the eigenvalues, such as (2-8), is difficult to evaluate for a complex system. As a result, it could not provide a perfect sense of time response by placing the eigenvalues in order to obtain the best value of “K” and to achieve the optimised engine response. Another reason is that the LQR system does not provide constraints of the input to accomplish the control

goals. For example, the solution of fuel input to the combustor given by LQR may not be applicable to the fuel metering units. “Q” and “R” are weighting matrices for the states and inputs. The weighting matrices penalise the control and state signals for the entire optimal solution. The matrix “Q” must be a definite positive. Therefore, it must be a symmetrical matrix and its diagonal value must be greater than zero. Selecting the values of weighting matrices affects the control solution to ARE. The iterative process is required to find the perfect tuning factors of “Q” and “R” so that the perfect control solution can satisfy all the performance requirements of the engine states [39].

The main feature of optimal control theory is to use quadratic functions to solve the optimal control problem in a complex system, and LQR is a typical case for solving general nonlinear optimal control problems and indicates the prospective design for the task of performance optimisation. The MPC used in this project is also an optimal control design based on this theory. The predications of future dynamic response in the MPC eliminate the iterative process as well as tuning the weighting matrix (“R”) of LQR. Constraints to the engine parameters can be easily implemented to the MPC, which overcomes the problem of handling the parameters in LQR.

2.7.2 H_2/ H_∞(Infinity) Control

$H_2$and H-infinity (H_∞) are a well-known model based and robust control methods. They are developed on MIMO feedback system for mixed-objective optimisation. These methods have been employed to solve the performance optimisation tasks on gas turbines [40,41]. Besides the advanced control methods, such as: LQR and MPC, the distinctive feature of H-infinity method is that the optimising process can be applied to the dynamic model containing a certain degree of uncertainties and disturbances from the plant. Unlike the dynamic model used in LQR, (2-8), the uncertainty and disturbances (w) have been included in the system model, (2-9), and the state space function of controlled outputs (z) is implemented. The controlled objectives are predefined by the user, and the control synthesis seeks a possible solution to maintain the

influence of exogenous inputs on a defined reference output below the prescribed performance limits.

$$\begin{aligned} \dot{x} &= Ax + B_1 w + B_2 u \\ z &= C_1 x + D_{11} w + D_{12} u \\ y &= C_2 x + D_{21} w + D_{22} u \\ u &= Ky \end{aligned} \quad \textbf{(2-9)}$$

The distinction between H_2 and H-infinity is the number of norms taken from the transfer matrix. The 2-norm from the H_2 method measures the system amplification in terms of root mean square averages. In contrast, the infinity norm measures the peak amplification of the system. The optimal H_2 result is equivalent to a control solution of LQR, which improves the tracking capability to the control reference. H-infinity attempts to optimise the performance with decreasing feedback gain so that the system stability can be enhanced. It has been attempted to consider the H_2 and H-infinity methods simultaneously with weighted objectives. The system will have a better tracking capability to minimise the difference between the performance target and measured outputs when H_2 is selected. The system stability can be enhanced when H-infinity is selected [25,42].

2.8 Summary of Literature Review

In this chapter, the conventional engine control system has been introduced, which is still commonly applied to nowadays gas turbine engines. The conventional design separates the controller and the constraints. The final control value is compensated by adding the engine constraints after the initial control value has been generated by the controller. In addition, the minimum and maximum engine limits are considered in one by one. In this project, the controller will integrate the control and constraint process together, which will be capable of making the control decision with the consideration of all engine constraints with both minimum and maximum limits. The introduction of compressor transient performance and operating frequencies at different shaft speeds between low and high pressure components provide an appreciation of the different dynamic characteristics when the engine constraints designed for

low and high pressure components in the controller. The controller developed in this project is validated through simulation. Different simulation techniques of gas turbine transient performance are also discussed in this chapter. Due to the accuracy requirement to the simulation, engine performance will be simulated by component level modelling techniques, such as CMF and ICV. The ICV modelling method has been selected in this project for engine performance simulation in the engine module of Figure 1-3 because the modular design of ICV allows individual engine component could be developed or improved in a separate project without interfering the overall engine transient simulation process. Then the number of commercial simulation software has been reviewed for application of modern control technology on engine transient performance simulation. The outcome of the review shows a majority of public engine simulation tools still use the conventional control methods to manipulate the engine transient operation. The classic control method requires number control lookup tables for entire range operation. Then, a number of advanced control technologies researched on the application of gas turbine engines has been reviewed in this chapter. The advantage of using advanced control techniques enables the controller can be adaptive to the change of engine performance during transient operation. However, all of them are model based control techniques, which require a supply of dynamic models. The dynamic models are estimated by model identification process. Due to the complexity of the advanced control methods, such as H infinity or Neural Networks, the constrained MPC introduced in this project is simpler, which does not require an accurate dynamic model to initialise transient operation and the engine constraints can be directly embedded in the control process. However, the control accuracy of the reviewed advanced techniques is more dependent on their initialised models and engine constraints must be implemented and calculated separately. Therefore, the constrained MPC method is the most suitable for gas turbine transient process control and performance optimisation.

3 ENGINE MODELLING AND SIMULATION

The closed loop engine system in Figure 1-3 starts from the engine module. The control and identification module are built onto the engine; the controller ensures the safe, efficient and high responsive of transient operation, and the identification module which supplies the identified dynamic models supports the controller. The purpose of the simulated engine in the closed loop is to clone a real engine operating process. The controller will only depend on the dynamic model provided by the identifier to produce control decision. This allows the engine model could be used as the real engine to validate the performance of the control system, and the engine model can be developed independently using different approaches to achieve high estimation accuracy.

This chapter presents the inter-component volume (ICV) technique for mathematical modelling of gas turbine engines, where the engine is modelled in details to component level [43]. The component level model is constructed by turbomachinery components, combustor, intake and nozzle. The engine working process follows the design of the Joule-Brayton cycle, where the air is absorbed from the inlet, compressed in the compressor, burned in the combustor, expanded in the turbine and finally released from the nozzle [44]. In the interests of overall engine performance, only the engine's combustor and major turbomachinery components (compressors and turbines) are modelled in detail, with consideration given to varying thermodynamics.

3.1 Component Level Modelling

A component level model consists of a number of individual components ranging from the engine inlet, through the compressor, combustor and turbine to the nozzle. Each of the components includes a number of mathematical equations, maps and tables, which describe the relationships of the thermodynamic and aerodynamic parameters (pressure, temperature and mass flow). Each component is subjected to different processes to estimate the values of these parameters.

3.1.1 Intake

Total temperature (T) and total pressure (P) from (3-1), are typically determined from ambient temperature (t), pressure (p) and flight Mach number (M) in the intake module.

$$T = \left(1 + \frac{\gamma - 1}{2} \cdot M^2\right) \cdot t \qquad \textbf{(3-1)}$$
$$P = \left(1 + \frac{\gamma - 1}{2} \cdot M^2\right)^{\frac{\gamma}{\gamma - 1}} \cdot p$$

Static pressure (3-2)and temperature(3-3) need to be normalised when the engine is not operating at standard atmospheric conditions [45].
The variation of ambient pressure due to change of altitude:

$$\begin{aligned} &\text{If}(ALT < 11000\ \text{m}) && P_{AMB} = 101.325 \cdot \left(\frac{288.15}{TAMB}\right)^{-5.25588} \\ &\text{If}(11000\ \text{m} \le ALT < 24994\ \text{m}) && P_{AMB} = 22.63253 \Big/ e^{0.00015768 \cdot (ALT - 10998.1)} \\ &\text{If}(24994\ \text{m} \le ALT < 30000\ \text{m}) && P_{AMB} = 2.5237 \cdot \left(\frac{216.65}{TAMB}\right)^{11.8} \end{aligned} \qquad \textbf{(3-2)}$$

The variation of ambient temperature due to change of altitude:

$$\begin{aligned} &\text{If}(ALT < 11000\ \text{m}) && T_{AMB} = 288.15 - 0.0065 \cdot ALT \\ &\text{If}(11000\ \text{m} \le ALT < 24994\ \text{m}) && T_{AMB} = 216.65 \\ &\text{If}(24994\ \text{m} \le ALT < 30000\ \text{m}) && T_{AMB} = 216.65 + 0.0029892 \cdot (ALT - 24994) \end{aligned} \qquad \textbf{(3-3)}$$

3.1.2 Compressor

Compression is assumed to be an isentropic process. The dynamic change of compressor mass flow and pressure ratio and shaft speed is nonlinear during transient operation. The compressor's non-dimensional mass flow (NDMF) and isentropic efficiency (η_{is}) are generalised to the functions of corrected rotational speed (CN) and compressor pressure ratio (PR):

$$NDMF = f(PR, CN); \eta_{is} = f(PR, CN) \qquad \textbf{(3-4)}$$

In the Turbomatch, the values of NDMF and isentropic efficiency are interpolated from compressor maps, Figure 3-1. The compressor characteristic is composed of lines at different relative corrected speeds (CN).

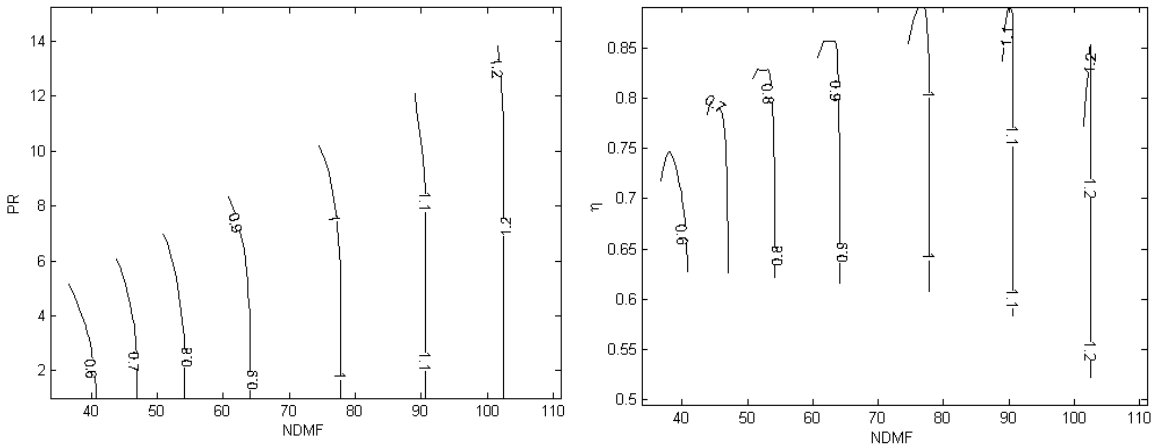

(a) (b)

Figure 3-1 Compressor map: compressor pressure ratio (a), compressor isentropic efficiency (b) (the numbers on the lines are relative shaft speeds)

The outlet temperature can be obtained from the temperature ratio calculated from isentropic function(3-5), which is introduced by textbook [12,46] and notes can be referred to the axial compressor chapter in the textbook: Gas Turbine Theory by HIH Saravanamuttoo [47].

$$\mathrm{TR} = 1 + \frac{\mathrm{PR}^{\frac{\gamma-1}{\gamma}} - 1}{\eta_{is}} \tag{3-5}$$

Instead of using (3-5), an alternative method allows the outlet temperature can be obtained from (3-6) for improvement of accuracy by considering the entropy change from individual gas substance [48].

$$s_{out} = s_{in} + R \cdot \ln(\mathrm{PR}) \tag{3-6}$$

where S_{in} is the engine component inlet entropy and S_{out} is the engine outlet entropy.

The inlet entropy can be obtained from (3-7) with inputs of inlet pressure and temperature. The exit compressor temperature can also be estimated through an equation by (3-7) with known entropy given by (3-6) and outlet pressure from compressor pressure ratio [49].

$$s_k = a_{k,II} - R\ln\left(\frac{P}{101.325}\right) + a_{k,I}\ln\left(\frac{T}{273.15}\right) + \sum_{i=2}^{10}\frac{a_{k,i}}{b_i}\left(\frac{T}{273.15}\right)^{b_i} \quad \textbf{(3-7)}$$

The total entropy estimated in (3-7) is contributed by the combination of gas elements. There are “k” number of gas elements. The values of constants (a, b) in (3-7) are difference to each of the gas elements and the list of elements are referred to the report by Bücker, D. [49].

The outlet temperature can be estimated by solving the equation: (3-8) by the iterative estimating approach, such as Newton Raphson method.

$$a_{k,II} - R\ln\left(\frac{P_{out}}{101.325}\right) + a_{k,I}\ln\left(\frac{T_{out}}{273.15}\right) + \sum_{i=2}^{10}\frac{a_{k,i}}{b_i}\left(\frac{T_{out}}{273.15}\right)^{b_i} = S_{in} + R\cdot\ln(PR) \quad \textbf{(3-8)}$$

The value of constants from each gas element in (3-8) can also be found in the report by Bücker, D. [49].

The compressor work (CW) is calculated from the increment of enthalpy between inlet and outlet, (3-9).

$$CW = W\cdot\left(H_{out} - H_{in}\right) \quad \textbf{(3-9)}$$

The inlet and outlet enthalpy are calculated from the sum of specific gas enthalpy, (3-10).

$$h_k = a_{k,I} + \sum_{i=1}^{10} a_{k,i}\cdot\frac{273.15}{b_i+1}\cdot\left(\frac{T}{273.15}\right)^{b_i+1} \quad \textbf{(3-10)}$$

For both entropy (s) in (3-7) and enthalpy (h) in (3-10) calculations, “k” is the index of the gas elements; and “a” and “b” are specific coefficients of substances [49].

3.1.3 Combustor

The fuel flow is the control input for transient operations. Its value is known and produced by the engine control module. The outlet gas flow is the sum of fuel flow (W_{ff}) and inlet flow (W_{in}) which is the outlet flow of an upstream

component. A constant pressure drop rate (dP) across the combustor is assumed. The outlet from upstream pressure (P_{in}) and temperature (T_{in}) are already available. An iterative process is required to approximate the combustor outlet temperature (T_{out}), shown by flow diagram: Appendix B.1. For starting the iteration, initial values of outlet temperature and combustor efficiency are required to be guessed. The values are normally chosen from results from the steady state point at current shaft speed or from the previous time step.

The outlet temperature from B.1 is calculated from the conservation of energy equation, (3-11).

$$T_{out} = \frac{W_{in} \cdot H_{in} + W_{fuel} \cdot \eta_{cc} \cdot LHV}{(W_{in} + W_{fuel}) \cdot C_{p\_out}} \quad \textbf{(3-11)}$$

The combustor efficiency (η_{cc}) is interpolated from the combustor map, Figure 3-2. The value is interpolated from inputs of temperature rise in the chamber at constant pressure ratio which is the ratio of pressure in the combustor to the engine inlet.

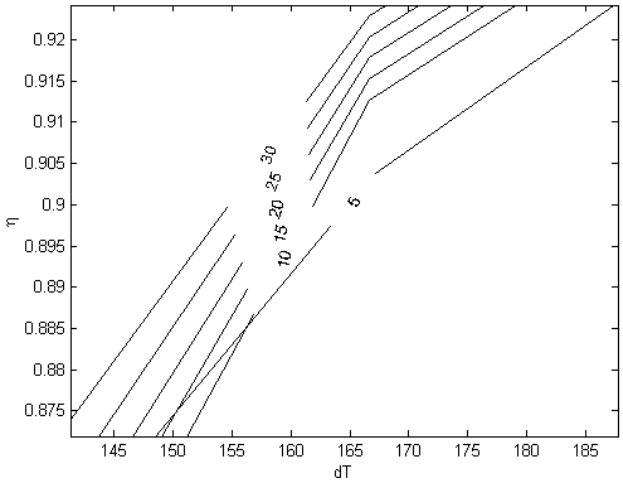

Figure 3-2 Combustor map (percentage of pressure drop is labeled on the lines)

The calculation of heat capacity at constant pressure (C_p) follows the formula (3-12) and procedures introduced by the report of Bücker, D. [49]. The total value of heat capacity is the sum of the values from each individual gas element which is provided by the list of elements by Bucker, D. [49]. Similarly as the

calculation of total entropy and enthalpy, the proportion of the fluid elements is determined by fuel air ratio of flow.

$$C_{p,k} = \sum_{i=1}^{10} a_{k,i} \left(\frac{T}{273.15} \right)^{b_i} \quad \textbf{(3-12)}$$

3.1.4 Turbine

The turbine performance is estimated through choked and unchoked conditions. The inlet non-dimensional mass flow (NDMF), (3-13), is checked against the maximum value of NDMF on the turbine map at current relative corrected rotational speed (CN).

$$NDMF = \frac{W_{in} \sqrt{T_{in}}}{P_{in}} \quad \textbf{(3-13)}$$

The turbine corrected relative shaft speed or non-dimensional shaft speed (NDSS) is calculated as:

$$CN = \frac{N/N_{DP}}{\sqrt{T_{in}}} \quad \textbf{(3-14)}$$

The enthalpy drop and isentropic efficiency, (3-15), are obtained from turbine map, Figure 3-3, by the input of NDMF and CN.

$$\Delta H = f(NDMF, CN); \eta_{is} = f(NDMF, CN) \quad \textbf{(3-15)}$$

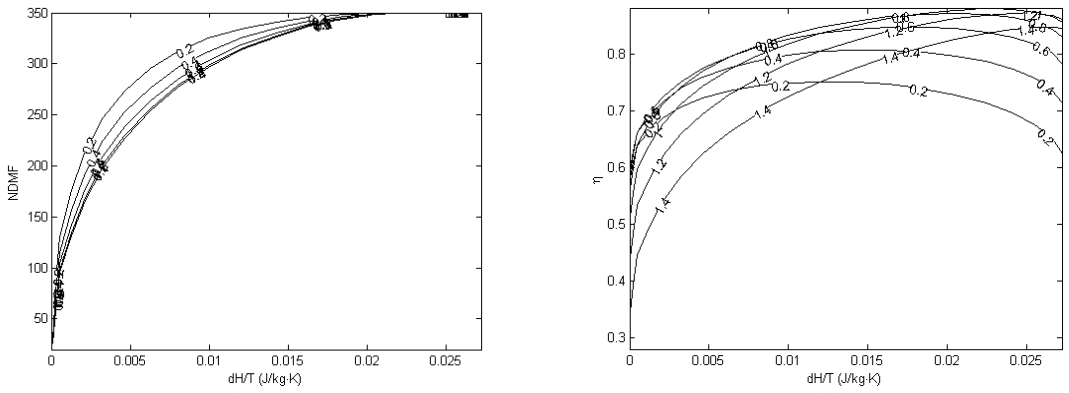

(a) (b)

Figure 3-3 Turbine map (a), turbine isentropic efficiency map (b) (the numbers on the lines are relative shaft speeds)

At the choked inlet condition, the inlet NDMF is limited by the maximum value of the turbine map in Figure 3-3 (a). If the inlet NDMF is higher than the value at choked turbine, the mass flow expanded through the turbine chamber has been reduced to satisfy the maximum NDMF. The mass flow is assumed constant through turbine inlet to the outlet. The outlet mass flow is also reduced to the same amount. Due to a plateau of the turbine map in Figure 3-3 (a), a unique value of enthalpy drop cannot be interpolated from the input of NDMF. An iterative process is required for matching the enthalpy drop on the turbine map from mathematical approximations. An isentropic efficiency value (η_{is}) is firstly estimated for the initiation of the iteration. The turbine pressure drop (PR) is given by the ratio between the turbine volume pressure and pressure from its upstream component or volume for transient operation. The outlet temperature is calculated from (3-16):

$$T_{out} = T_{in} \cdot \left[1 - \eta_{is} \cdot \left(1 - PR^{\frac{\gamma-1}{\gamma}} \right) \right] \quad \textbf{(3-16)}$$

The inlet and outlet enthalpy which are functions of temperature and fuel air ratio (FAR) are calculated by using the formula in (3-10). The enthalpy drop is given by (3-17).

$$\Delta H = H_{in} - H_{out} \quad \textbf{(3-17)}$$

The turbine isentropic efficiency is interpolated from the turbine efficiency map, Figure 3-3 (b), with inputs of non-dimensional enthalpy drop and corrected relative speed, (3-18).

$$\eta_{is} = f\left(\frac{\Delta H}{W \cdot T_{in}}, CN \right) \quad \textbf{(3-18)}$$

The new isentropic efficiency is compared with the initial estimated value. If the two values are different, the process will be repeated with the replacement of the new value until the error between the two values is reasonably small. Then, the turbine work can be calculated through (3-19).

$$TW = W \cdot (H_{in} - H_{out}) \quad \textbf{(3-19)}$$

The procedure of turbine performance estimation is shown by the flow diagram in B.2.

The same entropy process mentioned in Section 3.1.2 applied on the compressor can also be applied to estimate the values of thermodynamic parameters of the turbine. However, the enthalpy drop across turbine is unknown, which means the pressure ratio in (3-6) and outlet pressure in (3-7) are unknown. As the result, each iterative process of estimating turbine outlet temperature requires repeating the iterative estimating process of turbine pressure ratio. The total number of iteration becomes the number of iterations for estimating pressure ratio multiplies the number of estimating outlet temperature. Therefore, there is a concern of processing time if this method is applied.

3.1.5 Nozzle

The control system is designed for the engine with a convergent nozzle in this project. The design of a convergent-divergent nozzle is not included in this project due to the control requirement of a variable nozzle area while a transient operation is being conducted. Another control loop for nozzle area adjustment is required to be added on to the control system, which results in a change of design from a single input and single output (SISO) to a multi-input and multi-output (MIMO) system.

A constant pressure drop across the nozzle is assumed. The critical nozzle pressure ratio (the ratio between total pressure and static pressure) is calculated with an input of critical Mach number ($M = 1.0$) in (3-20).

$$\frac{P}{p} = \left(1 + \frac{\gamma - 1}{2} \cdot M^2\right)^{\frac{\gamma}{\gamma - 1}} \quad \textbf{(3-20)}$$

This value is then compared with the ratio between the nozzle exit total pressure and the atmospheric (static) pressure. The nozzle performance

estimation is separated by two routes, demonstrated by the flow diagram of B.3. If the critical pressure ratio is larger, the nozzle is unchoked. Otherwise, the nozzle is choked.

For a choked nozzle, the flow Mach number is fixed at 1. The static nozzle pressure is calculated from the critical pressure ratio, and the static temperature (t) can be obtained from (3-21).

$$\frac{T}{t} = 1 + \frac{\gamma - 1}{2} \cdot M^2 \quad \textbf{(3-21)}$$

The flow velocity (V) is the speed of sound, (3-22).

$$a = \sqrt{\gamma \cdot R \cdot t} \quad \textbf{(3-22)}$$

The value of gas constant (γ) can be calculated from the ratio between heat capacity (C_p) and gas constant (R), (3-23).

$$\gamma = \frac{C_p}{C_p - R} \quad \textbf{(3-23)}$$

where the value of Cp can be obtained from (3-12).

If the nozzle is unchoked, the nozzle exit static pressure is atmospheric pressure. The Mach number can be calculated from (3-24)which takes the Mach number as the subject of (3-20).

$$M = \sqrt{\frac{2}{\gamma - 1}\left(\left(\frac{P}{p_{atm}}\right)^{\frac{\gamma - 1}{\gamma}} - 1\right)} \quad \textbf{(3-24)}$$

The static temperature value can be calculated from (3-21), and the same formula, (3-22), calculates the speed of sound. The value of gas velocity is obtained from the multiplication of the speed of sound by the Mach number.

The calculation of engine thrust is the same for both choked and unchoked nozzles. The net thrust (3-26)from exhaust gas is the difference between gross thrust and momentum drag:

Net Thrust (FN) = Gross Thrust (F_G) – Momentum Drag (F_D) **(3-25)**

The thrust equation:

$$FN = W \cdot V + A_n \cdot (p_n - p_{atm}) - W \cdot V_{flight} \quad \textbf{(3-26)}$$

3.2 Engine Transient Performance Simulation

3.2.1 Shaft Dynamics

The engine transient states are achieved by an imbalance between compressor and turbine work. The imbalanced work is created by a disturbance of the injected fuel flow to the combustor which either increases or reduces the thermo-energy. The surplus power (ΔT) on the shaft between the compression and expansion sides is given by (3-27).

$$\Delta Q = TW - CW \tag{3-27}$$

The shaft angular acceleration is the ratio between the change of torque and shaft moment inertia:[50]

$$\dot{\omega} = \frac{\Delta Q}{I} \tag{3-28}$$

The linear acceleration can be calculated from (3-29).

$$\frac{d\,PCN}{d\,t} = \frac{3600 \cdot \Delta Q}{4\pi^2 \cdot I \cdot PCN} \tag{3-29}$$

The shaft relative rotational speed is the ratio of shaft rotational speed to its speed at the design point (N_{DP}), (3-30). (3-30)Design shaft speed is a constant. Therefore, shaft speed (N) in (3-29) can be replaced by PCN.

$$PCN = \frac{N}{N_{DP}} \tag{3-30}$$

Engine shaft speed (N) is measured in RPM (revolution per minute), which is converted to angular speed ($\omega = N \cdot \frac{2\pi}{60}$). The surplus power ($\Delta T$) is measured in watt, and torque (ΔQ) is measured in N·rad/s. The relationship between surplus power and torque is $\Delta T = \Delta Q \cdot \omega$. The relative rotational speed (PCN) is updated at each time step and is integrated from (3-29).

$$PCN(t) = PCN(t_0) + \int_0^t \frac{dPCN}{dt}\,dt \tag{3-31}$$

3.2.2 Inter-Component Volume Transient Modelling Technique

The inter-component volume (ICV) technique introduces the volume blocks to the downstream of the turbomachinery components, such as shown in Figure 3-4. The dynamic of the engine shaft affects the dynamics of the assembled turbomachinery components on the shaft, whilst the volume controls the dynamic of each individual component. The detailed design can be developed individually to these components according to the requirement of simulation accuracy and complexity. The constant mass flow (CMF) method was the initial approach for simulating the transient performance into component level. However, the CMF method is unlike the ICV method, where the fluid continuity must be kept at each time step. This introduces high complexity to the engine's performance simulation. In order to maintain the fluid continuity, the value of mass flow between two consecutive components must be kept the same. Therefore, matching the value of mass flow requires iterative estimations across the engine components. As the results, including the iterative estimation process required in the combustor and turbine modules, it requires a longer simulation time to estimate one operating point. The volume from the ICV method allows flow to be temporally imbalanced between the two consecutive components during transient operations. As a result, no iteration is required and computing time can be saved. The volume acts as a damping factor to the working fluids, which simulates the flow propagation through the chamber. Figure 3-4 shows the implementation of volumes to a twin-spool turbofan engine. Furthermore, the ICV method provides a continuous change of engine dynamic performance so that the simulation result looks more realistic. The integral terms in the volume calculation provide continuous change on the value of the fluid parameters. This avoids unrealistic step changes of the value of engine parameters due to the iterative processes from the CMF method.

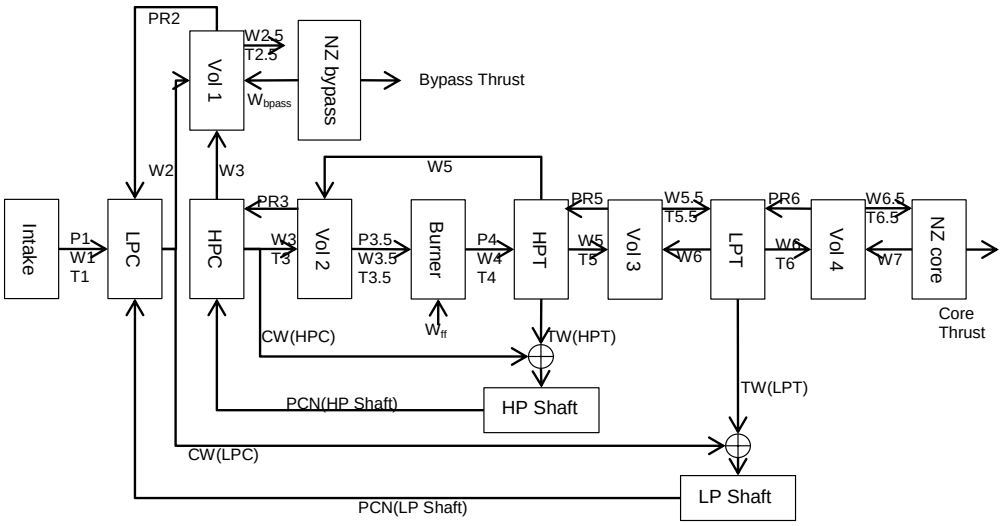

Figure 3-4 ICV model of 2-spool turbo-fan engine

Volumes in Figure 3-4are simulation modules; they are not a physical part of the engine, but each volume controls the pressure gain of its upstream component. The volume mass storage is caused by the imbalance between downstream and upstream flow capacity [51,52]. The stored mass flow:

$$\dot{m} = W_{out} - W_{in} \tag{3-32}$$

The temperature change inside the volume:

$$\dot{T}_v = \frac{\gamma(T_v W_{out} - T_{in} W_{in}) - T_v \dot{m}}{m} \tag{3-33}$$

The rate of change of pressure inside the volume:

$$\dot{P}_v = \frac{P_v}{T_v}\dot{T}_v + \frac{RT_v}{V}\dot{m} \tag{3-34}$$

The total value of volume parameters from their initial condition:

$$m = m_0 + \int_0^t \dot{m} dt$$
$$T_v = T_{v0} + \int_0^t \dot{T}_v dt$$
$$P_v = P_{v0} + \int_0^t \dot{P}_v dt \quad \textbf{(3-35)}$$

The volume exit flow is taken from the downstream components for the next step calculation and the value of the flow at the current step is used for the inlet of its downstream component.

3.3 Summary of Engine Modelling Technique

In this chapter, the component-level modeling technique has been introduced for accurately simulating engine performance, and the ICV simulation method allows the dynamic change of engine performance can be estimated due to change of fuel input in the combustor chamber. The engine model simulated by component ICV method is the engine module in Figure 1-3. Other modules in Figure 1-3 are developed to manipulate the fuel flow and to allow the engine delivering its optimal transient performance. The highly accurate engine model introduced by this project allows testing and validating the adaptability and capability of the control system could be possible on simulation basis and close to the real operations. The control system including both identification process and MPC module is introduced in the subsequent chapters. The nonlinear characteristics of the engine components produce overall nonlinear engine performance. The control system is required to accurately identify and be adaptive to the change of the engine dynamics which vary between different transient operations. The MPC module in the control system must always be capable of bringing the engine performance accurately, quickly, efficiently and safely through transient states to the final target steady state. The accurate engine model is essential that it allows the controller can be tested thoroughly. As the result, the design of this control technology can be applied to real engine control system.

4 ON-LINE PERFORMANCE IDENTIFICATION

The goal of the identification process is to estimate a dynamic function for the performance analysis of the engine control system. The identified model must be adequate to represent the dynamic of the engine for supplementing the control module. Five key steps are involved in identifying a complex system [53]. Firstly, the model structure must be defined, where model type (continuous or discrete model) and the order of the function in the model are decided. Secondly, the variables and excitation sources to affect the dynamic response must be defined. Thirdly, data is measured and recorded from the engine while the simulation is being performed; meanwhile, the fourth step is to apply an identification algorithm to identify the dynamic characteristic, and determine the quantities of the variables required to be identified and degree of their nonlinearity; the last step is the model refinement, which updates the model and minimises the error between the estimation and the original system. For the application to a real system, the information of the measurement system or sensors about the accuracy and spatial resolution must also be available before initialising the identification process, and filtering is required for identifying a real dynamic system.

A discrete model structure is used to represent the ICV engine model, and the method of selecting the source and states for the dynamic model is discussed.

Recursive least squares (RLS) and its modifications become the first choice of the identification techniques implemented in this project. The main benefit of RLS is its simplicity with a considerable level of identification accuracy. Because of this, the RLS method is still the preferred identification technique in the industry although advanced identification techniques have been developed, such as the methods reviewed in Section 2.6. The only weakness of RLS is its sensitive to noise. However, noisy data is unlikely to occur in this project because the engine block in the closed system (Figure 1-3) is a simulated model. In addition, development of identification process is not

the main focus in this project. As a result, the method based on RLS theory is the perfect choice of model identification for this closed system.

In this chapter, the conventional and modified recursive least squares methods: classical recursive least squares (RLS), RLS with directional forgetting factor (RLS-DF), stabilised RLS with invariant factors (RLS-SI)and stabilised RLS with variable factors (RLS-SV),are introduced to perform on-line identification for the dynamic of gas turbine engines, and their tracking performances are compared and discussed.

4.1 Reduced State Space Model

Before identification process can be applied to identify the dynamic of engine parameter, the order of dynamic function and other relative parameters in this dynamic function must be clarified. Most engine parameters are likely to be correlated with each other, creating a time-variant system. For example, the change of volume pressure in (3-34) is a function of the volume temperature and mass flow, so it can be rearranged to:

$$\dot{P}_v = \left(\frac{\dot{T}_v}{T_v}\right) P_v + \left(\frac{RT_v}{V}\right) \dot{m}_v \qquad \textbf{(4-1)}$$

The dynamic continuous function can be expressed as:

$$\dot{P}_v = A(T_v)\, P_v + B(T_v)\, \dot{m}_v \qquad \textbf{(4-2)}$$

The values of constants (A and B) in (4-2) are affected by the value of volume temperature. The value of volume temperature is changed by volume inlet and outlet mass flow. The mass flow changes nonlinearly due to the nonlinear dynamics of engine turbomachinery components. As a result, the volume temperature changes nonlinear, similar as the volume pressure.

For a discrete engine system, the generalized non-linear function can be expressed:

$$X(k+1) = f(X(k), U(k)) \qquad \textbf{(4-3)}$$

where X is state matrix and it is the matrix of relevant engine parameters, and U is the input matrix which is the matrix of control inputs.

The linearization for the engine transient performance can be realized if the sampling time is selected to be sufficiently small so that the dynamic behaviour between each time interval (k) can be assumed as a linear time invariant (LTI). Therefore, the complete transient performance can be superposed by the entire LTI systems. Each LTI can be expressed in a discrete format as:

$$X(k+1) = AX(k) + Bu(k) \tag{4-4}$$

where A, B in (4-4)are coefficient matrices.

The selection of state variables must be sufficient to describe the dynamics of the interested engine parameters [50]. For example, the dynamic of pressure ratio to each compressor in a multi-spool gas turbine engine is affected by its upstream and downstream compressors. Therefore, identifying its pressure ratio requires including the pressure ratio of its nearby components into (4-4). In addition, the fuel flow (W_{ff}) is the only control input. The change of fuel flow controls the thermodynamic in the combustor which disturbs the energy balance between compressors and turbines. The disturbed energy is located in the middle of the engine and is being transferred sequentially from high to lower pressure components with significant time delay. The time constant for each engine component is defined by the volume in (3-34) and the shaft inertia in (3-29). As a result, the required number of state variables (n) is defined by the number of interested engine parameters and their associated variables, and (4-4) can be written as:

$$\begin{bmatrix} x_1(k+1) \\ \vdots \\ x_n(k+1) \end{bmatrix} = \begin{bmatrix} a_{11} & \cdots & a_{1n} \\ \vdots & \ddots & \vdots \\ a_{n1} & \cdots & a_{nn} \end{bmatrix} \begin{bmatrix} x_1(k) \\ \vdots \\ x_n(k) \end{bmatrix} + \begin{bmatrix} b_1 \\ \vdots \\ b_n \end{bmatrix} u(k) \tag{4-5}$$

Where x is state variable, u is input variable and k is discrete time.

The values of elements from matrix A and B in (4-5) are unknown and are required to be estimated, which is the objective of the model identification process. The values of states variables and input variable can directly access from the output engine model, thus, the state variables must be both observable and controllable [54,55].For example, the discrete function for identifying relative spool speed of a twin-spool gas turbine engine is:

$$\begin{bmatrix} PCNL(k+1) \\ PCNH(k+1) \end{bmatrix} = \begin{bmatrix} a_{11} & a_{12} \\ a_{21} & a_{22} \end{bmatrix} \begin{bmatrix} PCNL(k) \\ PCNH(k) \end{bmatrix} + \begin{bmatrix} b_1 \\ b_2 \end{bmatrix} W_{ff}(k)$$ As this example, the engine shaft model mentioned in Chapter 3 can be reduced to a 2nd order discrete model. The transient operation is handled by fuel flow (W_{ff}) as a control input. The speed of high-pressure shaft (PCNH) responses first and the low-pressure shaft speed (PCNL) responses following after the response of high-pressure shaft with significant delay when the fuel flow is changed. The high or low-pressure shaft behaves as a load added to the other shaft. Due to the component level model containing iterative estimating process, there is no certain dynamic function for estimating engine parameters. As the result, developing discrete models for parameters of gas turbine engine mostly came from experiences and repetitive tests. The equations used to construct engine model in Chapter 3 can be suggestive for choosing the order of dynamic functions and the relative parameters.

4.2 Parameter Observability and Controllability

The properties of parameter observability and controllability determine the presence of the identified model. Understanding controllability and observability is crucial for the development of state space model and control design. If any of the state variables in the state space model is un-observable, the state variable is un-relative to the dynamic equation and can be eliminated from the state space model. If any of the parameters is uncontrollable, the change of the parameter value is an independent change of the control parameter and may introduce uncertainty or instability to the dynamic model. In this section, the technique to distinguish the parameter observability and controllability for a discrete-time model, (4-5), is represented. These properties

of state space parameters can be checked once the dynamic model has been developed through off-line identification.

4.2.1 Controllability in the Discrete-Time Domain

A variable from a discrete system, (4-5), is said to be controllable if any state ($x(k) = x_f$) can be reached from any initial state of the system ($x(0) = x_0$) in a finite time interval ($k < \infty$) by the action from controller [56]. The linear state space equation of (4-5) is assumed to be adequate to present the dynamic of transient operations between two steady state levels. The operation has been through "k" time steps. The dynamic response at each time step is shown by (4-6).

$$\begin{aligned} X(1) &= AX(0) - Bu(0) \\ X(2) &= AX(1) - Bu(1) = A^2X(0) + ABu(0) + Bu(1) \\ &\vdots \\ X(k) &= A^kX(0) + A^{k-1}Bu(0) + \cdots + Bu(k-1) \end{aligned} \tag{4-6}$$

The relationship of state variable to control input at final state where time step is at "k" becomes:

$$X(k) - A^kX(0) = \underbrace{\begin{bmatrix} B & AB & \cdots & A^{k-1}B \end{bmatrix}}_{P} \begin{bmatrix} u(k-1) \\ u(k-2) \\ \vdots \\ u(0) \end{bmatrix} \tag{4-7}$$

The constant matrix A is assumed to have distinct eigenvalues (λ). The system of (4-6) is controllable if, and only if multiplication of the constant matrix (B) with the square matrix (ψ) has no zero elements. The controllability matrix (P_c):

$$\begin{aligned} P_c &= \psi\psi^{-1}\begin{bmatrix} B & A\psi\psi^{-1}B & \cdots & A^{k-1}\psi\psi^{-1}B \end{bmatrix} \\ &= \psi\begin{bmatrix} \psi^{-1}B & \psi^{-1}A\psi\psi^{-1}B & \cdots & \psi^{-1}A^{k-1}\psi\psi^{-1}B \end{bmatrix} \end{aligned} \tag{4-8}$$

where Ψ is a square matrix. The elements in the matrix (P):

$$\begin{aligned}
&\psi^{-1}B = B_m \\
&\psi^{-1}A = \mathrm{diag}\left[\lambda_1, \lambda_2, \cdots \lambda_n\right] \\
&\psi^{-1}A^2\psi = \mathrm{diag}\left[\lambda_1^2, \lambda_1^2, \cdots \lambda_n^2\right] \\
&\vdots \\
&\psi^{-1}A^{k-1}\psi = \mathrm{diag}\left[\lambda_1^{k-1}, \lambda_1^{k-1}, \cdots \lambda_n^{k-1}\right]
\end{aligned} \tag{4-9}$$

where:

$$B_m = \begin{bmatrix} b_1 \\ b_2 \\ \vdots \\ b_n \end{bmatrix}$$

The controllability matrix becomes:

$$P_c = \psi \begin{bmatrix} b_1 & \lambda_1 b_1 & \cdots & \lambda_1^{k-1} b_1 \\ b_2 & \lambda_2 b_2 & \cdots & \lambda_2^{k-1} b_2 \\ \vdots & \vdots & \ddots & \vdots \\ b_n & \lambda_n b_n & \cdots & \lambda_n^{k-1} b_n \end{bmatrix} \tag{4-10}$$

If any element (b_i) in the controllability matrix is zero, then the engine variable in the i^{th} row is uncontrollable in (4-5). Therefore, the system's controllability means that the matrix, (4-10), must have full rank.

4.2.2 Observability in the Discrete-Time Domain

If a state variable (x(k)) at sample time (k) from (4-5) is observable if input ($u(k_i)$) and output ($y(k_i)$) over a finite time ($0 < k_i < k$) completely determines the value of this state. Because the MPC is a receding horizon controller, the output formula for the state space model ((4-5)) is:

$$Y(k) = CX(k) \tag{4-11}$$

The outputs from initial transient operation to sample time (k):

$$
\begin{aligned}
&Y(0) = CX(0) \\
&Y(1) = CX(1) = CAX(0) + CBu(0) \\
&\vdots \\
&Y(k-1) = CX(k) = CA^{k-1}X(0) + C\sum_{i=0}^{k-1} A^{i-1}Bu(i)
\end{aligned}
\tag{4-12}
$$

The observability matrix (P_o):

$$
P_o = \begin{bmatrix} C \\ CA \\ CA^2 \\ \vdots \\ CA^{K-1} \end{bmatrix} \tag{4-13}
$$

For completely observable of all states, the matrix, (4-13), must have full rank.

4.3 Recursive Methods of Least Squares Algorithms

Identification of coefficient matrix (A and B) is undertaken by the recursive least square algorithm (RLS). The RLS method was originally developed from least squares (LS) method. The LS assumes that all data about engine parameters are available, and that the selected state variables are both observable and controllable. This means that the engine estimation process can only be applied to simulation. Therefore, it is more suitable for off-line model identification. The recursive methods build on the LS method. Instead of a batch processing at the end of engine performance simulation, the estimation will be updated after each sample step. This allows the recursive approaches to be applied online or in a real-time identification process. The estimated model will be updated when new engine data is available at each time interval. This benefit can enable the later design of the model-based controller to provide control command from the latest engine model. Because of the feature of the adaptive capability, the estimation can be automatically evolved with the engine performance.

4.3.1 Recursive Least Squares

Recursive least squares (RLS) algorithm is an extension from least squares (LS) which has been mentioned in the literature review (Section 2.6.1). RLS introduces the covariance matrix instead of storing all the data to the matrix as LS method [57]. This removes the problem of expansion about matrix size in LS as time passes on, and makes online identification possible [58].

This self-adaptive capability allows the estimation to be updated at each sampling time with newly available data. The error is taken between the new engine data (y(k)) and estimated state value ($\hat{y}(k)$) with the system noise (n(k)) as shown in (4-14). Due to the engine data being taken from the simulated engine ICV model, the value of noise can be excluded.

$$\varepsilon(k) = y(k) - n(k) - \hat{y}(k) = y(k) - n(k) - \varphi(k)^{T}\,\theta(k-1) \tag{4-14}$$

where ε is the error between the estimation from the identification process and the engine output; parametric matrix (φ) is combined with measurement of input and states:

$$\varphi(k) = [X(k),\, u(k)]^{T} \tag{4-15}$$

The value of the objective parameter (θ) from previous time step:

$$\theta(k-1) = [A^{T}(k-1), B^{T}(k-1)]^{T} \tag{4-16}$$

The covariance matrix (P):

$$P(k) = \left[\begin{bmatrix} \varphi(0) \\ \vdots \\ \varphi(k-1) \end{bmatrix}^{T} \begin{bmatrix} \varphi(0) \\ \vdots \\ \varphi(k-1) \end{bmatrix}\right]^{-1} \tag{4-17}$$

The values in the covariance matrix can be estimated by using matrix inversion Lemma. This method saves computing memory and eliminates operation of matrix inversion from (3-17) [57]. The update of covariance matrix becomes:

$$P(k+1) = P(k)\left[I - \frac{\varphi(k)\,\varphi^{T}(k)\,P(k)}{1+\varphi^{T}(k)\,P(k)\,\varphi(k)} \right] \quad \textbf{(4-18)}$$

The new constant matrices (A and B) of (4-5) are a sum between the value from last time step and the correction of the error at the current time step, (4-19).

$$\theta(k+1) = \theta(k) + P(k+1)\,\varphi(k)\,\varepsilon(k) \quad \textbf{(4-19)}$$

The main advantage of RLS is its simplicity and computational efficiency. The estimation of A and B only requires where the engine data from one step backward.

The error created by linear interpolation from compressor and turbine performance maps creates results the engine performance never reaches steady state. Instead, the operating points are oscillating about the final steady state point, which creates control noise for the engine controller. The existing stochastic noise with zero mean from the engine outputs consistently excites the engine parameters when the engine is operating near steady states. Such white noise ensures the parameter's controllability or full rank for covariance matrix [34]. For adaptation of both transient and steady state operations, the tracking performance can be improved by introducing forgetting factors so that the estimation weight can be shifted to the latest data.

4.3.2 RLS with Forgetting Factors

The RLS algorithm with the implementation of a constant forgetting factor can be simply modified on the covariance matrix:

$$P(k+1) = \lambda^{-1}P(k)\left[I - \frac{\varphi(k)\,\varphi^{T}(k)\,P(k)}{\lambda+\varphi^{T}(k)\,P(k)\,\varphi(k)} \right] \quad \textbf{(4-20)}$$

Forgetting factor allows the RLS algorithm could update the identified dynamic model towards to the latest data, and reduces the effectiveness of estimating the coefficients of the dynamic model by the old data. As a result, this is especially useful to identify step or ramp change instead of identifying steady state performance from conventional RLS algorithm. The value of λ

(forgetting factor) is selected between 0.9 and 1.0 for a fixed forgetting process. The forgetting factor controls the dumping rate to the old data. If unity is selected, the algorithm is the same as RLS, which considers all past data. Recent research has been focused on improving the converging speed to a real system. A robust variable forgetting factor to RLS (RLS-VFF) is introduced by Paleologu (2008) [36]. The selection of forgetting factors is controlled by the error between the measurement and its estimation:

$$\lambda = \min\left\{\frac{\sigma_q(k)\,\sigma_v(k)}{\zeta + \left|\sigma_e(k) - \sigma_v(k)\right|}, \lambda_{max}\right\} \quad \textbf{(4-21)}$$

where σ_e and σ_v are the power from the square of the error at current time step. However, when the error (ε) approaches to zero, the value of σ_e and σ_v are approaching to zero. The minimum value of λ can be as close as zero in (4-21).This is most likely to happen near steady states. Because of this, the value of elements in the covariance matrix of (4-20) can be increased or decreased exponentially. If the engine is operating close to a steady state, the values of elements in the covariance matrix are expected to approach constant. However, the forgetting factor (λ) in (4-20) with value less than 1 increases the covariance trace if the engine outputs are lack of excitation [57], and the inversed λ causes the divergence on the covariance matrix.

A directional forgetting algorithm (RLS-DF) is designed to avoid covariance wind-up by removing the multiplication of inverse forgetting factor from (4-20) to (4-22) [57]. However, this method compromises the tracking speed.

$$P(k+1) = P(k)\left[I - \frac{\varphi(k)\,\varphi^T(k)\,P(k)}{\lambda^{-1}(k) + \varphi^T(k)\,P(k)\,\varphi(k)}\right] \quad \textbf{(4-22)}$$

The value of the variable forgetting factor is determined by the direction of vector “φ” [57]. The direction forgetting factor is selected as:

$$\lambda(k+1) = r - \frac{1-r}{\varphi^T(k)\,P(k)\,\varphi(k)} \quad \textbf{(4-23)}$$

“r” acts as a fixed forgetting factor, which controls the tracking speed to the engine performance. The value of “r” is suggested to be selected between 0 and 1.

4.3.3 Stabilised RLS algorithms

For time variant systems, such as gas turbine engines, the covariance matrix must not be asymptotically singular. The method suggested by F. J. Kraus (1991) stabilizes the estimation process in RLS by introducing the stabilizing invariant factors (RLS-SI) or variable factors (RLS-SV) [59,60]. The modification on covariance with a linear forgetting algorithm becomes:

$$P(k+1) = \mu\hat{P}(k+1) + gI \tag{4-24}$$

$\hat{P}(k+1)$ in (4-24) is normalized $P(k+1)$ in (4-22). “I” is an identity matrix. The additional term added to the end of (4-24) is the adjustable matrix, which damps the growth on the value of covariance matrix. The constrained covariance matrix stabilizes the change on the value of poles and zeros from discrete transfer function (4-5).

The modification of the covariance matrix can either lead the value to diverge if the estimator is not a persistent excitation, or the adaption ability is lost by the growth of stored information content. Therefore, the eigenvalues (λ) of the covariance matrix must be limited, and cannot be less than 0:

$$0 < \lambda_{min} < \lambda < \lambda_{max} \tag{4-25}$$

The value of eigenvalue can be calculated as:

$$\lambda(k+1) = \mu\lambda(k) - \frac{\lambda(k)\left|\varphi(k)\right|^2}{1+\left|\varphi(k)\right|^2} + g \tag{4-26}$$

The engine parameter matrix (φ(k)) has been normalized $\hat{\varphi}(k)$.

$$\hat{\varphi}(k) = \varphi(k)/\left|\varphi(k)\right| \tag{4-27}$$

The normalized value of parameter matrix ($\hat{\varphi}(k)$) and the normalized covariance ($\hat{P}(k+1)$) are obtained by iterations from an initial estimate of covariance matrix, and the bounded eigenvalues of $\hat{P}(k+1)$ are checked through (4-28).

$$\lambda_{max} = \frac{g}{1-\mu}$$
$$\lambda_{min} = \frac{\mu + g|\varphi(k)|^2 - 1 + \sqrt{(1-\mu-g|\varphi(k)|^2)^2 + 4g|\varphi(k)|^2(2-\mu)}}{2|\varphi(k)|^2(2-\mu)} \quad \textbf{(4-28)}$$

where $0 < \mu < 1$, and $\rho > 0$,

$$g = \mu \cdot \rho \quad \textbf{(4-29)}$$

In RLS-SV, the performance of RLS-SI is improved by including the variable adjustable term in (4-24). Instead of using a constant adjusting value (g) in RLS-SI, a variable value is determined by signal levels (φ(k)) from (4-30). The procedure of other estimation steps remains the same as RLS-SI.

$$g(k) = \frac{g}{\varphi^T(k)\,\varphi(k)} \quad \textbf{(4-30)}$$

The RLS and modified RLS identification process are validated through estimating the dynamic model of a twin-spool gas turbine engine and there are two validation cases shown in Section 6.2.1 and Section 6.2.2.

In Section 6.2.1, the online identification capability to identify the dynamic model of compressor pressure ratio by the RLS algorithms introduced in this chapter: RLS, RLS-DF, RLS-SI and RLS-SV, are tested. From the results, all modified RLS methods are capable of forgetting irrelevant old data and adjusting the dynamic model to follow the repetitive large transient operation cycles and produce the results nearly or identical to the outputs from the twin-spool engine model. The dynamic model should be identical through the same transient operation under the same operating condition. When RLS methods are applied to online model identification, the dynamic model can be updated while the engine is in operation according to the reading of previous engine dynamics because the future engine response is unknown. The identification

results show that simply adding forgetting factor cannot guarantee the consistent identical roots of the dynamic models can be produced through the same transient cycles. The control module in the closed system produces the control signal to the fuel flow base on the prediction of engine future response. The predictions could be generated according to the analysis of the dynamic models. The inconsistent dynamic model could result in unstable control inputs and finally results in unstable engine response. Therefore, the stabilised RLS (RLS-SI and RLS-SV) methods produce the consistent dynamic models, and the forgetting factor ensures the results from the identified model could keep close track of the engine outputs. Referring the test results in section 6.2.1, the RLS-SV produces better results than RLS-SI due to its variable adjusting factor.

Section 6.2.2 demonstrates the process of determining the order of the dynamic model and the parameters relative to the dynamic model. In this section, the dynamic model of combustor outlet temperature (COT) was estimated by RLS-SV method in order to use MPC to monitor and protect combustor temperature as shown in Figure 1-3. From engineering experience, the combustor temperature rise is mainly affected by the change of input fuel flow if a small change or constant pressure drop across combustor chamber was assumed within small time interval and temperature change is mainly affected by the injected fuel flow. However, the simulation results in Section 6.2.2 show that the 1storder discrete model which only contains the fuel flow as input variable cannot successfully track the dynamic change of COT value. Equation: (3-11) is not a dynamic equation, but it provides a hint of the parameters which are affective to the dynamic change of COT. They are the fuel-gas ratio (FGR) and air- gas ratio (AGR), and gas is the sum of fuel flow and air flow. If the dynamic change of COT value is tracked accurately, the parameters: FGR and AGR must be included in the dynamic model, which made up 3rd order discrete model. However, the fuel-air ratio (FAR) contains both parameters: fuel and air, which can replace both FGR and AGR. Although there is a slight reduction in tracking accuracy to the COT value produced by the engine model, one parameter can be reduced in the discrete model which can greatly enhance the calculation speed of producing control value (the

comparison of estimated results by 2nd and 3rd discrete model are shown in Section 6.2.2 Figure 6-47). This is because the control decision made by MPC must predict the possible outcome of future engine outputs and constrained parameters. Although FGR and AGR are not part of engine constraints or outputs, the controller is still required to make a prediction on these variables to the effectiveness of the future response of COT. If FAR can be used to reduce 1 state variable in this model, the reduction of predictions equals to the prediction length at each time step (the details of prediction and control process of MPC will be introduced in Section 5.2). Therefore, the least and sufficient number of engine parameters are selected to develop the dynamic models allowing faster control decisions produced from MPC without loss of control accuracy.

4.4 Summary of On-line Model Identification Process

In summary, the RLS algorithm and its modified versions are applied to identify engine dynamic models and the identification algorithm is an essential module situated between the gas turbine engine and the model based controller. It is responsible for estimating and updating the dynamic model of the gas turbine engine and the controller produces the engine control signal based on the prediction from the dynamic model. The gas turbine engine in the real life is a nonlinear complex system. Its dynamic response changes nonlinearly according to the operating point and transient operations. In this project, the real engine was replaced by a simulated model which is developed to component level and is sufficient to represent the real engine performance. As the result, the engine dynamics cannot be represented by a single dynamic function. It requires nonlinear dynamic models to represent the dynamic response for the entire operating envelope. Linearization is a simple method and commonly applied by the industry. The engine transient response can be assumed that the dynamic response is linear in a small time period. In this project, the identification process uses the advantage of linearization the modified RLS algorithm could be successfully implemented to perform online dynamic model identification for gas turbine engines.

5 ENGINE CONTROLLER DESIGN

The PID controller has been successfully used by the commercial gas turbine engine performance simulation platforms: Gasturb and GSP, for gas turbine simulations and also for practical applications. The effective control actions from the PID controller cannot be guaranteed if the controller has been used at different operating conditions and outside its design range. To ensure control effectiveness, gain scheduling is required [27]. The design of MPC allows predictions about the engine performance to be made on the basis of the identified engine models. According to the predictions, the MPC is capable of managing its control gains and providing an optimal control solution in order to adapt the changes of operating environment and operating points as well as protecting engine operations within its safety range during transient operations.

In this chapter, designs of proportional-integral-derivative (PID) and constrained model predictive control (MPC) are presented. The two designs bring new approaches for controlling and optimising the transient performance of gas turbine engines and for improvement of the functionality from the classic control schedules to Turbomatch.

5.1 PID Controller

The proportional-integral-derivative (PID) controller is a linear controller installed on a closed-loop feedback mechanism. The PID controller is shown by the shaded area in Figure 5-1. The controller signals of the PID are determined from the error between the measured process variable and the desired control reference. An initial control input, fuel flow ($W_{ff}(0)$), is required to be added to the system because the control input produced by PID is the difference of fuel flow from the initial state.

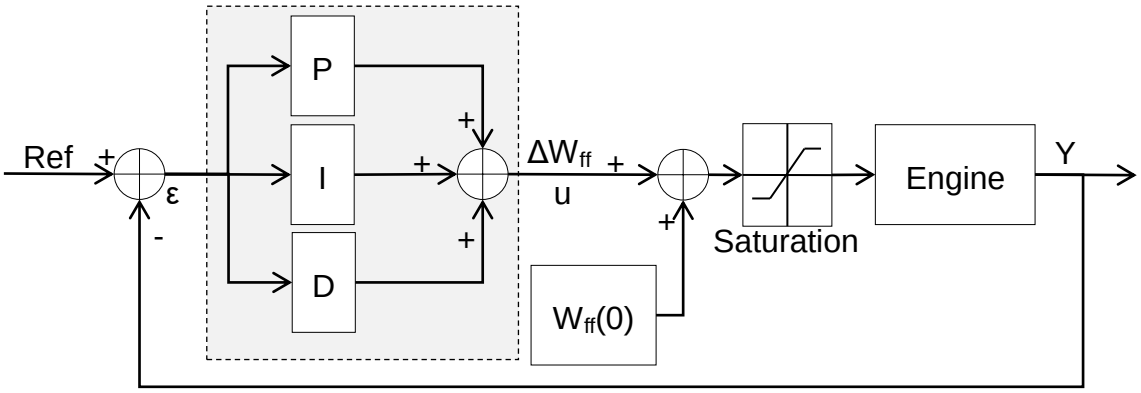

Figure 5-1 Implementation of PID controller to the closed-loop engine system

The continuous formula of PID is:[61]

$$u(t) = K_p \varepsilon(t) + K_i \int_0^t \varepsilon(\tau)\, d\tau + K_d \frac{d\varepsilon(t)}{dt} \quad \textbf{(5-1)}$$

where "K_p" is the proportional gain, "K_i" is the integral gain, and "K_d" is the derivative gain. The values of gains must be manually tuned for each system to achieve control response.

Because the engine model is a discrete time system, the PID controller must be developed in the discrete format. There are three ways to convert continuous (5-1) to discrete PID controller: Forward Euler, Backward Euler and Trapezoidal Method, shown in Table 5-1. "T_s" is the sampling time, and "N" is the filter coefficient. "z" is the discrete time and means the transfer function is on a discrete domain, and it defines the one step forward of the input or output signal.

	Forward Euler	Backward Euler	Trapezoidal
P	K_p	K_p	K_p
I	$K_i \frac{T_s}{z-1}$	$K_i \frac{T_s z}{z-1}$	$K_i \frac{T_s(z+1)}{2(z-1)}$
D	$K_d \frac{N}{1+N\frac{T_s}{z-1}}$	$K_d \frac{N}{1+N\frac{T_s z}{z-1}}$	$K_d \frac{N}{1+N\frac{T_s(z+1)}{2(z-1)}}$

Table 5-1 Discrete-time PID controller

As the name suggests, the proportional gain is the signal amplifier. Therefore, the proportional term remains the same in all discrete controller models as well as in the continuous model. The effects on the integration results by taking different sampled data from the three discrete control methods are shown in Figure 5-2. The Forward Euler uses the data from one time step ahead, and overestimates the original system. Underestimation appears for Backward Euler when one set of previous step data is being used in the controller. The trapezoidal creates the most accurate estimation of the system performance. The derivative term of PID shows the same pattern as in the estimation of the original system.

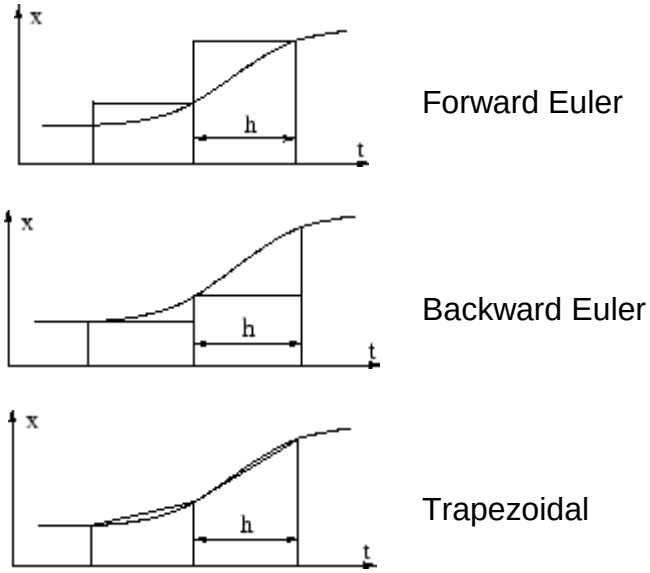

Figure 5-2 Different integration results from Forward Euler, Backward Euler and Trapezoidal methods [62]

To obtain optimum transient results from the control of PID, there are 3 coefficients (K_p, K_i and K_d) in the PID controller which needs to be tuned. They are the control gains of the PID controller.

Increasing the value of K_p increases amplification to the error between control reference and engine output. It reduces the rise time and the line moves closer to the reference at the initial stage of transient operation as shown in Figure 5-3. Due to a reduction of error near the final steady state, the effect of

K_p on the entire control gain reduces on the improvement of transient performance.

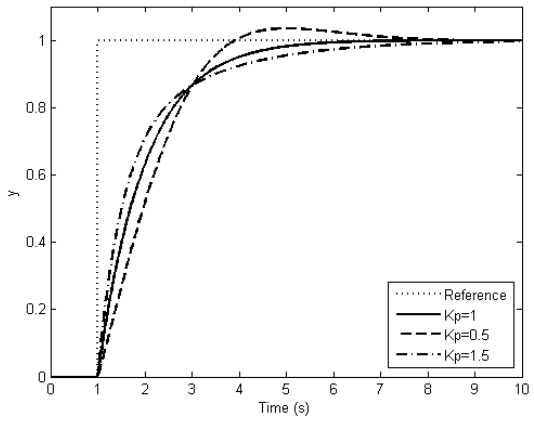

Figure 5-3 Change value of K_p to the effect on transient results

Unlike proportional gain, the change of the integral gain (K_i) is not as much effective as proportional gain at the initial transient states. However, it improves the approach time to the final steady state. The larger value of integral gain provides a faster approaching speed. However, it also introduces overshoot and a higher number of oscillations of the system, as shown in Figure 5-4.

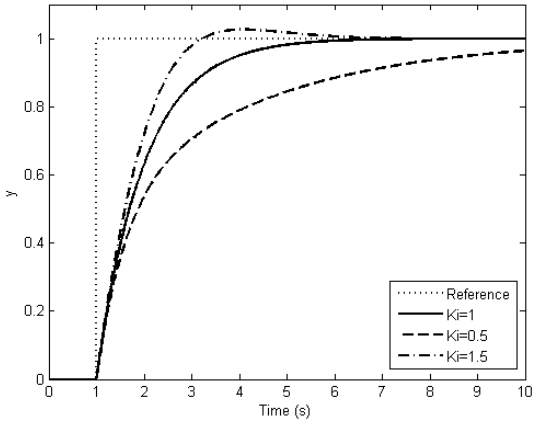

Figure 5-4 Change value of K_i to the effect on transient results

The derivative gain (K_d) determines the gradient of the error over time. At the initial stage, a larger K_d value is applied to the system due to the existence of the largest error. However, the derivative term is rarely used in practice. The implementation of K_d can provide an impact on the system stability due to

enlargement of noise and high-frequency gains. Therefore, it is common to add an additional low pass filter before the derivative term. The low pass filter allows passing the signal at the low frequency to the controller.

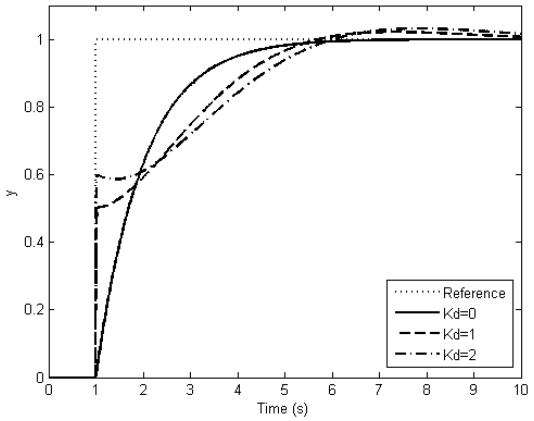

Figure 5-5 Change value of K_d to the effect on transient results

For the same reason, K_d is also rarely added to the gas turbine control system. Tuning the control loop on the engine system must be given extra care because the combustor might not be able to react to the large change in fuel flow, especially high gains chosen by K_p and K_d.

The PID controller with selected control gains is not only capable of performing the transient operation within the time requirement specified by the regulations (FAA's Part 33-Section 33.73), but the controller is also required to avoid the constraints of the engine parameters. Due to the limited range of component maps, the transient performance must be controlled by the PID within the boundaries. In order to obtain the optimal performance by the control of PID controller, the repetitive simulations are normally attempted with the slight amendment of control gains at each time. Therefore, an algorithm which can simplify the above controller design process is urgently needed. The implemented MPC is capable of seeking the optimal control solution as well as ensuring the safety of operation.

5.2 Model Predictive Controller

The model predictive controller (MPC) is an optimal control algorithm. The optimal control decisions are produced based on the predictions of engine

future behaviours as well as considering the constraints for the safety of operation. The MPC cannot directly analyse the engine performance from the component level model; the hypothesis of future engine performance is developed from the discrete engine model, (5-2) (developed from (4-5)). The control decisions from MPC are based on the linear predictions of the state space model, and the predictions are amended due to the updates of state space model by RLS-SV at each time interval.

$$\begin{aligned} X(k+1) &= AX(k) + BU(k) \\ Y(k) &= CX(k) \end{aligned} \tag{5-2}$$

The prediction by MPC uses incremental state space model with discrete differences ($\Delta U, \Delta X$) instead of exact engine parameters (U,X). The discrete increments can be obtained from(5-3) [63].

$$\begin{aligned} \Delta X(k+1) &= X(k+1) - X(k) \\ \Delta U(k) &= U(k) - U(k-1) \end{aligned} \tag{5-3}$$

The state space model (5-2) can be written into a difference model, (5-4).

$$\underbrace{\begin{bmatrix} \Delta X(k+1) \\ Y(k+1) \end{bmatrix}}_{X(k+1)} = \underbrace{\begin{bmatrix} A & 0 \\ C\cdot A & 1 \end{bmatrix}}_{A} \underbrace{\begin{bmatrix} \Delta X(k) \\ Y(k) \end{bmatrix}}_{X(k)} + \underbrace{\begin{bmatrix} B \\ C\cdot B \end{bmatrix}}_{B} \Delta U(k) \tag{5-4}$$

$$Y(k) = \underbrace{\begin{bmatrix} 0 & C \end{bmatrix}}_{C} \underbrace{\begin{bmatrix} \Delta X(k) \\ Y(k) \end{bmatrix}}_{X(k)}$$

Due to the principle of receding horizon, the output parameters (Y) must be a subset of the state matrix (X). The performance prediction is only possible when the output of the state space model, (5-4), only involves the receded control inputs. The new coefficient and variable matrices in (5-4) have replaced the original matrices in (4-5). N_c and N_p define a finite length of control and prediction horizon of MPC, and the length ($N_p \geq N_c$) can be customized according to system complexity, parameters' natural frequencies and sampling time. According to (5-4), the linear prediction of state variables at each future time step within the prediction length (N_p) can be expressed as:

$$
\begin{aligned}
X(k+1) &= AX(k) + B\Delta U(k) \\
X(k+2) &= A^2X(k) + AB\Delta U(k) + B\Delta U(k+1) \\
X(k+3) &= A^3X(k) + A^2B\Delta U(k+1) + B\Delta U(k+2) \\
&\vdots \\
X(k+N_p) &= A^{N_p}X(k) + \sum_{i=1}^{N_c} A^{N_p-i}B\Delta U(k+i-1)
\end{aligned}
\tag{5-5}
$$

The linear prediction for the outputs can be written as:

$$
\begin{aligned}
Y(k+1) &= CAX(k) + CB\Delta U(k) \\
Y(k+2) &= CA^2X(k) + CAB\Delta U(k) + CB\Delta U(k+1) \\
Y(k+3) &= CA^3X(k) + CA^2B\Delta U(k) + CAB\Delta U(k+1) + CB\Delta U(k+2) \\
&\vdots \\
Y(k+N_p) &= CA^{N_p}X(k) + \sum_{i=1}^{N_c} CA^{N_p-i}B\Delta U(k+i-1)
\end{aligned}
\tag{5-6}
$$

The matrix equation from (5-6)for predicted output (Y) where “Y” is a matrix with dimension: Np×1, and contains predicted output from Y(k+1) to Y(k+N_p):

$$
Y = \begin{bmatrix} CA \\ CA^2 \\ \vdots \\ CA^{Np} \end{bmatrix} X(k) + \begin{bmatrix} CB & 0 & \cdots & \cdots & \cdots & 0 \\ CAB & CB & 0 & \cdots & \cdots & 0 \\ CA^2B & CAB & CB & 0 & \cdots & 0 \\ \vdots & \vdots & \vdots & \ddots & \ddots & \vdots \\ CA^{Np-1}B & CA^{Np-2}B & CA^{Np-3}B & \cdots & \cdots & CA^{Np-Nc}B \end{bmatrix} \begin{bmatrix} \Delta U(k) \\ \Delta U(k+1) \\ \Delta U(k+2) \\ \vdots \\ \Delta U(k+N_c-1) \end{bmatrix}
\tag{5-7}
$$

Simplification of(5-7):

$$
Y = E\cdot X(k) + F\cdot \Delta U
\tag{5-8}
$$

The benefit of(5-8) is that the prediction of future outputs (Y) from time step “k+1” to “k+N_p” only requires the values from variables in state matrix (X) at currently time step (k) The optimization for engine transient performance can be achieved by penalizing the control inputs from minimizing the objective(or cost) function (5-9) so that the predicted outputs (Y) track to the control reference (W). The predicted outputs are estimated from the linear identified state space model and the planned control actions in (5-8).

$$
J = \left(W - \left(F\Delta U + EX(k)\right)\right)^T \left(W - \left(F\Delta U + EX(k)\right)\right) + \Delta U^T \overline{W} \Delta U
\tag{5-9}
$$

(5-9) is expanded as:

$$J = (W - EX(k))^T (W - EX(k)) - 2\Delta U^T F^T (W - EX(k)) + \Delta U^T (F^T F + \overline{W})\Delta U \quad \textbf{(5-10)}$$

The minimization of the cost function is obtained from the derivative of (5-10):

$$\frac{\partial J}{\partial \Delta U} = 2(F^T F + \overline{W})\Delta U - 2F^T (W - EX(k)) = 0 \quad \textbf{(5-11)}$$

The optimal solution for future input signals as:

$$\Delta U = (F^T F + \overline{W})^{-1} F^T (W - EX(k)) \quad \textbf{(5-12)}$$

where $\overline{W} = w \cdot I$; "I" is an identity matrix with dimension: $N_c \times N_c$; "ω" is a weighting factor.

"$\overline{W}$" is a weighting diagonal matrix, which adds the weights to the signals for the future control inputs. The weighting matrix is used to control the amount of change in control input, i.e. fuel flow, at each sampling time. The value of diagonal elements (ω) is chosen between 0 and 1, which can be different depending on different engine configurations and the natural frequency of the system. The frequency indicates the sensitivity of engine responses to the change of fuel input. When the value is close to 0, the future control inputs become more proportional to the difference between the future control reference (W) and engine output ($E \cdot X(k)$) according to (5-12). Conversely, when the value is closer to 1, more control weight is added and a slower fuel rate is supplied to the engine's combustor.

The objective function represented in (5-12) minimizes the number of control actions for reaching the final control reference, which is capable of providing the fastest transient performance of a gas turbine engine. However, such a control signal cannot be directly accepted by the engine because it discards the concerns of operating limitations, such as shaft over-speed, compressor surge and maximum turbine entry temperature (TET). The constraints to input, states and outputs can be applied to the engine system. In

the design of MPC, inequality constraints, such as (5-13), can be applied to specify the control and performance boundaries of the engine parameters.

$$\begin{cases} U_{min} \le U \le U_{max} \\ \Delta U_{min} \le \Delta U \le \Delta U_{max} \\ X_{min} \le X \le X_{max} \\ Y_{min} \le Y \le Y_{max} \end{cases} \quad \textbf{(5-13)}$$

For computational convenience, the constrained variables can be moved to the right hand side of (5-13), and the left side of the inequality becomes unity. The input variable at discrete time "k" (U(k)) equals to the sum of input from last time step (U(k-1)) and the change of input value (ΔU(k)): U(k)=ΔU(k)+U(k-1). The rearrangement of the input constraint matrix from (5-13) is shown by (5-14).

$$\underbrace{\begin{bmatrix} 1 \\ -1 \\ 1 \\ -1 \end{bmatrix}}_{M} \Delta U(k) \le \underbrace{\begin{bmatrix} U_{max} - U(k-1) \\ -U_{min} + U(k-1) \\ \Delta U_{max} \\ \Delta U_{min} \end{bmatrix}}_{\gamma} \quad \textbf{(5-14)}$$

In this project, the inequality state and output variable constraints are developed and introduced to the MPC algorithm. The development allows all engine parameters can be added to the MPC algorithm to be monitored or constrained if those parameters can be identified to dynamic models, and the control decisions are produced by considering all the added constraints.

Taking input variables (ΔU) as the matter in hand, the incremental state space predictions, (5-8), can be substituted as the outputs' constraints of (5-13). The unequal constraints are shown by (5-15).

$$\begin{cases} I\cdot\begin{bmatrix}\Delta U(k)\\ \vdots \\ \Delta U(k+N_c)\end{bmatrix} \le F^{-1}\cdot\left(I\cdot Y_{max}-E\cdot X(k)\right) \\ -I\cdot\begin{bmatrix}\Delta U(k)\\ \vdots \\ \Delta U(k+N_c)\end{bmatrix} \le F^{-1}\cdot\left(-I\cdot Y_{min}-(-E)\cdot X(k)\right) \end{cases} \quad \textbf{(5-15)}$$

Implementing constraints to engine parameters can be developed as the same limiting process as designing for output parameter from state space equation, (5-2). Output limit only requires constraining values to one parameter. Engine constraints often require being developed on several engine parameters based on their limits. These parameters must be continuously monitored and the dynamic equations are continuously adjusted while the engine is in operation. Their future dynamic responses are predicted based on the dynamic equations in order to penalise the engine performance before reaching their limits.

The 1st state space function in (5-16) produces an estimation of a dynamic model for all constrained engine parameters. These constrained parameters are the outputs in the 2nd function in (5-16). The development and validation of (5-16) is illustrated on a twin-spool turbo-fan engine in Section 6.2, and they are applied to the speed, pressure and temperature protection and transient performance optimisation. MPC uses the 1st function predicting the future dynamics of the constrained variables. Engine constraints are applied to the output function of (5-16). The penalised control output is derived from the analysis of the overall impact to the engine performance by the output function.

The 2nd function from (5-16) shows an example of the discrete state space function about the constrained engine parameters. In this function, the corrected relative speed of high-pressure shaft (CN_H), the pressure ratio of high-pressure compressor (PR_{HPC}), overall thrust ratio ($TR_{overall}$), turbine entry temperature (TET) and specific fuel consumption (SFC) are the constrained engine parameters. The constraint of high-pressure shaft speed is designed to avoid over-speed. The upper limit of high-pressure compressor is designed to avoid

compressor surge while the engine is accelerating and the lower limit of it is designed to prevent low-pressure delivery to the combustor during deceleration. The constraint of TET is to protect over-temperature in the high-pressure turbine. The constraints, such as overall thrust ratio and SFC, are used for trimming the engine transient performance. The constrained thrust output is proportional to the target thrust output. It provides an opportunity for a faster transient performance by supplying dramatic change of fuel input with controlled percentage overshoot of a delivery thrust. Implementing SFC allows controlling fuel consumption for a fuel economy. The implementation of engine multi-variable constraints to engine transient operation optimising process have been validated through transient performance simulation on a twin-spool turbo-fan engine, and the design and validation results are shown in Section 6.2.3.

$$\underbrace{\begin{bmatrix} CN_L \\ CN_H \\ PR_{LPC} \\ PR_{HPC} \\ TR_{Bypass} \\ TR_{Core} \\ FAR \\ TET \\ SFC \end{bmatrix}_{k+1}}_{X_{con}(k+1)} = \underbrace{\begin{bmatrix} a_{11} & a_{12} & & & & & & & 0 \\ a_{21} & a_{22} & & & & & & & \\ & & a_{33} & a_{34} & & & & & \\ & & a_{43} & a_{44} & & & & & \\ \vdots & & & & a_{55} & a_{56} & & & \vdots \\ & & & & a_{65} & a_{66} & & & \\ & & \ddots & & & & a_{77} & a_{78} & \\ & & & & & & a_{87} & a_{88} & \\ 0 & & & & \cdots & & & & a_{99} \end{bmatrix}}_{A\_con} \underbrace{\begin{bmatrix} CN_L \\ CN_H \\ PR_{LPC} \\ PR_{HPC} \\ TR_{Bypass} \\ TR_{Core} \\ FAR \\ TET \\ SFC \end{bmatrix}_{k}}_{X_{con}(k)} + \underbrace{\begin{bmatrix} b_1 \\ b_2 \\ b_3 \\ b_4 \\ b_5 \\ b_6 \\ b_7 \\ b_8 \\ b_9 \end{bmatrix} U|_k}_{B\_con} \quad \textbf{(5-16)}$$

$$\underbrace{\begin{bmatrix} CN_H \\ PR_{HPC} \\ TR_{Overall} \\ TET \\ SFC \end{bmatrix}_k}_{Y_{con}(k)} = \underbrace{\begin{bmatrix} 0 & 1 & 0 & 0 & 0 & 0 & 0 & 0 & 0 \\ 0 & 0 & 0 & 1 & 0 & 0 & 0 & 0 & 0 \\ 0 & 0 & 0 & 0 & TR_{Bypass}|_{design} & TR_{Core}|_{design} & 0 & 0 & 0 \\ 0 & 0 & 0 & 0 & 0 & 0 & 0 & 1 & 0 \\ 0 & 0 & 0 & 0 & 0 & 0 & 0 & 0 & 1 \end{bmatrix}}_{C\_con} \underbrace{\begin{bmatrix} CN_L \\ CN_H \\ PR_{LPC} \\ PR_{HPC} \\ TR_{Bypass} \\ TR_{Core} \\ FAR \\ TET \\ SFC \end{bmatrix}_k}_{X_{con}(k)}$$

The process which derives (5-3) and (5-4) can also be applied to state space model of engine constraints, (5-16). As the result, the increment state and input of (5-16) can derive from (5-17).

$$\Delta X_{con}(k+1) = X_{con}(k+1) - X_{con}(k) \qquad \textbf{(5-17)}$$
$$\Delta U(k) = U(k) - U(k-1)$$

The increment state space model of (5-16) becomes (5-18). Developing increment model for engine constraints model is because the engine control value derived from MPC measures the delta values of engine parameters. The dimension of a matrix containing state variables in (5-18) is 14×1, X_{con_in}. The coefficient matrix, A_{con_in}, is a square matrix, which has dimension 14×14, and coefficient matrix, B_{con_in}, has dimension 14×1.The coefficient matrix in the output function, C_{con_in}, has dimension 1×14, which produces multiple outputs. According to this example, there are 5 constrained engine parameters.

$$\underbrace{\begin{bmatrix}\Delta X_{con}(k+1)\\ Y_{con}(k+1)\end{bmatrix}}_{X_{con\_in}(k+1)} = \underbrace{\begin{bmatrix}A\_con & 0\\ C\_con\cdot A\_con & 1\end{bmatrix}}_{A_{con\_in}}\underbrace{\begin{bmatrix}\Delta X_{con}(k)\\ Y_{con}(k)\end{bmatrix}}_{X_{con\_in}(k)} + \underbrace{\begin{bmatrix}B\_con\\ C\_con\cdot B\_con\end{bmatrix}}_{B_{con\_in}}\Delta U(k) \qquad \textbf{(5-18)}$$

$$Y_{con}(k) = \underbrace{\begin{bmatrix}0 & C\_con\end{bmatrix}}_{C_{con\_in}}\underbrace{\begin{bmatrix}\Delta X_{con}(k)\\ Y_{con}(k)\end{bmatrix}}_{X_{con\_in}(k)}$$

The same function for prediction of engine output: (5-7), can also be applied to produce the prediction for engine constrained parameters in (5-18), the prediction is shown as (5-19) from discrete time: k+1 to k+N_p. Once the prediction function, (5-19), has been developed, the constraints of engine parameters can now be designed by using the same constraint process as the output of (5-2). Increment input matrix (ΔU) contains the predicted control inputs from discrete time k+1 to k+N_c-1.

$$Y = \underbrace{\begin{bmatrix}C_{con\_in}A_{con\_in}\\ C_{con\_in}A_{con\_in}^{2}\\ \vdots\\ C_{con\_in}A_{con\_in}^{Np}\end{bmatrix}}_{E_{con\_in}} X_{con\_in}(k) + \underbrace{\begin{bmatrix}C_{con\_in}B_{con\_in} & \cdots & \cdots & 0\\ C_{con\_in}A_{con\_in}B_{con\_in} & C_{con\_in}B_{con\_in} & \cdots & 0\\ \vdots & \ddots & \ddots & \vdots\\ C_{con\_in}A_{con\_in}^{N_p-1}B_{con\_in} & C_{con\_in}A_{con\_in}^{N_p-2}B_{con\_in} & \cdots & C_{con\_in}A_{con\_in}^{N_p-N_c}B_{con\_in}\end{bmatrix}}_{F_{con\_in}}\Delta U \qquad \textbf{(5-19)}$$

Once the predictive function is established, the limits of engine parameters can be designed. The limits of engine parameters can be designed to be constant, linear or quadratic functions where the limits are varying depending on the operating points. For example, the limits of high-pressure shaft speed, overall thrust ratio, TET and SFC are constant values, and limit of pressure ratio

of high-pressure compressor can be designed to a linear function which is relative to the value of high-pressure shaft speed, as shown in (5-20).

$$\underbrace{\begin{bmatrix} CN_{min} \\ a_{HPC\_min}\cdot CN_H + b_{HPC\_min} \\ 0.95\cdot TR_{Min\_Target} \\ TET_{min} \\ N/A \end{bmatrix}}_{M_{con\_MIN}} \le \underbrace{\begin{bmatrix} CN_H \\ PR_{HPC} \\ TR_{overall} \\ TET \\ SFC \end{bmatrix}}_{Y_{con}} \le \underbrace{\begin{bmatrix} CN_{max} \\ a_{HPC\_max}\cdot CN_H + b_{HPC\_max} \\ 1.05\cdot TR_{Max\_Target} \\ TET_{max} \\ SFC_{max} \end{bmatrix}}_{M_{con\_MAX}} \quad \textbf{(5-20)}$$

The constraint in (5-20) can be separated into factor and constant terms as (5-21) showing.

$$\underbrace{\begin{bmatrix} CN_H \\ PR_{HPC} \\ TR_{overall} \\ TET \\ SFC \end{bmatrix}}_{Y_{con}} \le \underbrace{\begin{bmatrix} 0 & 0 & \cdots & \cdots & 0 \\ 0 & a_{HPC\_max} & 0 & \cdots & 0 \\ 0 & 0 & 0 & \cdots & 0 \\ 0 & 0 & \cdots & \cdots & 0 \\ 0 & 0 & \cdots & \cdots & 0 \end{bmatrix}}_{A_{max}} \underbrace{\left\| \begin{bmatrix} CN_L \\ CN_H \\ PR_{LPC} \\ PR_{HPC} \\ TR_{Bypass} \\ TR_{Core} \\ FAR \\ TET \\ SFC \end{bmatrix} \right\|_k}_{X_{con}(k)} + \underbrace{\begin{bmatrix} CN_{max} \\ b_{HPC\_max} \\ 1.05\cdot TR_{Max\_Target} \\ TET_{max} \\ SFC_{max} \end{bmatrix}}_{M_{con\_MAX}}$$

$$-1\cdot \underbrace{\begin{bmatrix} CN_H \\ PR_{HPC} \\ TR_{overall} \\ TET \\ SFC \end{bmatrix}}_{Y_{con}} \le -1\cdot \underbrace{\begin{bmatrix} 0 & 0 & \cdots & \cdots & 0 \\ 0 & a_{HPC\_min} & 0 & \cdots & 0 \\ 0 & 0 & 0 & \cdots & 0 \\ 0 & 0 & \cdots & \cdots & 0 \\ 0 & 0 & \cdots & \cdots & 0 \end{bmatrix}}_{A_{min}} \underbrace{\left\| \begin{bmatrix} CN_L \\ CN_H \\ PR_{LPC} \\ PR_{HPC} \\ TR_{Bypass} \\ TR_{Core} \\ FAR \\ TET \\ SFC \end{bmatrix} \right\|_k}_{X_{con}(k)} - \underbrace{\begin{bmatrix} CN_{min} \\ b_{HPC\_min} \\ 0.95\cdot TR_{Min\_Target} \\ TET_{min} \\ 0 \end{bmatrix}}_{M_{con\_MIN}} \quad \textbf{(5-21)}$$

The prediction of future control inputs regarding the consideration of engine constraints can be produced from the rearrangement of (5-21) with the substitution of (5-19), as shown in (5-22).The change of control inputs (ΔU) contains N_c length of control predictions.

$$\underbrace{F_{con\_in}}_{M}\cdot\Delta U \le \underbrace{A_{max}X_{con}(k)-E_{con\_in}X_{con\_in}(k)+M_{con\_Max}}_{\gamma}$$
$$\underbrace{-1\cdot F_{con\_in}}_{M}\cdot\Delta U \le \underbrace{-A_{min}X_{con}(k)-E_{con\_in}X_{con\_in}(k)-M_{con\_Min}}_{\gamma} \quad \textbf{(5-22)}$$

The combination of (3-14), (3-15) and (5-22) can be simplified to (5-23).

$$M\cdot\Delta U \le \gamma \quad \textbf{(5-23)}$$

Using Lagrange's theorem estimates the compensated control action, which minimises the objective function with consideration of constraints to the derivative form as shown in (5-24).

$$\max_{\lambda\ge 0}\min_{\Delta U}\left[\Delta U^T(F^TF+\overline{W})\Delta U-2\Delta U^TF^T(W-EX(k))+2\lambda^T(M\Delta U-\gamma)\right] \quad \textbf{(5-24)}$$

The optimal control solution of (5-25) is given by the minimization of the Lagrange multiplier from (5-24).

$$\Delta U=-\left(F^TF+\overline{W}\right)^{-1}\left[F^T\left(EX(k)-W\right)+\lambda^TM\right] \quad \textbf{(5-25)}$$

"λ" is a weighting factor, which determines the impact of the constraints to the future control inputs. The optimal solution of "λ" is solved by Hildreth's quadratic programming method [63]. The Hildreth method is an element-by-element searching algorithm, and it does not require matrix inversion in the process. The maximum value of "λ" is picked from (5-26). The value of "w" in (5-26) is determined from the iteration process by (5-27). The iteration is repeated for all constrained engine parameters ((5-13)) on each predicted time.

$$\lambda_i^n=\max\left(0,w_i^n\right) \quad \textbf{(5-26)}$$

where:

$$w_i^n=-\frac{1}{h_{ii}}\left(k_i+\sum_{j=1}^{i-1}h_{ij}\lambda_j^n-\sum_{j=i+1}^{m}h_{ij}\lambda_j^{n-1}\right) \quad \textbf{(5-27)}$$

The optimal control solution with consideration of parameter constraints is the substitution of the minimum control actions, (5-25), to (5-24) and gives (5-28).

The maximum value of "λ" is substituted to (5-28) for each time step prediction in order to ensure the satisfaction of all active constraints.

$$\max_{\lambda \geq 0}\left(-\lambda^{T} H \lambda - 2\lambda^{T} K - \left(F^{T}\left(W - EX(k)\right)\right)^{T}\left(F^{T} F + \overline{W}\right)^{-1}\left(F^{T}\left(W - EX(k)\right)\right)\right) \quad \textbf{(5-28)}$$

where:

$$\begin{cases} H = M\left(F^{T} F + \overline{W}\right)^{-1} M^{T} \\ K = \gamma + M\left(F^{T} F + \overline{W}\right)^{-1}\left(F^{T}\left(EX(k) - W\right)\right) \end{cases} \quad \textbf{(5-29)}$$

The small letters: "h" and "k" are the elements of the matrix "H" and "K". Letters: "i" and "j" in (5-27) indicate the row and column number in the matrix "H". "m" is the total number of iterations and "n" is the iteration number. If the total number of constraints is assumed to be "r", the dimension of matrix "H" is $r \times r$; the dimension of "K" is $r \times 1$ and the dimension of "λ" is $r \times 1$. The iteration starts where no iteration is taken: $n = 0$. The initial value of "λ" can be set to 0, such as: $\lambda_1^0 = \lambda_2^0 = \cdots \lambda_r^0 = 0$, if the initial condition is unknown. If the value of any element in "λ" equals 0, the constraint of this parameter is inactivated. If any element in "λ" has a value greater than 0, the optimal solution of (5-12) will be compensated by the constraint. The final value of "λ" can be substituted back to (3-32) to obtain the constrained optimal control solution. The constraints must be linearly independent and the number of active constraints must be less than or equal to the number of control or decision variables, so that there will be a converged control solution. Only the first sample input from the sequence is used by the controller, although the optimal control plan has been predicted through to the horizon. The process is repeated for each sampling step when the new data is available and the predictions by the constrained MPC will be updated.

5.3 Summary of Engine Controller Design

In this chapter, constrained model predictive control process (MPC) has been introduced to the application of the gas turbine engine control system. The engine control values are produced from the prediction of engine future dynamic responses. The predictions rely on the estimated models (discrete state space

models). In addition, the engine performance can also be predicted with influence of engine constraints. Through tuning the future control inputs, the transient operating points can be protected within assigned operating limits for safety concerns. The constraints can be designed on any of engine parameters, and instead of safety protection, they can also be designed for performance tuning, such as for lower fuel consumption or smooth transient thrust transition. The design and application of MPC with engine constraints are described in more details on the test cases of single and multi-spool gas turbine engines in Chapter 6. Therefore, the MPC allows more appropriated control inputs can be produced to deliver outcome of the fastest transient response through the prediction of future engine dynamic responses with the consideration of input and performance or safety restrictions. As the results, higher safety level of transient operation and faster and smoother transient response can be achieved by the implementation of constrained MPC for gas turbine transient operations.

6 APPLICATION, RESULTS and ANALYSIS

6.1 Application to a Single-spool Turbojet Engine

This case study illustrates and compares different control strategies: scheduling methods, PID control and MPC, to optimise the transient response on a single-spool turbojet engine. Furthermore, the design to optimise fuel economy and performance of the transient optimisation, under dynamic conditions, is also demonstrated.

The design of this engine was based on the design point shown by Table 6-1 [64]. The schematic sketch is shown in Figure 6-1. The volume sizes are measured from technical drawing [65]. The dimension has been returned to the scale of the actual engine according to length 3,200mm and diameter 907mm from data sheet [64]. The design, off-design and transient simulations were performed on Turbomatch 2.0baccording to the design point from Table 6-1 as the input.

Ambient condition	ISA SLS	[-]
Intake Mach number	0	[-]
Intake mass flow	76.0	kg/s
High-pressure compressor pressure ratio	8.80	[-]
High-pressure compressor isentropic efficiency	89	%
Fuel flow	1.1102	kg/s
High-pressure turbine isentropic efficiency	89	%
Moment of inertia for high-pressure shaft	30	Nm^2
Percentage of corrected rotational speed at high-pressure shaft to 131.67 RPS	100	%
Volume 1	0.6749	m^3
Volume 2	0.3384	m^3
Volume 3	0.1241	m^3

Table 6-1 The design point of the single-spool turbojet engine

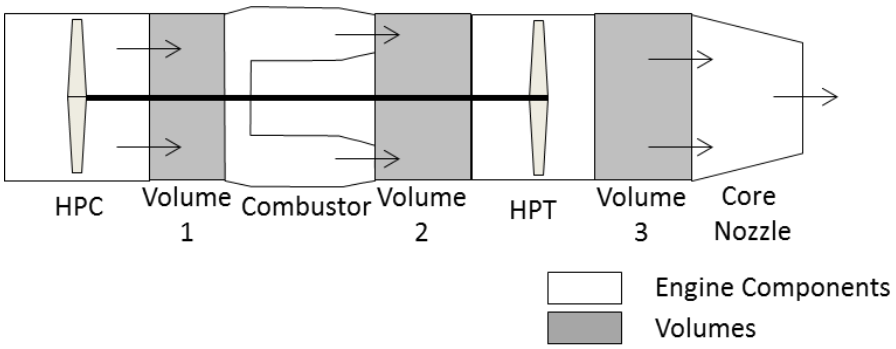

Figure 6-1 Single spool turbojet engine

The design of the controller is an attempt at optimising the acceleration and deceleration operation between idle and the design point, which corresponds to the range shown in Table 6-2.

PCN	60.0~100.0	%
HPC-PR	3.93~8.80	[-]
GTR	26.2~100.0	%
W_{ff}	0.3754~1.1102	kg/s

Table 6-2 Transient range for single spool turbojet engine

The off-design performance from the simulation on Turbomatch has been compared and validated with the result from Gasturb 11. The similar off-design running lines are shown by Figure 6-2. However, in general, the steady state running line from Gasturb has a slightly lower value of compressor pressure ratio than the steady state results from Turbomatch.

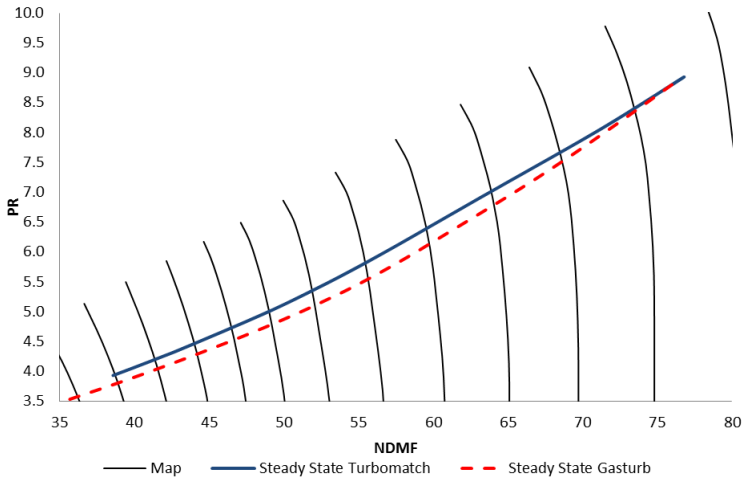

Figure 6-2 Steady state performance of the single spool turbojet engine

The gross thrust at design point is 50.624kN from Turbomatch, approximately 0.4% less than the prediction from Gasturb (50.819kN).However, the difference increases from 0.4% to over 24% on both SFC and gross thrust while the PCN reduces from design point (100%) to idle (60%), Figure 6-3. A larger difference on the estimation results in lower power operating points. The different steady sate results from both simulation tools are caused by different approximation of gas properties and different combustor maps. The steady state lines of SFC and gross thrust from both simulation tools show similar trends. The lines agree as in the demonstrated engine performance shown by

figure 14.4 in the textbook: Dynamic Modelling of Gas Turbines [52]. Furthermore, both sets of results agree that the optimal performance with minimum SFC is at the operating point between 0.80 and 0.85 of PCN.

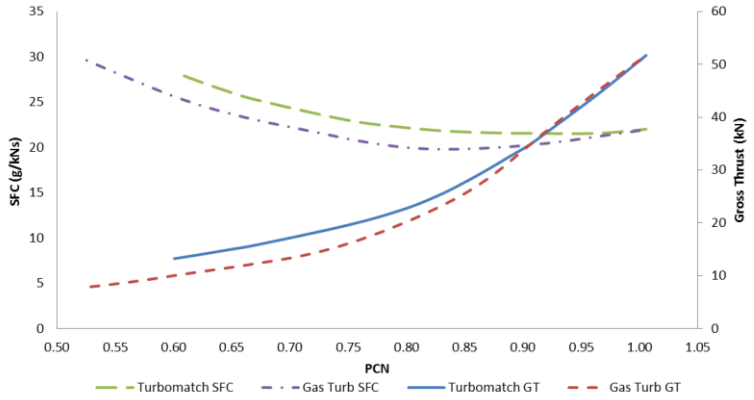

Figure 6-3 Steady state fuel consumption and gross thrust

6.1.1 Transient Response Optimisation

6.1.1.1 PID Controller

PID is designed for controlling linear time-invariant (LTI) systems. A linear characteristic is assumed for the operating range between idle and design point (60% to 100% PCN). There are two ways of tuning the PID controller, Ziegler-Nichols and manual tuning, to obtain the optimum transient time with an acceptable percentage overshoot (<5%).

Ziegler Nichols (ZN) tuning is the most common method used in the process control to determine the appropriate value of gains in PID controller. The parameters, time delay (L) and time constant (T), characterise the open-loop step response of the engine system. The time delay is the time from the start of the transient operation to the point where there is an interception of the tangent of inflection point to the time axis. The time constant is the time of this intercept point to the time where the transient line first reaches the final steady state point. The graphical representation for estimating delay and time constant is shown in Figure 6-4.

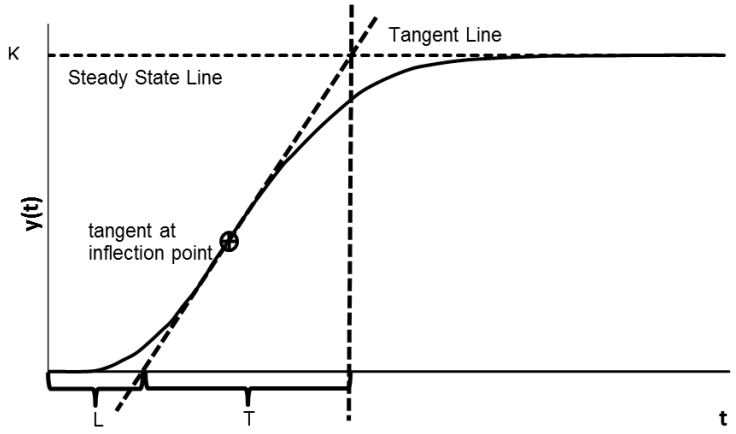

Figure 6-4 Estimation of time delay and time constant for transient response

The values for the coefficients of PID can be determined from Table 6-3 by ZN method [66].

	k_p	k_i	k_d
P	T	0	0
PI	$0.9 \cdot T/L$	$L/0.3$	0
PID	$1.2 \cdot T/L$	$2L$	$0.5L$

Table 6-3 Gains of PID controller by Ziegler Nichols method

In order to estimate the value of delay and time constant for the single spool engine, an open loop step system was set up for the simulation, Figure 6-5.

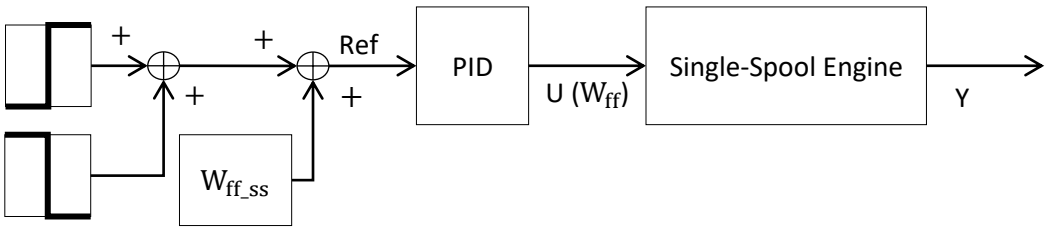

Figure 6-5 Open loop single-spool engine system

PID controller is normally applied to a closed-loop system and provides the change to the input signals by considering the error between the reference signal (Ref) and the output signal (Y). In an open loop system, due to an absolute value of fuel input, the proportional gain is set to 1 and the integral and differential parts are de-activated (set values to 0) so that the fuel flow shown in

Figure 6-5 can be directly injected into the engine. A step change from 0kg/s to 0.7348kg/s at 1sadded to the initial fuel flow allows the engine to accelerate from idle to 100% power. The 2nd step block returns the fuel flow back to its initial value at 10s, which provides the opposite command of the 1st step block in Figure 6-5. The result of PCN from an open-loop simulation performed on Turbomatch 2.0b is shown in Figure 6-6.

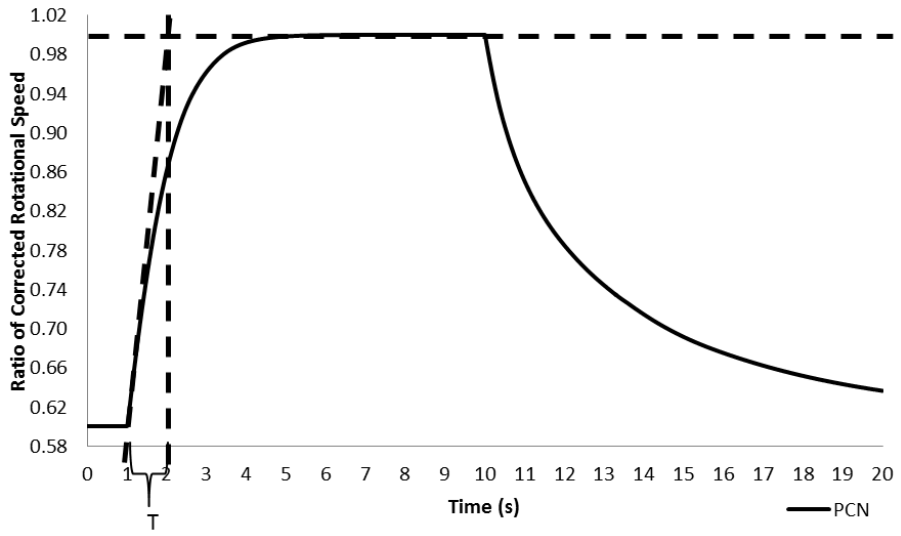

Figure 6-6 Open loop response of corrected shaft speed for the single spool turbojet engine

The delay and time constant on PCN can be estimated from the graph given by the open-loop response. The time constant (1s) can be easily approximated from the time where the largest tangent line intercepts with the initial steady state to the time where the operation reaches the final steady state, Figure 6-6. The time delay can be almost neglected (0.01s).

The design of a PID controller sometimes only includes the proportional and integral terms because the derivative gain is easily magnified by the interference of high-frequency noise. According to the Ziegler Nichols method of Table 6-3, the value of proportional gain (K_p) is 900, and the integral gain (K_i) is 0.0333. However, the values of these gains are not applicable to the engine system because the proportional gain is too large and will directly exceed the fuel limits during transient operations.

The manual tuning method is firstly to set K_i and K_d value to zero. The K_p value is increased until the output starts to oscillate or reaches resonance. Then, the value of K_i should be increased until any steady state error has been eliminated within sufficient time. A large K_i provides a system excessive response, increases the percentage of overshoot and number of oscillations, and increases the chance of instability. The increase of K_d value reduces the offset to the final steady state. The summary of increase in PID control gains to the system response is shown in Table 6-4 [67].However, a manual tuning method is practically difficult to apply on a gas turbine engine because the limitation on the fuel air ratio in the combustor normally does not allow large changes in fuel flow. When this method is applied to the corresponding transfer function (6-3), the K_p value is approximately 162 which is 45% of the K_p value given by ZN method, and K_i is 183.6.

	Rise Time	Overshoot	Settling Time	Steady State Error	Stability
K_p	Decrease	Increase	Negligible	Decrease	Decrease
K_i	Decrease	Increase	Increase	Decrease	Decrease
K_d	Negligible	Decrease	Decrease	Negligible	Negligible

Table 6-4 Effects of increased PID gains

According to the graphical representation in Figure 6-6, the dynamic response of PCN for this engine can be identified as a 1storder transfer function by the least squares (LS) algorithm if a linear response is assumed for this transient behaviour between idle (60%)and 100% of PCN [57,68]. In the model estimation process, it often assumes the input signal (u(t)), fuel flow, is ‘sufficiently and consistently exciting’, so that a unique set of parameters can generate a unique dynamic function. Therefore, a closed-loop engine system with PI controller, Figure 6-7, can be designed to replace the open loop system, Figure 6-6. An arbitrary value of control gains (K_p=0.7, K_i=0.7) was imported to PI control to perform the transient operation. During the initial attempt, smaller values of control gains are chosen to ensure that no fuel saturation could be reached and that the PCN can reach its control reference for both acceleration and deceleration. The closed-loop simulation repeated the same process as the open-loop simulation, in which the command of acceleration was started at 1s from idle to 100% shaft speed, and returned to idle at 10s.

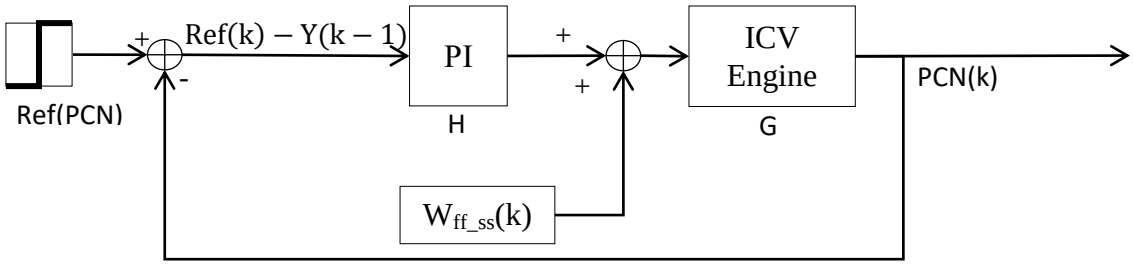

Figure 6-7 Closed-loop PID control on ICV engine model

Fuel flow and PCN data can be gathered from the simulation and subjected to an off-line identification of LS algorithm. A discrete state space function with a sampling time of 0.001s has been produced according to the outputs of the ICV model:

$$\mathrm{PCN(k+1)} = 0.9958\mathrm{PCN(k)} + 0.004767\mathrm{W_{ff}(k)} \quad \textbf{(6-1)}$$

The discrete transfer function:

$$\frac{\mathrm{PCN(k)}}{\mathrm{W_{ff}(k)}} = \frac{0.004767}{\mathrm{z} - 0.9958} \quad \textbf{(6-2)}$$

The conversion from discrete to continuous model gives the 1st order transfer function (TF):

$$\mathrm{G} = \frac{4.776}{\mathrm{s} + 4.169} \quad \textbf{(6-3)}$$

Since the transfer function of the shaft speed has been identified, the closed-loop response from system Figure 6-8 can be viewed on the root locus (s-plane) by choosing arbitrary values of K_p and K_i. The closed-loop transfer function can be written as:

$$\frac{\mathrm{Y}}{\mathrm{Ref}} = \frac{\mathrm{H \cdot G}}{1 + \mathrm{H \cdot G}} \quad \textbf{(6-4)}$$

Substitute the PI formula and (6-3) to (6-4):

$$\frac{\mathrm{H \cdot G}}{1 + \mathrm{H \cdot G}} = \frac{\frac{\mathrm{K_p s + K_i}}{\mathrm{s}} \cdot \frac{4.776}{\mathrm{s}+4.169}}{1 + \frac{\mathrm{K_p s + K_i}}{\mathrm{s}} \cdot \frac{4.776}{\mathrm{s}+4.169}} = \frac{4.776\mathrm{K_p s} + 4.776\mathrm{K_i}}{\mathrm{s^2} + \left(4.776\mathrm{K_p} + 4.169\right)\mathrm{s} + 4.776} \quad \textbf{(6-5)}$$

Two roots of the denominator and one root of the numerator can be solved from the closed loop transfer function (6-5). Roots of the denominator are called poles, and roots of the numerator are called zeros. An example of a root locus plot is shown in Figure 6-10.For any asymptotic stable discrete system, the real parts of poles and zeros are located inside the unit circle. Therefore, the value of zeros and poles must be less than one. If the location of poles or zeros are on the line of the unit circle, the system is marginally stable. For any pole or zero outside the unit circle, the system becomes unstable. The optimal design of a PID controller is to shift the system response as close as possible to the imaginary axis for the fastest transient response.

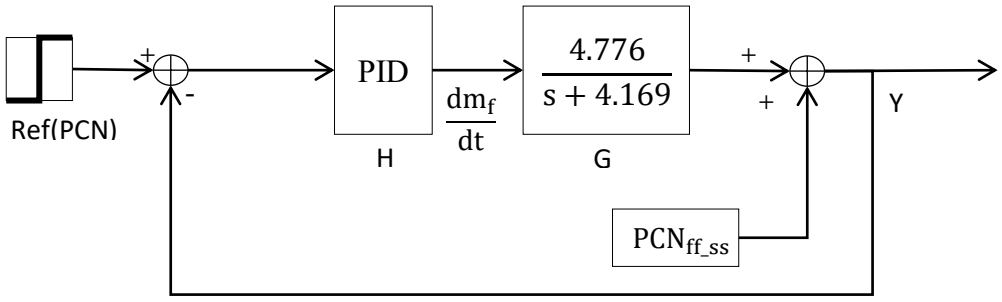

Figure 6-8 Closed-loop control on transfer function of $\Delta PCN/\Delta W_{ff}$

A group of K_p and K_i values substituted to (6-5) predicts the location of zero and poles on the s-plane, Figure 6-9, so that the change of poles and zero can be observed. According to Figure 6-9, the fastest transient response can be achieved by selecting the value of K_p and K_i which can provide the lowest values of poles and zero. The graphs indicate that increasing K_p brings the values of one of the poles and a zero infinitely close to 0 (imaginary axis). The engine is a stable system; it responds to any disturbance from input (fuel flow) and is capable of restoring the performance to a new steady state point. The transfer function about the dynamic of PCN, (6-3), also shows a stable characteristic because the value of pole is -4.169 which is located far away from the imaginary axis. Therefore, for any value of PI gains, the response of PCN will always be stable. As a result, the roots of the closed-loop system,(6-5), will not reach or cross the imaginary axis. However, the other poles will move infinitely away from this imaginary axis, and it provides little influence to the

shaft dynamic compared to the other pole. Both ZN and the manual tuning method attempt to choose the optimum value of K_p and K_i (infinitely large) by bringing poles and zero close to the imaginary axis in order to match the step change of control reference. When a value of K_p is large, the value of Ki can be either small or large because it has little contribution to the improvement of rising time.

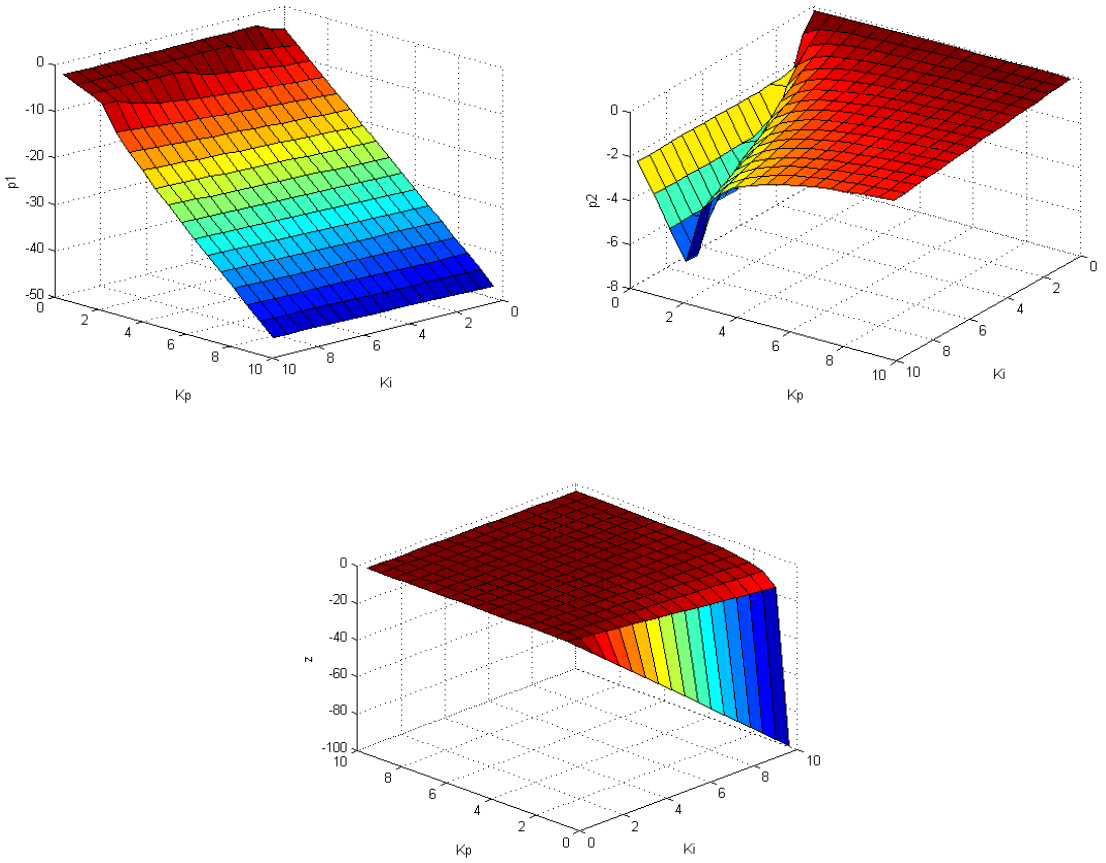

Figure 6-9 The results of poles and zero of dynamic of PCN controlled by PI with different control gains

The values of zero and poles are reaching a plateau and so the improvement of transient response becomes insignificant while K_p and K_i values are being further increased. The optimum engine transient response also requires the control signals to avoid the operational boundaries, such as fuel rate and change of loadings on the engine components. The control design is still acceptable to the performance requirements of most engines if the rise time

can be maintained within 3~5s [45]. Therefore, only seeking the shortest transient time is not always the best solution for a control design. Therefore, smaller values of K_p (0.1) and K_i (1.4) were selected. The values still allow the location of poles and zero to be reasonably close to the origin according to Figure 6-9. However, they are further away from the imaginary axis than the values given by ZN method, Figure 6-10, hence a much slower transient response (longer rise time) is expected, Figure 6-11. The rise time of the acceleration of the estimated TF in Figure 6-8 is approximately 4s from the PI controller with the reduced value of control gains, and it is approximately 4s longer than the results given by ZN method (0.004s). The transient acceleration shows approximately 3s of rising time when the reduced gain of the PI controller is simulated on Turbomatch.

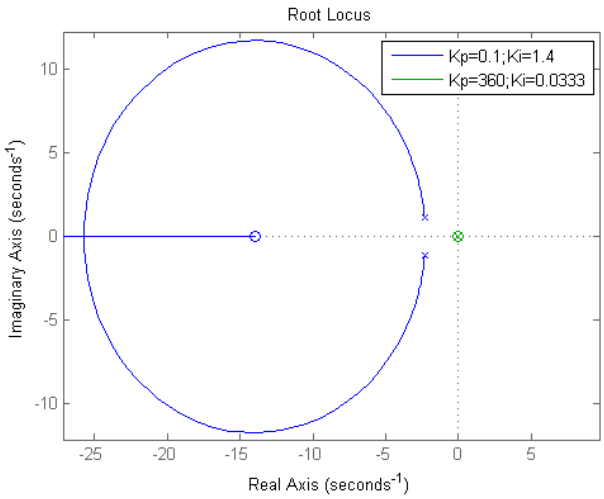

Figure 6-10 Root loci design at (6-5) when K_p=0.1 K_i=1.4; K_p=360 K_i=0.0333

A linear system should have the deceleration running line which is centrosymmetric image to the acceleration running line, as shown by the transient performance of the transfer function in Figure 6-11. However, the transient result from the component-level model shows different dynamic characteristics between acceleration and deceleration, Figure 6-11.Therefore, different values of PI gains must be designed separately in order to obtain the optimum performance for both acceleration and deceleration. As a result, the gain-scheduled control technique can be developed including the table of

control gains for different levels of power change as well as for the operations at different Mach number and altitudes [54].

Furthermore, a 1st order transfer function (6-3) cannot sufficiently match the transient acceleration and deceleration of the ICV model, Figure 6-11. The transient response from the ICV model shows significant delay over the TF. Due to the delay response of PCN to the change of fuel flow, the ICV model provides more overshoot (1%) during acceleration and 1s less of rising time than the 1st order TF. According to the research from Hanz Richter [54], using a linear parameter-varying (LPV)algorithm can improve the accuracy of the transfer function; and the coefficients of the TF associated with the set of parameters, ie Mach number, altitude and the imbalance of power between compressor and turbine work. The method, such as: LPV or RLS, allows the coefficients of (6-3)to be updated according to the change of shaft dynamics. Therefore, in order to develop an accurate model for a better control design, the identified model should be updated adaptively to the changes in engine performance. The gains of PID should be updated according to the change of the dynamic model. In some design cases, scheduling tables of PI gains are built and constructed within the designs for various combinations of conditions. A linear interpolation is used to find the appropriate controller gains from real-time measurements[54].

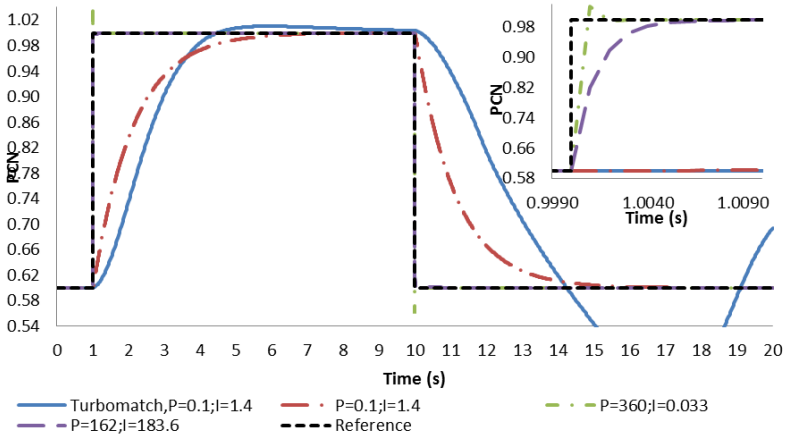

Figure 6-11 The transient response from estimated transfer function controlled by PI controller

6.1.1.2 Constrained Model Predictive Controller

The above PID design proves that a single classic control design is not enough to satisfy the performance requirements for both acceleration and deceleration. As a result, a control schedule is required for the control of entire operating range. In this section, a single design of MPC is demonstrated to achieve the transient performance requirements for both acceleration and deceleration operations. In addition, obtaining the optimal performance with different reference variables can be easily modified on the MPC.

Before designing the constrained MPC, the engine system must be simplified to a reduced order of state space (SS) model for the convenience of control analysis. A few engine parameters which matter to the transient operations are selected. The SS dynamic models are built around these parameters. In this case, the selection of control input, state and output variables are shown by Table 6-5. Fuel flow (W_{ff}) is the only variable to control the engine performance to achieve the transient objective. There are four state variables as shown in Table 6-5. The constraints are designed to these variables for shaft speed protection, compressor surge potection and fuel consumption optimisation. The output variable must be a subset of the state variables and include at least one of the state variables. In this case, the same transient cycle was simulated by selecting the three engine variables separately as output variables: PCN, HPC-PR and GTR in order to compare the transient performance given by the control of MPC with different control references.

Type	Name
Control Variable, U(k)	W_{ff}
State Variables, X(k)	PCN, HPC-PR, GTR and SFC
Output Variables, Y(k)	PCN, HPC-PR or GTR

Table 6-5 The control and state engine variables

Prior knowledge about dynamics of the variables is required for designing the SS model, such as: the order of function and the initial value of the coefficients. Most parameters of a single spool gas turbine can be assumed to 1^{st} order functions. A discrete model for most engine parameters, (6-6), according to (4-5)can be identified accurately by RLS-SV. Adjustable parameters of RLS-SV are set to 0.99 for ρ and 0.96 for μ.

$$\begin{bmatrix} \text{PCN} \\ \text{PR}_{\text{HPC}} \\ \text{GTR} \\ \text{SFC} \end{bmatrix}_{k+1} = A \begin{bmatrix} \text{PCN} \\ \text{PR}_{\text{HPC}} \\ \text{GTR} \\ \text{SFC} \end{bmatrix}_{k} + \text{BW}_{\text{ff}}|_{k} \tag{6-6}$$

where the initial value in matrix A and B from LS steady state estimation:

$$A = \begin{bmatrix} 0.9964 & 0 & 0 & 0 \\ 0 & 0.9970 & 0 & 0 \\ 0 & 0 & 0.9931 & 0 \\ 0 & 0 & 0 & 0.9989 \end{bmatrix}; B = \begin{bmatrix} 0.006051 \\ 0.003021 \\ 0.006230 \\ 0.000835 \end{bmatrix}$$

The MPC was designed for performance optimisation of a single input and single output (SISO) system in the Turbomatch. The output parameters can be selected among PCN, HPC-PR or GTR by switching the value “0” to “1” in matrix C of (6-7). If the engine output is its corrected relative rotational speed (PCN), the output can be set as shown by (6-7) according to output function of (5-4).

$$[\text{PCN}]_{k} = \underbrace{\begin{bmatrix} 1 & 0 & 0 & 0 \end{bmatrix}}_{C} \begin{bmatrix} \text{PCN} \\ \text{PR}_{\text{HPC}} \\ \text{GTR} \\ \text{SFC} \end{bmatrix}_{k} \tag{6-7}$$

The value of control reference changes according to the selection of output parameters for step simulation. The transient between 0.6 and 1.0 of PCN corresponds to a compressor pressure ratio (HPC-PR) between 3.93 and 8.80, or a gross thrust ratio (GTR) between 0.262 and 1.000.

A smaller weighting factor value ($\omega = 0.01$) ensures that the transient operation can be completed within 3~5s for any transient level. The length of prediction and control horizon ($N_p = 70;\ N_c = 70$) is chosen for sufficient prediction steps to prevent the engine parameters exceeding their constraints. Unequal constraints are added to the input and state as well as output parameters, shown in Table 6-6.

$0.25\text{kg/s} \le W_{ff} \le 1.67\,\text{kg/s}$
$-0.8602\text{kg/s} \le \Delta W_{ff} \le 0.9568\text{kg/s}$
$0.55 \le PCN \le 1.15$
$10.334\,PCN - 4.3961 \le PR \le 14.958\,PCN - 4.4721$
$0.95 \cdot Ref \le Y \le 1.03 \cdot Ref$
$SFC \le 1.00\ \text{kg/kNs}$

Table 6-6 Constraints to the engine parameters

The constraint of the control input is to limit the total amount of fuel flow integrated through the simulation. The amount of fuel changed in the combustor at each sampling time is also limited in order to protect the instantaneous change of chamber temperature and limit the mixture of fuel and air. In this example, the maximum instantaneous change of fuel flow (0.9568kg/s) which can be sustainedis86% of the value at design point (1.1102kg/s), and the minimum value (-0.8602kg/s) is the difference between design point and minimum fuel flow limit (0.25kg/s).Shaft over-speed protection limits the PCN so it cannot be lower than the idle power and cannot have more than15% over-speed. Compressor surge and burner blowout are protected by limiting the value of HPC-PR [50]. The surge line is made up of the surge point from the map shown in Figure 6-2. The boundary of HPC-PR (Figure 6-12) can be written as the subject of PCN which is approximated to linear function from the compressor map in Figure 6-2. Above 0.95 of $R^2$of both linear approximations means the linear functions provide a high quality of alignment to the points on the map. The constraint on specific fuel consumption is not included for optimisation on transient time. The unequal equation: (5-13), for the state and output variables of the single spool engine becomes:

$$\begin{bmatrix} 0 & 0 & 0 & 0 \\ 10.334 & 0 & 0 & 0 \\ 0 & 0 & 0 & 0 \\ 0 & 0 & 0 & 0 \end{bmatrix} \begin{bmatrix} PCN \\ PR_{HPC} \\ Y \\ SFC \end{bmatrix} + \begin{bmatrix} 0.55 \\ -4.396 \\ 0.95 \cdot Ref \\ 0 \end{bmatrix} \le \begin{bmatrix} PCN \\ PR_{HPC} \\ Y \\ SFC \end{bmatrix}$$

$$\begin{bmatrix} 0 & 0 & 0 & 0 \\ 14.958 & 0 & 0 & 0 \\ 0 & 0 & 0 & 0 \\ 0 & 0 & 0 & 0 \end{bmatrix} \begin{bmatrix} PCN \\ PR_{HPC} \\ Y \\ SFC \end{bmatrix} + \begin{bmatrix} 1.14 \\ -4.472 \\ 1.03 \cdot Ref \\ 1 \end{bmatrix} \ge \begin{bmatrix} PCN \\ PR_{HPC} \\ Y \\ SFC \end{bmatrix} \quad \textbf{(6-8)}$$

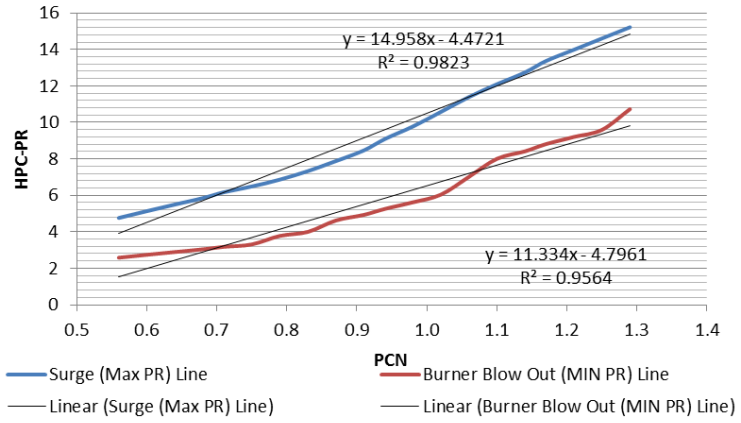

Figure 6-12 Maximum and minimum limit of HPC-PR in function of PCN

Similar transient performance is provided by the control of MPC with control references (PCN, HPC-PR and GTR) and the same weighting factor value (0.01) in Figure 6-13. Compared with the transient line from PID control, the acceleration line by the MPC has been shifted closer to the surge line, which improves the transient time. The HPC-PR had been limited within the surge boundary which is estimated on-line according to the constraint functions in Table 6-6.

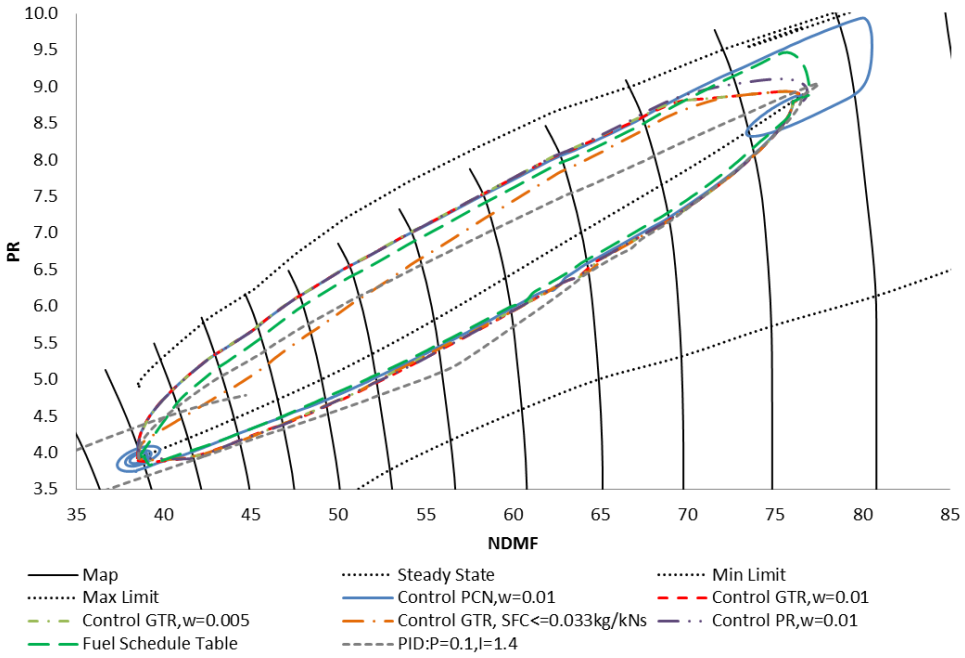

Figure 6-13 Transient performance given by the MPC with different control objectives and control weights

Different natural frequencies of engine parameters provide different transient results. The transient line given by the control reference of PCN has a longer settling time than the results from other control references due to its lower natural frequency. The steady state vibrations demonstrated by the circles around steady state points in Figure 6-13 shows longer lag to input signals. The frequency response for the engine parameters: GTR, HPC-PR, PCN, is shown by the bode plot of Figure 6-14. The higher cut-off frequency allows the engine parameter. For example, GTR (24.6rad/s) is more sensitive to the input signals than the parameter (HPC-PR: 11.0rad/s) on the transient response. As the results of Figure 6-17 and Figure 6-18 show, the transient performance can be more easily controlled within the constraints. The significant lag of PCN to the control signal creates a higher difficulty for the control system settling the transient response (longer settling time) due to the lowest frequency (4.15rad/s). From the plot of PCN, Figure 6-15, the acceleration by control reference of PCN result exceeds the steady state overshoot by 3% and the oscillations decay slowly while the transient line approaches steady state. Because the frequency of HPC-PR is in between the other parameters' frequencies, the percentage of overshoot is also expected to be located between the values of the other two parameters, as shown in Figure 6-15.

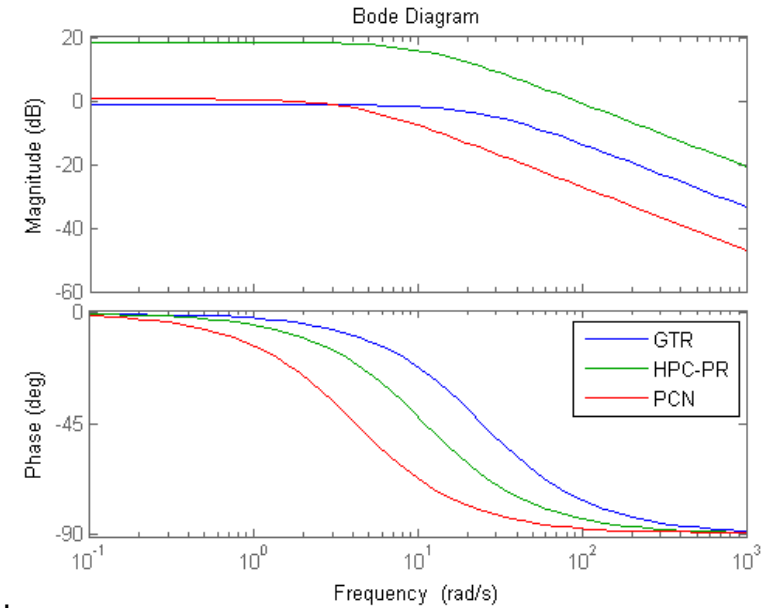

Figure 6-14 Frequency response of engine parameters: GTR, HPC-PR, PCN

A smaller value of weighting factor ($\omega = 0.005$) was also attempted for the control of GTR. The result (Figure 6-15) shows little improvement on the transient time than the original value ($\omega = 0.01$).

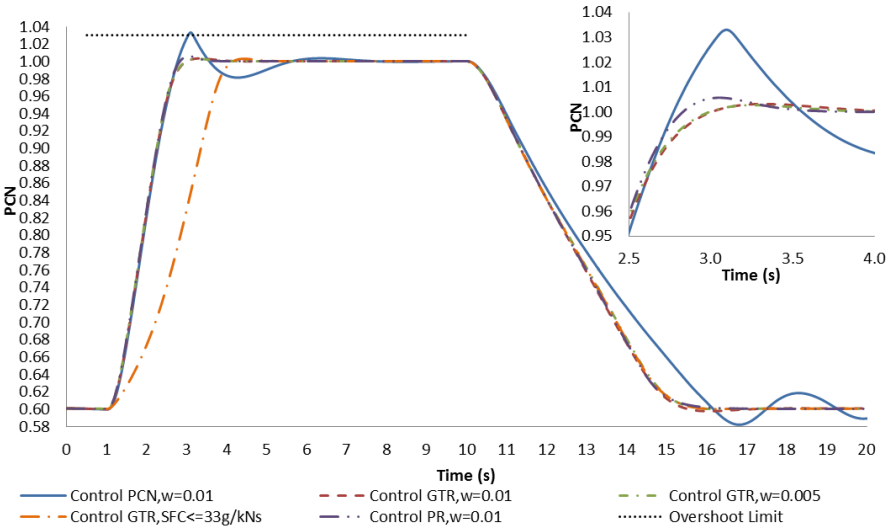

Figure 6-15 Transient result of PCN

The optimal fuel input is adjusted automatically from the control of MPC along the transient simulation. The MPC is capable of adapting to the change of engine performance and constraints and calculates the optimal control solution regardless of the parameter of control references, Figure 6-16. Because of its adaptability, unlike PID control, only one MPC design can satisfy the performance requirements for both acceleration and deceleration.

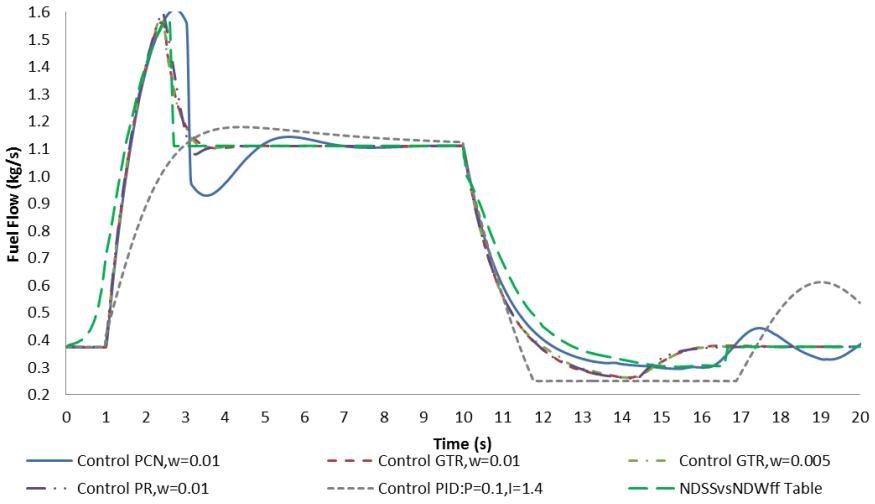

Figure 6-16 Transient fuel flow for single spool turbo-jet

The estimated system output (Y) follows the parameter of the control references. The value of the system output can be successfully kept within the 103% overshoot limit to the control references: PCN (Figure 6-15), HPC-PR (Figure 6-17) and GTR (Figure 6-18). From the results, the overshoot for PCN, HPC-PR and GTR can be all achieved by referring to GTR. Therefore, the transient performance requirements for the most engine parameters with a minimum number of active constraints can be achieved by applying the control to the parameter with the highest cut-off frequency.

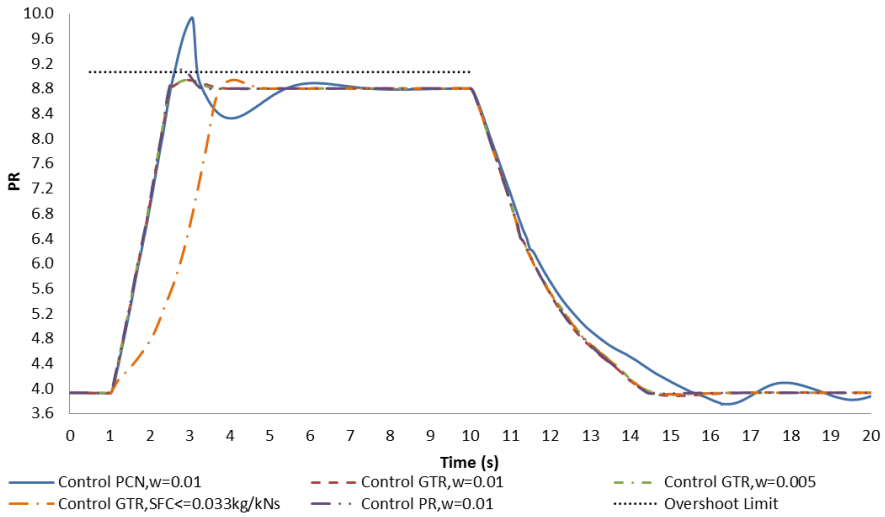

Figure 6-17 The transient results of HPC-PR from different control of MPC

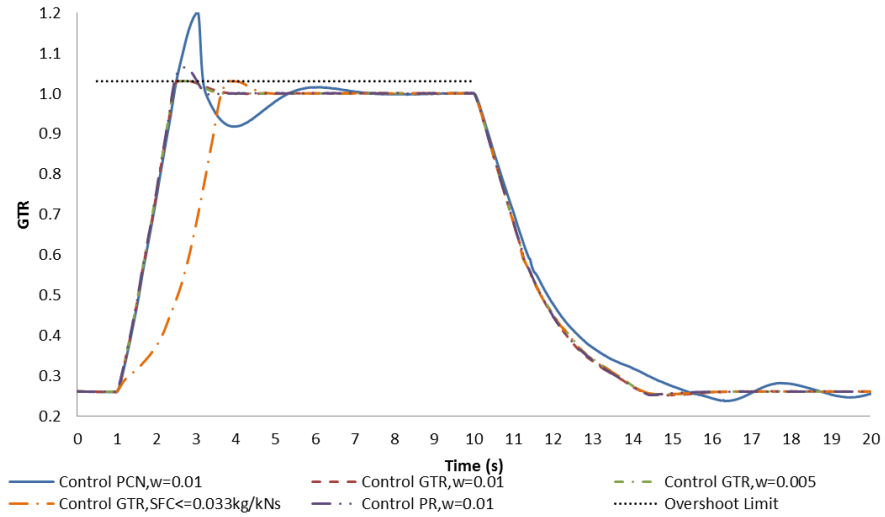

Figure 6-18 The results of engine gross thrust ratio from different control of MPC

In summary, the simulation results demonstrate that the MPC is capable of providing the satisfied transient response as well as maintaining the output within its limit. The performance for the same acceleration and deceleration shows significant improvement by the control of MPC than PID controller. Due to the natural frequencies, the engine response will be dissimilar if different engine parameters are chosen for control reference.

The transient simulation could only be performed by the control of the fuel scheduling method in original Turbomatch 2.0. The transient fuel flow from the control of MPC can be suggestive of the design of transient fuel schedule. Turbomatch 2.0 supports two types of fuel schedule: fuel flow against time and non-dimensional fuel flow (NDW_{ff}) against non-dimensional shaft speed (NDSS) according to (3-14). The result of fuel flow from MPC can be directly summarised to fuel-time schedule and exactly the same simulation result can be obtained. From the fuel schedule referring to the non-dimensional shaft, the engine fuel flow table in the simulation is generated from the non-dimensional parameters related to the HPC inlet pressure, combustor inlet pressure and temperature. The nonlinear dynamic of HPC increases the difficulty in manually producing the optimal fuel schedule. However, the optimal solution can be easily summarised from the transient results given by the control of MPC, and the optimal engine transient fuel flow and performance from the control of non-dimensional fuel schedule are shown by Figure 6-16 and Figure 6-13.

6.1.1.3 Fuel Consumption Optimisation

The constraints to engine parameters can also be designed to reach a particular performance requirement, such as the limit of specific fuel consumption (SFC). The constraint of SFC in Table 6-6 is activated by setting its value to 0.033kg/kNs. The limited SFC value has been reduced to more than half of the difference between the steady state and peak of value during transient operation from Figure 6-19. Figure 6-19 shows that the maximum SFC value has been successfully limited below the threshold. The consequence of limiting SFC is the reduction of fuel rate added to the engine during acceleration, Figure 6-20. This also adds the rise time to the transient

performance of other engine parameters as shown in Figure 6-15, Figure 6-17and Figure 6-18. The reduction of the transient rate can be also observed by the performance where the transient line moves closer to the steady state line on the compressor map, Figure 6-13.

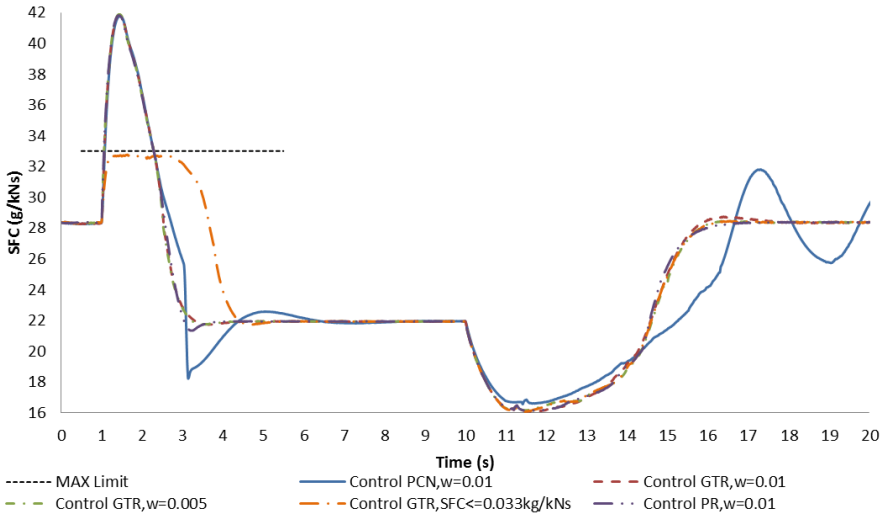

Figure 6-19 Transient specific fuel consumption with control of constrained MPC

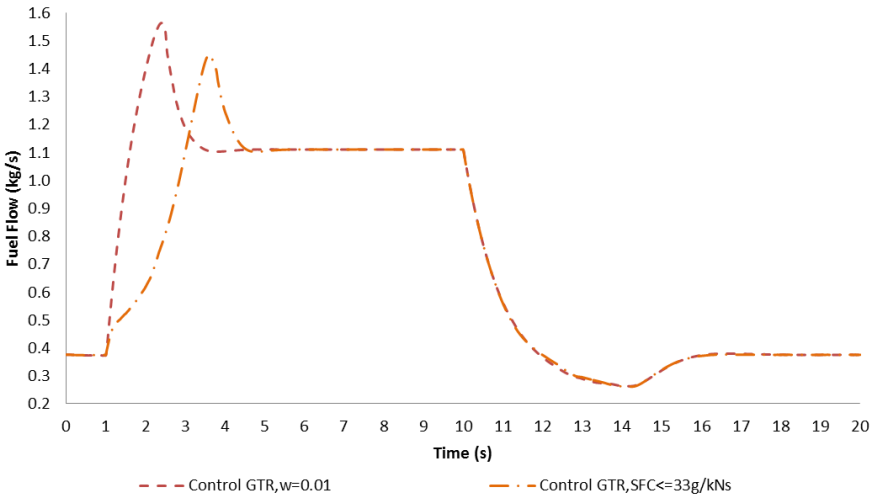

Figure 6-20 The fuel flow with additional SFC constraint

6.1.1.4 Transient Performance at Varying Operating Conditions

Any disturbance on the power output of the engines will affect the flight condition of an aircraft. The transient operation is more likely to execute under a varying environmental condition in the real life. A take-off procedure has been simulated in this example. The simulation of aircraft model and flight physics are

not the scope of this project. The flight of aircraft has been assumed to a centre of mass. The purpose of this simulation is to examine the application of a constrained MPC for the control of the transient performance of a gas turbine engine in varying environmental conditions.

The engine is assumed to accelerate from idle to 100% thrust whilst stationary for the first 5s at standard atmospheric conditions. The aircraft starts the take-off run when the net thrust reaches approximately at 100% of design point thrust. The thrust ratio is commanded to keep at the maximum (100%) output right up to the design point where the shaft speed is at 100%, at standard atmospheric conditions. The inlet Mach number increases linearly until reaching 0.182 which is approximately 120knots or 61.73m/s when the aircraft starts to take-off. A constant Mach number (0.34) is assumed to be kept for horizontal flight vector. The change of atmospheric temperature is calculated according to (3-3). A constant climb angle of attack (20^{o}) is assumed, as shown in Figure 6-21. The horizontal flight speed is varied and is the multiplication between the Mach number and speed of sound (a). The speed of sound varies according to the ambient temperature as the flight altitude (H) increases. The flight altitude is integral to the climb rate($\dot{h}$). The climb rate is calculated at (6-9). The aircraft finally level off at 3000ft (914.4m). The complete taking off, climbing and leveling off process is shown in Figure 6-22.

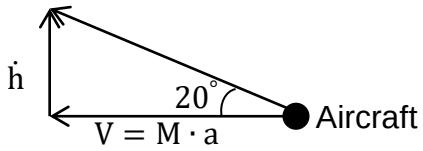

Figure 6-21 Flight vectors

$$\dot{h} = \frac{dh}{dt} = \tan(20) \cdot \left(M \cdot \sqrt{\gamma \cdot R \cdot t_{amb}}\right) \qquad \textbf{(6-9)}$$

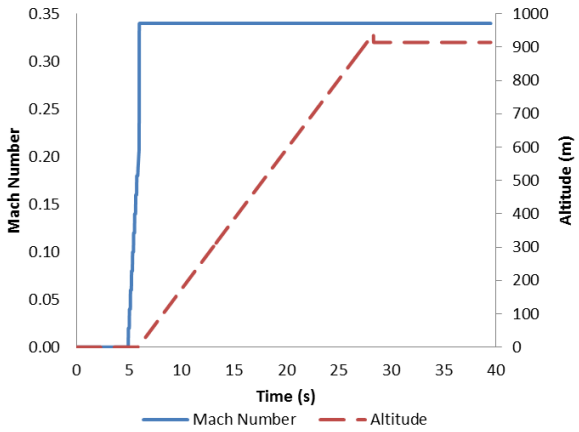

Figure 6-22 The engine input of Mach number and altitude

The control reference is taken to be the thrust ratio which is the ratio of the net thrust to the gross thrust at the design point. Figure 6-23 shows the performance of thrust output from the engine for the entire taking off procedure. A disturbance is created when the aircraft starts to climb, and the thrust quickly returns to the target steady state throughout the remaining operation. From the close up graph, Figure 6-24, violent oscillation about the final steady state point occurs while the aircraft is climbing to the cruising altitude due to the change of engine inlet conditions which further affects the change of engine dynamic. The performance is settling down when the aircraft is leveling off at its cruising altitude after approximately 27s.

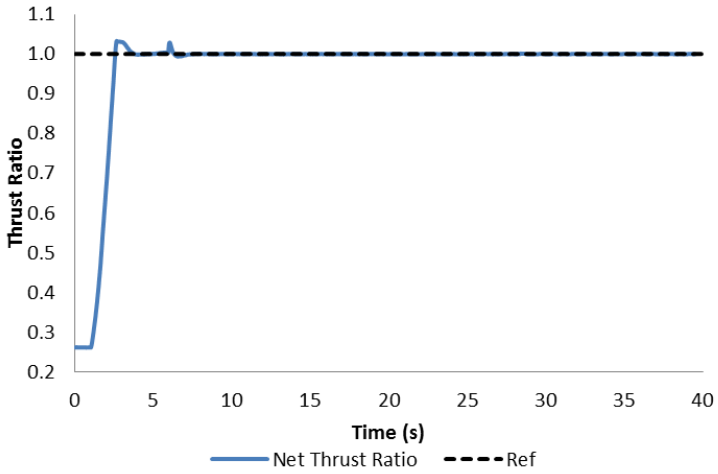

Figure 6-23 The performance of engine thrust output for the taking off process

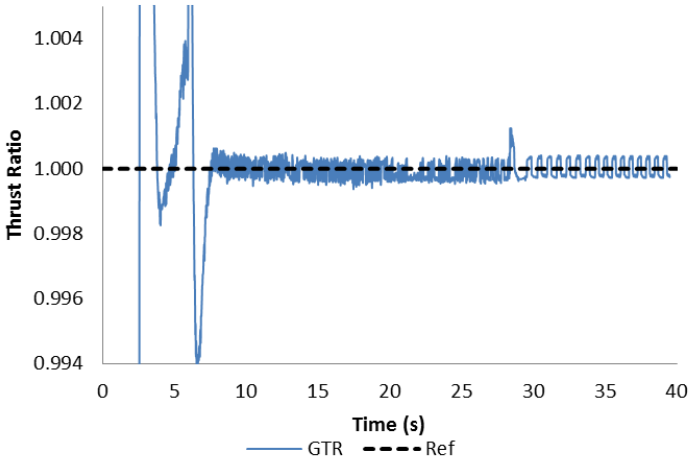

Figure 6-24 Close up from Figure 6-23

The relative shaft speed reaches to its design point before 5s. An instant drop of shaft speed is shown by Figure 6-25 while the altitude is being increased. Due to the lower natural frequency of the shaft as shown in Figure 6-14, a longer recovery time is expected from the thrust ratio as shown in Figure 6-24. A higher value of relative shaft speed is reached due to engine thrust drop caused by the increase of altitude and flight velocity as shown in Figure 6-25 (b). The reduction of air density, temperature and pressure cause shaft over-speed in order to maintain the constant value of thrust delivery.

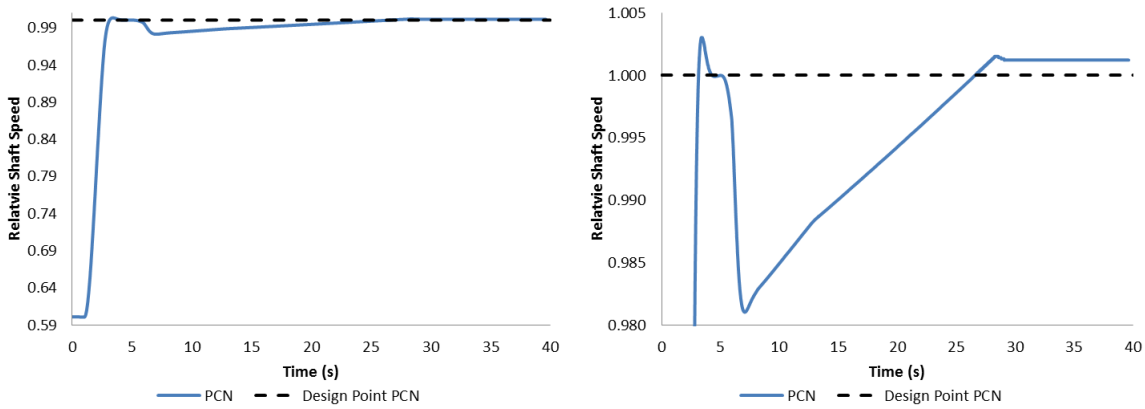

(a) (b)

Figure 6-25 Shaft dynamic for the taking off process (a), the close up plot of shaft dynamic near the final steady state point (b)

In this simulation case, the thrust output of the engine is required to remain the same as the 100% power output at the standard atmospheric condition with 0 intake Mach number. The results have shown that the MPC adjusts the control to maintain the control reference. As the result, the shaft is over-speed in order to encounter the loss of air density, pressure and temperature.

6.1.2 Transient Performance Validation

The transient fuel flow from the control of MPC with the control reference of GTR and without consideration of SFC constraint has been applied to GSP for transient performance validation. Similarly to Turbomatch, GSP also uses constant rotor inertia and volume dynamic to simulate gas turbine transient performance. Due to only accepting the “time vs. fuel flow” schedule, the fuel flow data is selected for the simulation of transient acceleration from idle to maximum (100%) power output. GSP also takes the heat soakage into consideration. A slightly higher over-fuelling to approximately1.8kg/s (by 0.2kg/s) is applied for a closer matching of transient time given in the results from Turbomatch. The transient performance of the compressor is shown in Figure 6-26. GSP does not support customising the compressor, combustor and turbine maps. Only the default component maps can be used for simulation. A different transient performance for the same engine is expected.

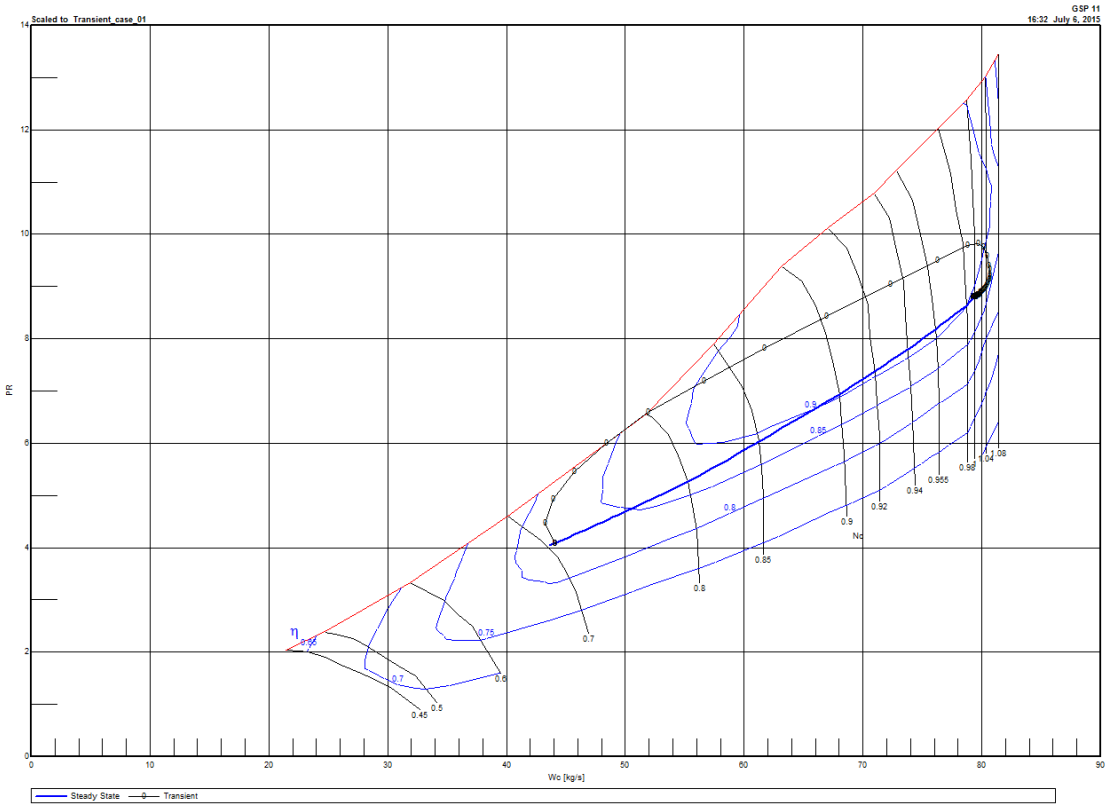

Figure 6-26 Transient performance of compressor from estimation of GSP

The performance of the engine acceleration is shown by Appendix C. Appendix C shows the results of fuel flow, proportional shaft speed, compressor pressure ratio and SFC. The same fuel schedule provides a transient response from 70% to 100% PCN on GSP, instead of 60% PCN on Turbomatch. The amount of PCN and compressor PR overshoot is also higher than the results from Turbomatch by 4~5% of PCN from Figure 6-15 and 0.8 of HPC-PR according to Figure 6-17.Due to different turbomachinery components' characteristics, the SFC is also much lower than the estimation from those results given by Turbomatch in Figure 6-19, where the corresponding SFC is 25g/kN·s at 70% PCN. However, the results of SFC at design point or 100% (22g/kN·s) and at the peak value during transient acceleration (39g/kN·s) are almost the same as the results from Turbomatch. Therefore, the differences on the transient performance are mainly caused by the components' maps. The agreement on the simulation results can be improved if exactly the same maps can be applied to both simulation platforms.

6.2 Application to Twin-spool Turbofan Engine

The twin-spool turbofan engine adds additional low-pressure components to the original single spool engine, which results in increased complexity of the configurations. The complexity has been increased in the dynamic of most engine parameters where the order of the transfer functions has been increased from 1st order to 2nd order or higher, and the transient performance for high-pressure components: HPC and HPT, becomes more difficult to predict due to the nonlinear behaviour low-pressure components.

In this design case, a detailed investigation of the design of a new engine control system has been carried out. The selection of online identification algorithms and the method of choosing the values of tuning factor in identification algorithms in order to produce accurate and reliable dynamic model, are being discussed. In addition to model identification, the design of MPC and engine constraints, to achieve optimum transient performance, has been investigated on the multi-spool turbofan engine.

The engine modeling was based on the ICV method and the design point shown in Table 6-7. The schematic of the twin-spool engine is shown in Figure 6-27.

Ambient condition	ISA SLS	[-]
Intake Mach number	0	[-]
Intake mass flow	44.8	kg/s
Low-pressure compressor pressure ratio	1.70	[-]
Low-pressure compressor isentropic efficiency	88	%
High-pressure compressor pressure ratio	5.60	[-]
High-pressure compressor isentropic efficiency	88	%
Bypass ratio	0.69	[-]
Fuel flow	0.2466	kg/s
High-pressure turbine isentropic efficiency	89	%
Low-pressure turbine isentropic efficiency	89	%
Moment of inertia for low-pressure shaft	10	Nm2
Moment of inertia for high-pressure shaft	8.4	Nm2
Percentage of low-pressure shaft corrected rotational speed at 170 RPS	100	%
Percentage of high-pressure shaft corrected rotational speed at 177 RPS	100	%
Volume 1	1.50	m3
Volume 2	0.50	m3
Volume 3	0.38	m3
Volume 4	0.50	m3

Table 6-7 Design point of the twin-spool turbofan engine

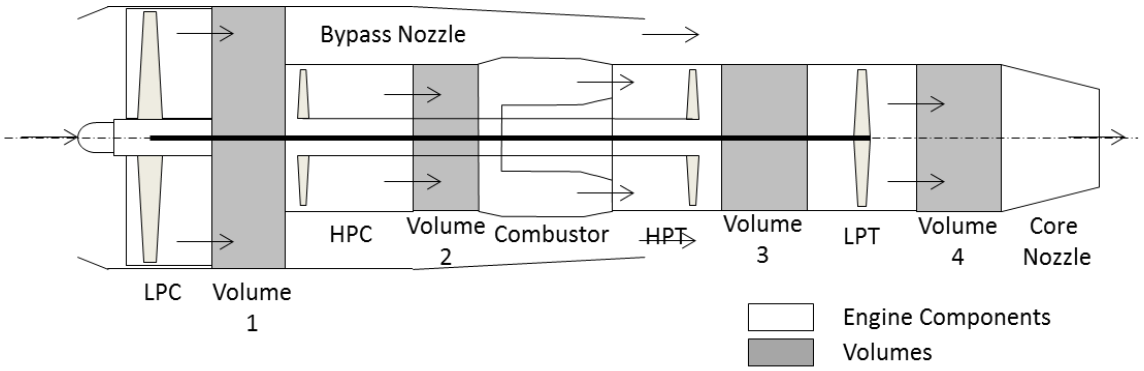

Figure 6-27 The sketch of the twin-spool turbofan engine

In Figure 6-27, no volume is added downstream of the combustor because of the assumption of a constant pressure drop and no flow change in the chamber. The settings of the transient simulation are shown in Table 6-8.

Percentage of corrected rotational speed at low-pressure shaft to 170 RPS	60~100	%
Percentage of corrected rotational speed at high-pressure shaft to 177 RPS	78.6~100	%
Low-pressure compressor pressure ratio	1.21~1.70	[-]
High-pressure compressor pressure ratio	3.41~5.31	[-]
Fuel flow	0.07~0.24	kg/s
Volume 1	1.50	m^3
Volume 2	0.50	m^3
Volume 3	0.38	m^3
Volume 4	0.50	m^3

Table 6-8 The settings for transient simulation

6.2.1 Online Dynamic Identification for 2-Spool Turbofan Engine

The nonlinear engine performance is created by the non-linear characteristics of the components: compressor, turbine and combustor, and variable gas properties. The nonlinearity can be observed from the frequency distribution throughout its operating range in Figure 6-28. The natural frequency of compressor pressure ratio changes because of increments of shaft speed at different shaft inertias. The natural frequency of LPC-PR increases while the change of shaft speed increases at constant shaft inertia. The opposite occurs for HPC-PR, where the peak value occurs at the smallest change of shaft speed at lowest inertia. The natural frequency for pressure ratio of both compressors decreases while shaft inertia increases with a constant increment of shaft speed.

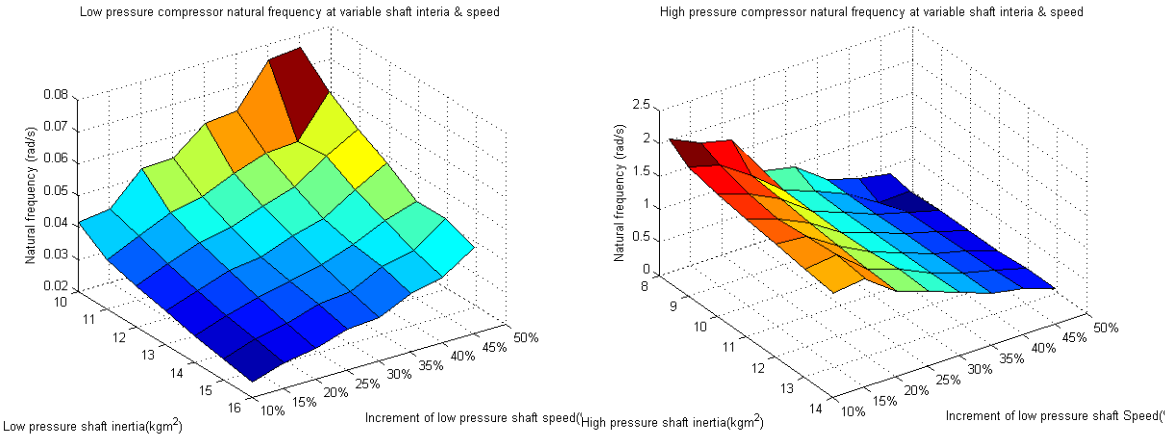

Figure 6-28 The frequency of LPC-PR (left) and HPC-PR (right) for different level of power transition and shaft inertias

The recursive identification algorithms: RLS, RLS-DF, RLS-SI and RLS-SV, applied to the engine system should be able to adapt the nonlinear performance of the engine model. A closed-loop engine system was simulated with a linear PID control, and the identification process is installed in parallel with the engine without the interference of the engine system, Figure 6-29. The algorithms estimate and update the open-loop model of the gas turbine engine from the reading at each sampling time. The estimated results from the identified model are produced by the state space (SS) model, Figure 6-30. The tracking accuracy and stability of the estimated model are being compared to the results from the engine and between each identification process.

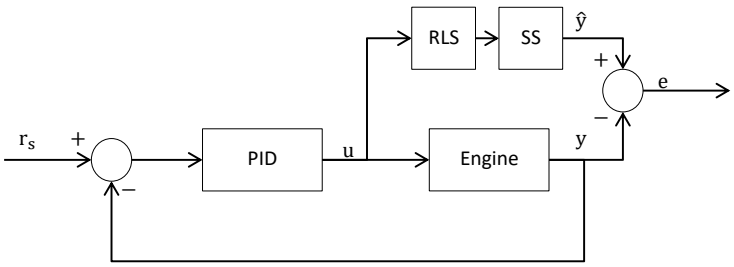

Figure 6-29 Open loop identification of RLS algorithm to the engine system

The state space model, Figure 6-30, is a linear model. The non-linearity is obtained by consistently superposing the values in matrix A and B at each time step. The performance of the algorithms: RLS, RLS-DF, RLS-SI and RLS-

SV, are compared through the errors between the outputs from their SS models and the engine outputs, shown in Figure 6-29.

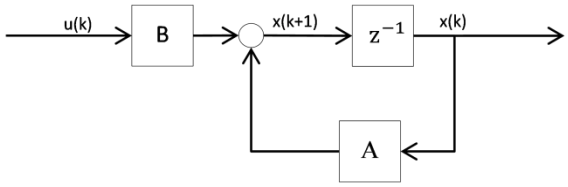

Figure 6-30 Discrete state-space model

The proportional gain is 0.4, the integral gain is 0.2 and derivative gain is 0.0. The value of control input (W_{ff}) is determined from the difference between the control reference (demand PCN) and the low-pressure shaft speed by the PID controller. Five identical consecutive transient cycles between idle (60%) and 100% low-pressure PCN have been simulated in order to evaluate the reliability of the identification processes. For a reliable process, the estimated dynamic of the system (poles and zeros) should be identical for each transient cycle with repetitive values of poles and zeros.

The identified engine variables are the pressure ratios of compressors (LPC-PR, HPC-PR). Due to the fact that a 2-spool engine was simulated, the dynamic of most parameters in the compressor is correlated to the same parameter of its up- and downstream compressors. Therefore, the pressure ratio from both compressors must be included in the discrete state space equation.

$$\begin{bmatrix} PR_{LPC}(k+1) \\ PR_{HPC}(k+1) \end{bmatrix} = A \begin{bmatrix} PR_{LPC}(k) \\ PR_{HPC}(k) \end{bmatrix} + BW_{ff}(k) \qquad \textbf{(6-10)}$$

where the dimensions of matrix A and B depends on the size of state and input variables. According to (6-10), A is a 2×2 square matrix. The control input is only the fuel flow so that B is a 2 by 1 matrix. Therefore, the values in matrix A and B are the objective for the identification processes.

The collecting factors from RLS-SV and RLS-SI are set to: $\rho = 0.99$ and $\mu = 0.96$; the forgetting factor for RLS-DF is chosen as $r = 0.80$. Because of unknown initial values of elements in the covariance matrix from (4-24), an identity matrix was assumed. The dimension of the identity matrix is 3×3, which contains two engine states (compressors' pressure ratio) and one input (fuel flow).

The comparison among the identification algorithms on the estimation of compressor pressure ratio (PR) from the engine model is shown by Figure 6-31 and Figure 6-32. The figures show that all modified RLS methods are capable of providing an accurate approximation to the running line given by the ICV engine model through the entire 225s with a 0.004s sampling time.

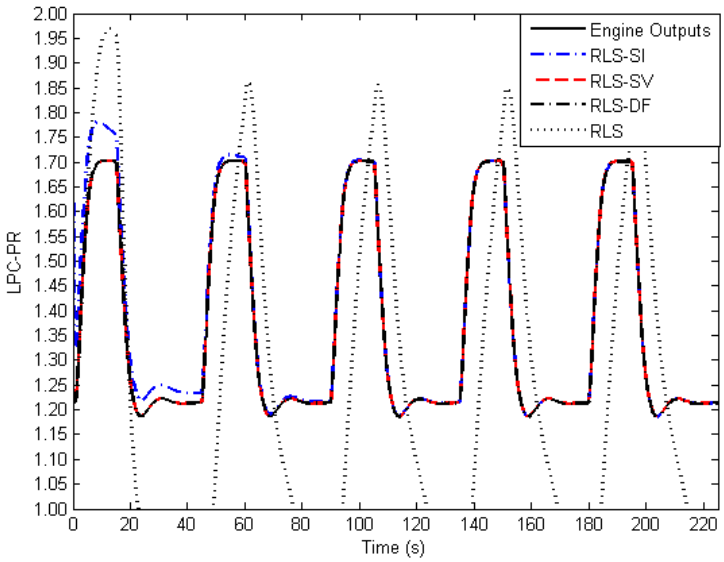

Figure 6-31 The comparison of tracking performance on the dynamic of pressure ratio for low-pressure compressor

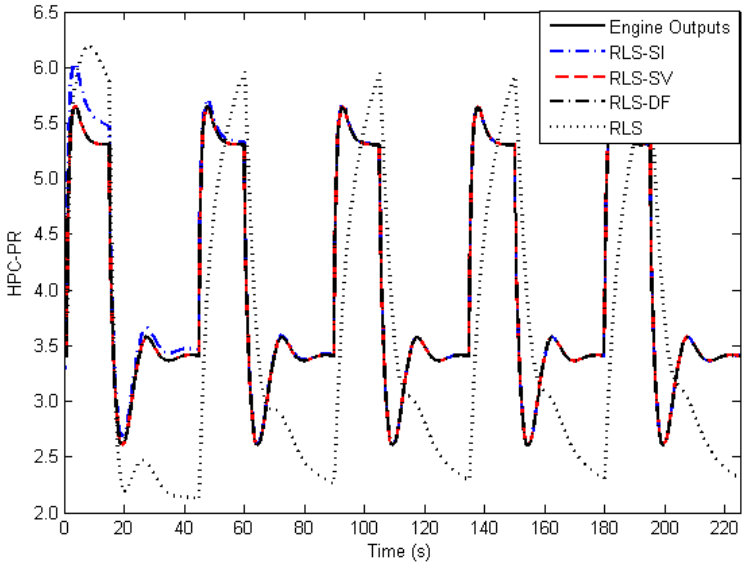

Figure 6-32 The comparison of tracking performance on the dynamic of pressure ratio for high-pressure compressor

The influence of nonlinearity was investigated by examining the Fast Fourier Transform (FFT) to the PR, Figure 6-33, from the results of Figure 6-31 and Figure 6-32. Only one frequency (below 0.04Hz) has the dominant coherence in the outputs of LPC-PR and HPC-PR. The presence of non-linear effects is indicated by the peaks at other frequencies given by additional periodic components. The spectrum shows that more harmonics existed in HPC-PR signals than in LPC-PR. The nonlinearity increases the difficulty of generating an averaged dynamic model for the entire operating range of all RLS algorithms. The conventional RLS method shows the significant error to the engine output which is the largest deviation among all the modified RLS algorithms. Although the result of the conventional RLS is being improved over transient cycles, the slow convergence speed is unacceptable for the application of system identification on gas turbine engines. Therefore, it is important to introduce the adaptive features to the algorithm, such as including the tuning terms in RLS-SV and RLS-SI or the forgetting factor in RLS-DF.

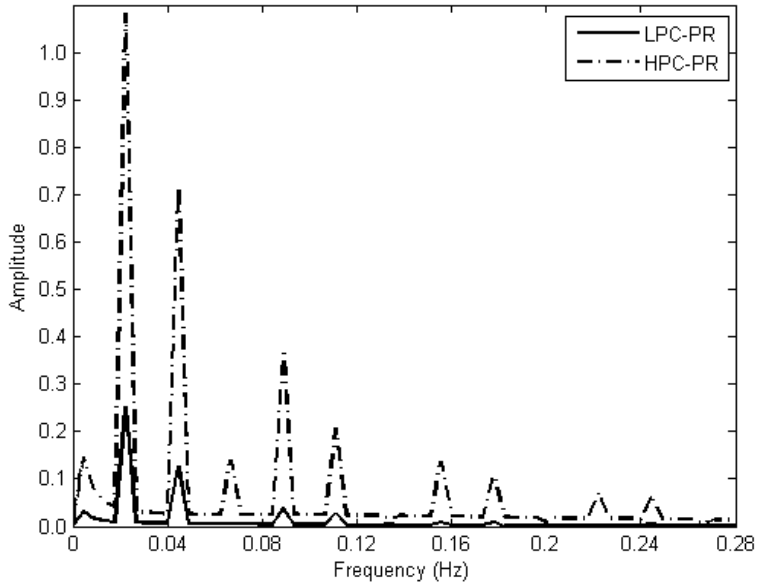

Figure 6-33 Single-sided spectral amplitude of LPC-PR and HPC-PR

The close up of figures, Figure 6-34, shows clearer comparisons of the tracking performances among the modified RLS algorithms. Due to the adjustable term in (4-24) controlled by the engine parameters, the RLS-SV shows the closest estimation to the engine outputs. By selecting a suitable value of the forgetting factor, the RLS-DF is capable of providing an accurate estimation. Like the selection of the forgetting factor in RLS-DF, the performance of RLS-SI is controlled by the value of 'g' and 'μ'. In this case, RLS-SI shows a slight overestimation to the engine outputs.

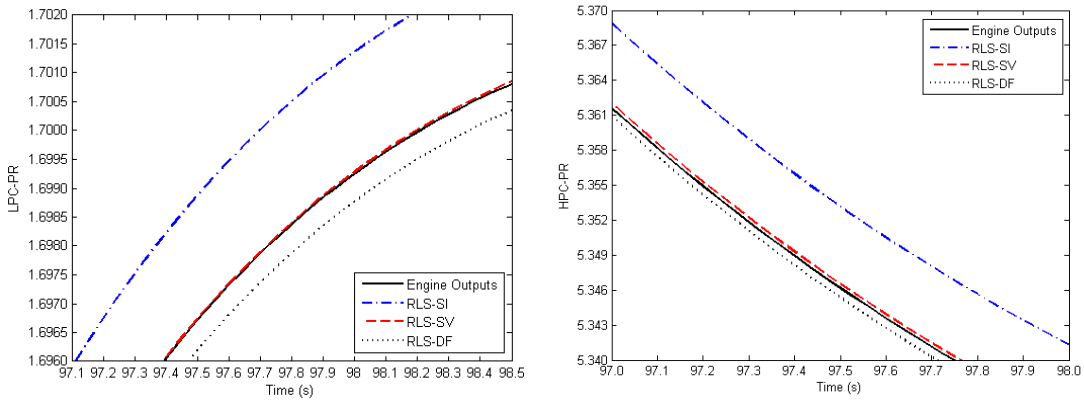

Figure 6-34 Close ups of Figure 6-31 and Figure 6-32; Left: close up of LPC-PR, Right: close up of HPC-PR

The errors from the estimations to the engine outputs shown by Figure 6-35 and Figure 6-36 provide a clearer presentation of the tracking performance over the repetitive transient cycles. All modified RLS methods drop their tracking accuracy while the engine is operating at transient states. This reduction in accuracy is caused by the greater gradient change on the transient line during acceleration and deceleration than operating near steady states. Overall, the tracking performance can be optimised to reduce the error within $\pm 1\%$for LPC-PR and $\pm 2\%$for HPC-PR by implementing the modified methods. The negative percentage error which appears during engine acceleration means an underestimation and an opposite trend appears while the engine's power is being reduced. This phenomenon means that the estimated model contains a lag to the actual engine response. The lag is caused by the estimations algorithms recursively requiring the data from previous time steps. The largest value on the errors always appears at the beginning of the transient stage where the gradient of the operating line is steepest.

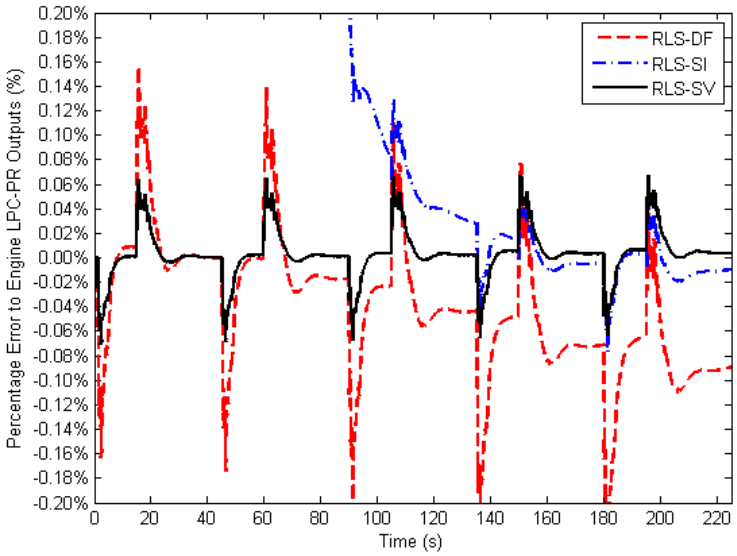

Figure 6-35 The percentage error of the estimations from RLS algorithms to the engine LPC-PR

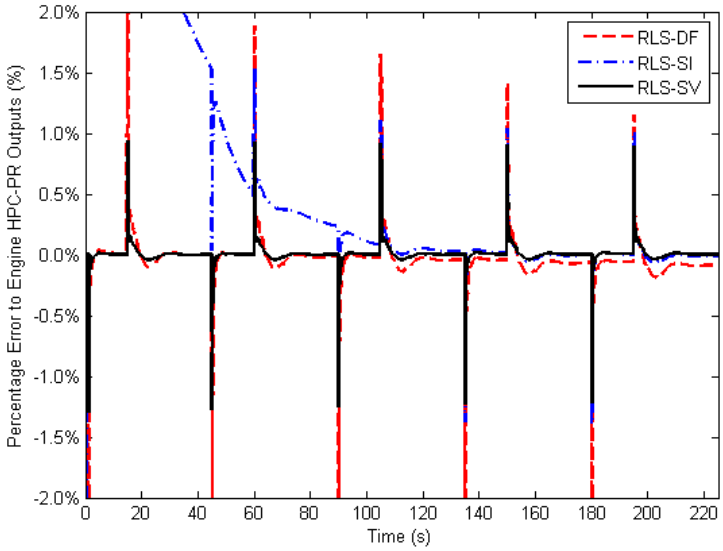

Figure 6-36 The percentage error of the estimations from RLS algorithms to the engine HPC-PR

The fixed values of collecting factors (μ and g) in RLS-SI control the convergent speed of the estimated model of the engine system. The error of estimation of the LPC-PR is gradually decreased from 10% to below 0.1% in approximately 150s in Figure 6-35 and the same amount of error is also reduced in 100s for HPC-PR in Figure 6-36. A smaller value of μ can reduce the recursive power to the normalised covariance matrix ($\hat{P}$) in (4-24); it also reduces the power of the correcting term in (4-24). Therefore, the mean error through (6-11) has been calculated to measure the accuracy of RLS-SI with different combinations of the values of collecting factors. Figure 6-37 shows the distribution mean error on the estimation of compressor performance by different combinations of collecting factors. In this case, the best performance can be obtained by choosing the values close to 1 in order to maintain a sufficient recursive capability as well as containing a forgetting capability.

$$\bar{e} = \frac{\left(\sum_{k=0}^{k=225} \frac{\hat{y}(k) - y(k)}{y(k)} \right)}{k} \times 100\% \qquad \textbf{(6-11)}$$

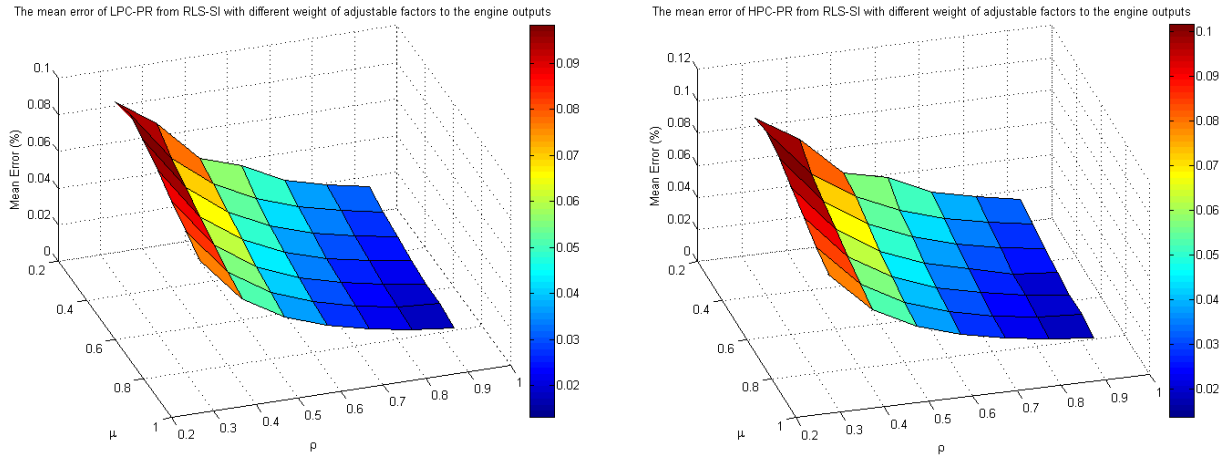

Figure 6-37 The mean error to the estimation of LPC-PR (left) and HPC-PR (right) by RLS-SI with different weight of adjustable factors

Unlike RLS-SI, the adjustable term in (4-24) from RLS-SV is controlled by the engine data (φ). The change in the covariance matrix is adaptive to the engine states and input so that RLS-SV can change its tracking speed according to the gradient of the operating line. Because RLS-SV and RLS-SI share the same estimating procedures, reducing the value of the collecting factors also reduces the tracking capability for both compressors' pressure ratio as shown in Figure 6-38andFigure 6-39. The largest error can reach up to $\pm 2\%$ for LPC-PR and $\pm 3\%$ for HPC-PR to the ICV engine output when the minimum value of collecting factors ($\mu = 0.1; \rho = 0.9$) is selected. The reason is that the adaptive capability has been reduced due to the significant reduction of recursive power on the covariance matrix.

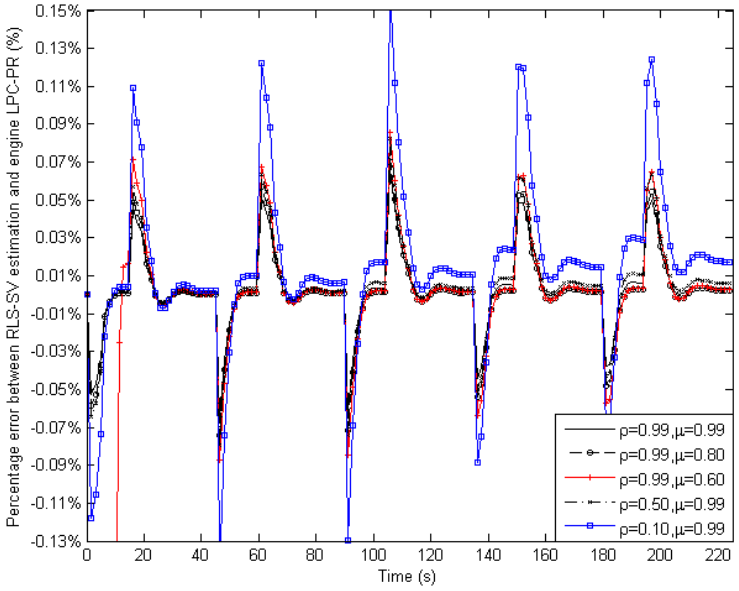

Figure 6-38 The percentage error of estimation from different collecting factors of RLS-SV to engine LPR-PR

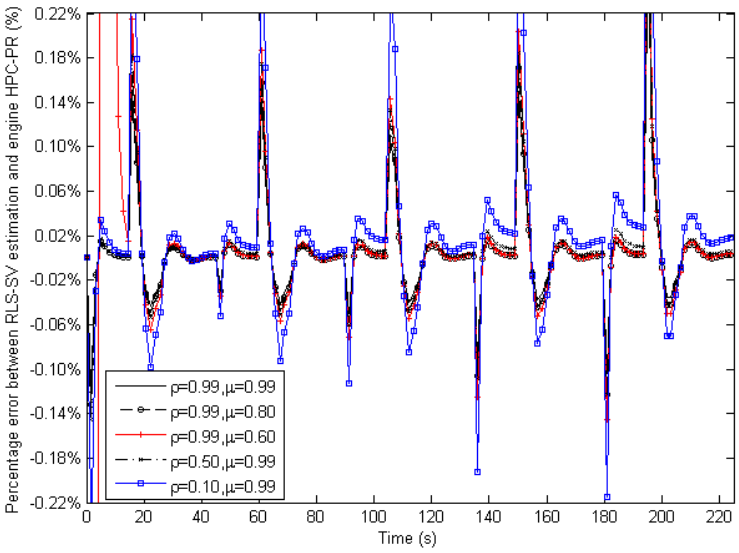

Figure 6-39 The percentage error of estimation from different collecting factors of RLS-SV to engine HPR-PR

Due to the time-variant characteristic of the engine system, the estimated system's dynamic and stability can be observed from the change of the roots from transfer functions (eigenvalues of the state space model) on the s-plane. The state space (SS) system was substituted by the open-loop identified model in Figure 6-30. The linear discrete model at each sampling time

only represents the dynamic of these selected engine parameters over a short period of time.

The SS system from (6-10) can be written into a 2^{nd} order function with 2 poles and 1 zero. Figure 6-40and Figure 6-41 show the variance of 2 poles for SS model through the simulation. A linear system has a constant value of poles and zeros. However, Figure 6-31 and Figure 6-32 show that the gas turbine engine is a non-linear system due to its different dynamics between acceleration and deceleration. The varying location of the poles and zeros from the SS model is also due to the restricted knowledge of the engine future performance. Therefore, it is important to check the stability and reliability of the estimation through the location of zeros and poles along the simulation.

For a reliable estimation, the poles and zeros should be repeated for each identical transient cycle. In Figure 6-40, the repetitive values to one of the poles are shown by all RLS methods. However, RLS-DF shows a divergence on the estimation of the other pole in Figure 6-41.

For any asymptotic stable discrete system, the real part of poles and zeros are located inside the unit circle. Therefore, the value of zeros and poles must be less than 1. If the location of poles or zeros are on the line of unit circle, the system is marginally stable. For any pole or zero outside the unit circle, the system is unstable. Figure 6-41 shows that one of the two poles can exit the unit circle when the engine is operating in its transient state. For any new input of fuel flow, the engine performance will deviate from its original steady state, and through an unsteady state region, until eventually the work between compressor and turbine is rebalanced and enters into a new steady state level. Because of unknowns about the engine's overall response, its dynamic can only be predicted based on its previous outputs. When the operating line approaches steady state as shown in Figure 6-31, the value of this pole returns to the unit circle (<1) in Figure 6-40.

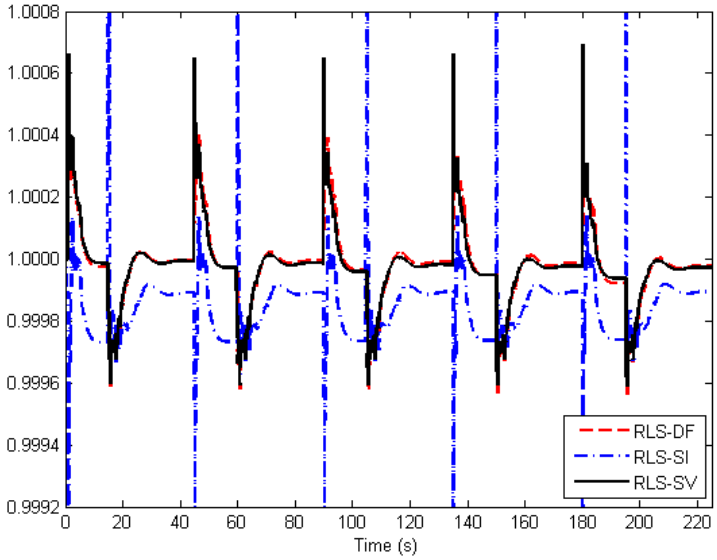

Figure 6-40 1st pole of the discrete state space model from RLS algorithms

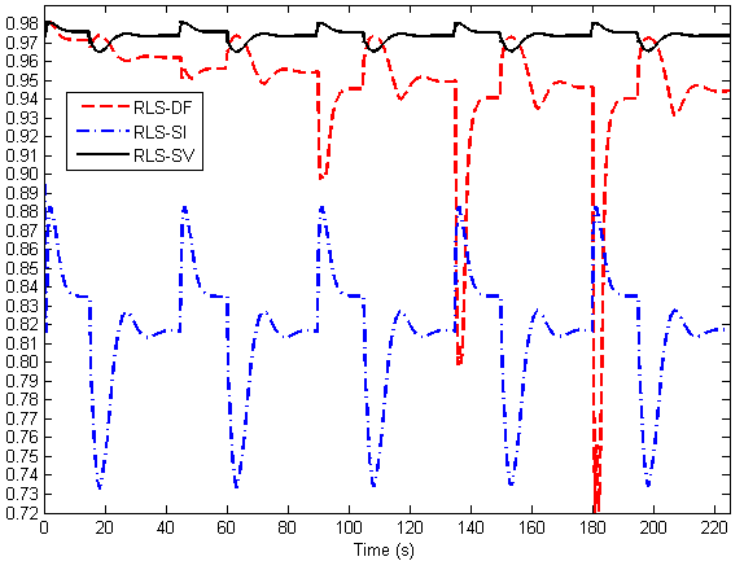

Figure 6-41 2nd pole of the discrete state space model from RLS algorithms

Figure 6-42 shows the values of zero for the 1st state space function which is from the SS model of LPC-PR, and Figure 6-43 shows the zero value from the 2nd state function for HPC-PR according to (6-10). Zeros from the transfer functions of both compressors are located further away from the marginally stable circle than the poles. Zeros have a strong attraction to poles. This means that although the engine may perform unsteadily, its performance can always be directed to a stable zone of operation.

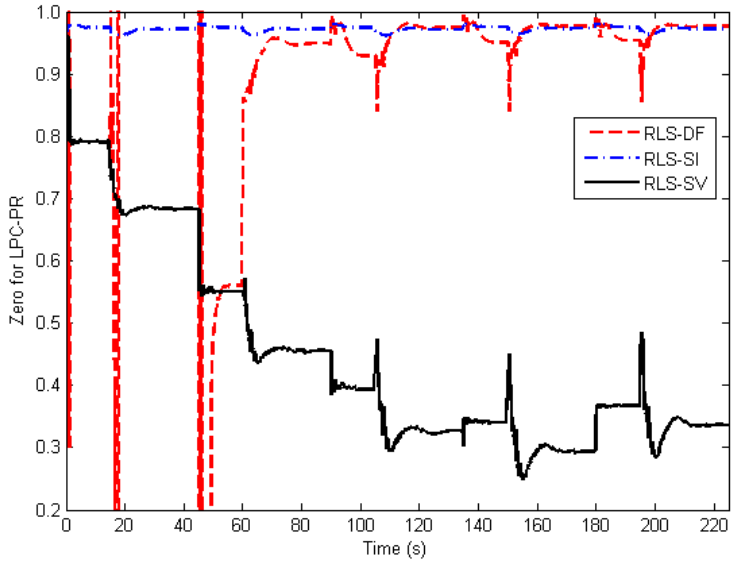

Figure 6-42 Zero for state space equation of LPC-PR given by different RLS algorithms

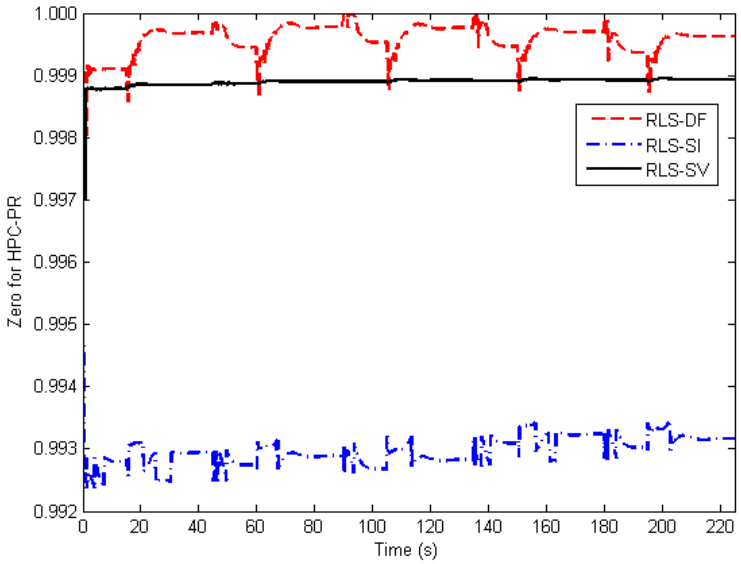

Figure 6-43 Zero for state space equation of HPC-PR given by different RLS algorithms

The stabilized RLS algorithms show effective constraints to the growth of poles and zeros along the transient cycles, from Figure 6-40 to Figure 6-43. The forgetting factor allows the RLS-DF to have a fast convergent speed by considering only the recent data. However, it compromises its stability; the number of oscillations with a large amplitude at the transient region is more likely to occur (Figure 6-42) if the initial covariance is not accurately estimated

or the transient line has a large gradient. The instantaneous value of the zero can be as high as above 40 or as low as below -100 by RLS-DF estimation. The estimating performance can be improved by reducing the sampling frequency so that the more excited engine outputs can be imported to the estimation between the two consecutive sampled points. However, a lower sampling rate can break the continuity to the estimation of the working stream in (3-33) and (3-34), especially for the multi-spool engines, because the thermodynamic parameters are calculated through an iterative process in the components of the ICV model. Therefore, a compromised choice to select an appropriate sampling time should be made to achieve a balance between simulation capability by ICV and the stability of the RLS algorithm.

Decreasing values of the collecting factors of RLS-SV reduces tracking speed as well as stability to the estimated model. The consequence affecting stability is shown by the divergence on the value of zeros shown by Figure 6-44 for LPC-PR and Figure 6-45 for HPC-PR. The figures show that the larger value of ρ (closer to 1) improves the converging speed to a stabilised value of zero and poles. Reducing the value of μ from 0.99 to 0.10 affects both the covariance matrix and the adjustable term in (4-24) so that poles and zeros diverge faster as the value of μ becomes smaller, as shown in Figure 6-44and Figure 6-45. Decreasing the value of ρ is not as much effective as decreasing μ because ρ only controls stabilising power and the value given by an adjustable term is usually much smaller than the adaptive term ($\widehat{\mathrm{P}}$) from (4-24). Therefore, in RLS-SV, μ controls power in order to minimise the error between the estimation and engine outputs, whilst ρ tunes the eigenvalues to the direction of engine state vectors within an acceptable range.

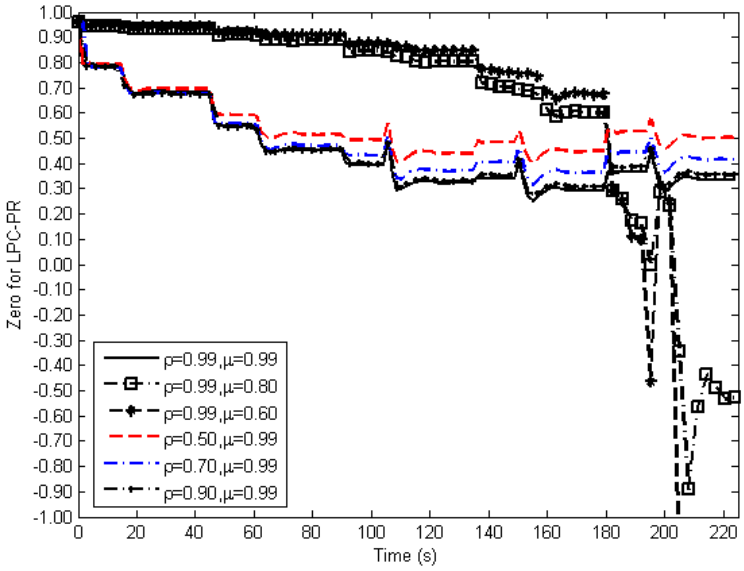

Figure 6-44 Zero for state space equation of LPC-PR given by RLS-SV with different values of weight factors

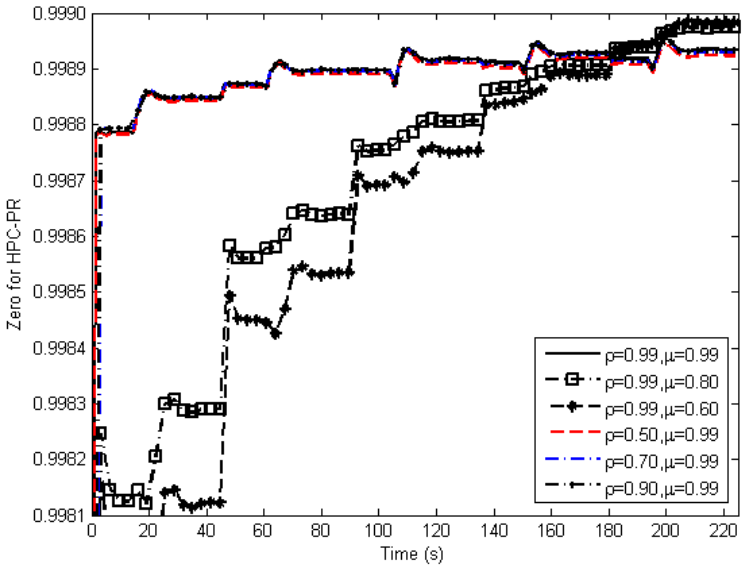

Figure 6-45 Zero for state space equation of HPC-PR given by RLS-SV with different values of weight factors

Overall, the factor (μ) in both RLS-SI and RLS-SV performs as the forgetting factor in RLS-DF, which allows the estimation to be more adaptive to the engine's performance, especially during the transient operations. On the other hand, the adjustable term constrains the change on the covariance matrix, which can be either defined by linear factors in RLS-SI or controlled by the engine data in RLS-SV. This stabilises variation to poles and zeros from the

estimated model, which makes the dynamic of the estimated model more predictable. Furthermore, to identify engine parameters, the value of the forgetting factor should not be too small so that the change in dynamic in the estimation can be compensated by the adjustable term in (4-24).

6.2.2 Identification of Combustor Outlet Temperature

The turbine entry temperature (TET) is a common engine parameter required to be limited during transient operations. Without the turbine cooling, the combustor outlet temperature (COT) will be same as the TET, whereas the identification process of COT will be the same as TET with or without the turbine cooling. The constraints to COT or TET have not been included in the optimisation control of MPC in this project. It is because the dynamic model of COT cannot be directly identified as the method, such as (6-12), of estimating the dynamic of engine parameters, such as: compressor pressure ratio and relative shaft speed as the function: (6-15).

$$T_{COT}(k+1) = A \cdot T_{COT}(k) + B \cdot W_{ff}(k) \qquad \textbf{(6-12)}$$

According to (3-11), the discrete model of COT can be expressed as a parameter varying function:

$$T_{COT}(k+1) = A \cdot T_{COT}(k) + B_1(H_{in}) \cdot \frac{W_{air}}{W_{air} + W_{fuel}}(k) + B_2(\eta_{cc}, C_p) \cdot \frac{W_{fuel}}{W_{air} + W_{fuel}}(k) \qquad \textbf{(6-13)}$$

(6-12) is insufficient to describe the dynamic of combustor gas temperature. The dynamic of the COT is relative to air to gas and fuel to gas ratios, (6-13). The RLS-SV method has been applied to identify both (6-12) and (6-13) and the comparison of results of the engine outputs is shown in Figure 6-46.

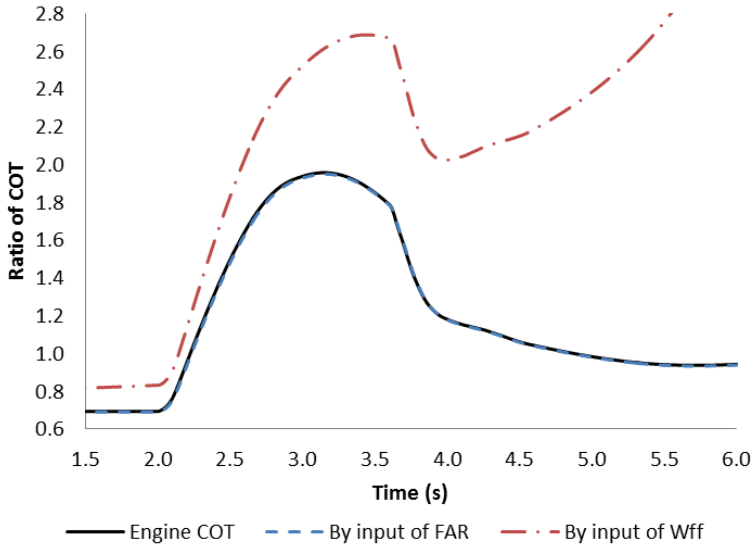

Figure 6-46 Comparison of Identification of COT results from the discrete model with input of fuel flow and the model involved with input fuel, air to gas ratios

The MPC is designed for SISO system in this project. The dynamic model of COT does not share the same input variables as the dynamic models of the other parameters. Including the constraint of COT requires estimating penalised values of multi-input variables from (5-15). The design of a MIMO control system will be carried out for future research. Although (3-11) suggests the dynamic of COT can be estimated accurately by containing air-flow ratio and fuel-flow ratio in (6-13), the fuel-air ratio can be implemented to replace both variables: air-flow ratio and the fuel-flow ratio (FAR) because FAR contains both terms of fuel flow and air flow. The benefit of using FAR is to allow reducing one term in (6-13). If the prediction length is 70 steps in MPC, one term reduction in the dynamic model can save 70 calculations for dynamic prediction. Therefore, choosing least number of necessary parameters to monitor could save process memory and increase processing speed to produce control values. The discrete function which replaces (6-13) is shown in (6-14).

$$T_{COT}(k+1) = A_1 \cdot T_{COT}(k) + A_2 \cdot FAR(k) + B \cdot W_{fuel}(k) \qquad \textbf{(6-14)}$$

The transient performance estimation of COT from both (6-13) and (6-14) are almost identical according to the results illustrated in Figure 6-47. The comparison of percentage error from the estimation results given by (6-13)

and (6-14) as shown in Figure 6-48 shows slight reduction accuracy on the estimations when FAR has been used. However, the reduction is negligible. Therefore compromising estimation accuracy is acceptable in order to save computation memory when identifying dynamic of engine variables, such as COT.

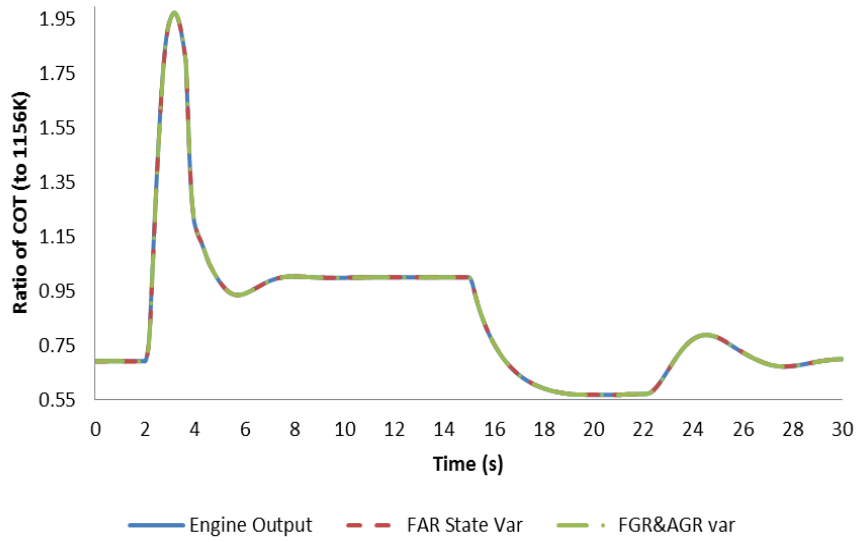

Figure 6-47 Comparison of transient estimations from (6-13) and (6-14)

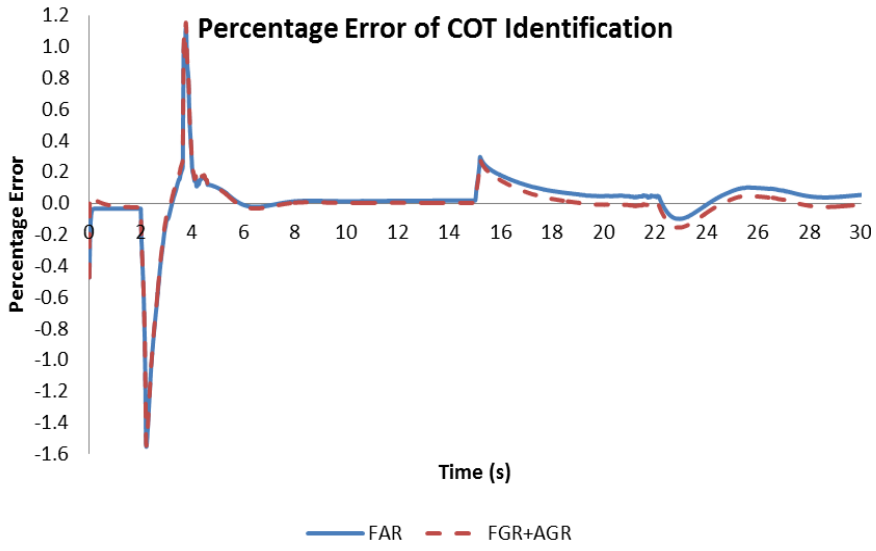

Figure 6-48 Percentage error of COT identification from (6-13) and (6-14) to the value of real engine COT output

6.2.3 Transient Response Optimisation

The engine system is assumed to behave linearly within a short period of time and when a small sampling time (0.001s) is taken. Most dynamic functions about the parameters of twin-spool engines, ie: relative shaft speed and compressor pressure ratio can be estimated as 2nd order function due to a serial association between high and low-pressure components. Due to the fact that the high-pressure components are more likely to exceed the operational boundaries, the over speed and surge protections are only included on high-pressure shaft (CN_H) and compressor (PR_H) for the safety of operation. Total gross thrust, which is the sum of bypass (GT_{bypass}) and core gross (GT_{core}) thrust, is the output variable. An additional variable: specific fuel consumption (SFC) can be included for improvement of engine performance on fuel economy. The engine control parameter is fuel flow (W_{ff}). As a result, the state space system from (5-2) becomes (6-15), which has a total of seven state variables, one control variable and one output variable.

$$\begin{bmatrix} CN_L \\ CN_H \\ PR_L \\ PR_H \\ GT_{Bypass} \\ GT_{Core} \\ SFC \end{bmatrix}_{k+1} = \begin{bmatrix} a_{11} & a_{12} & 0 & 0 & 0 & 0 & 0 \\ a_{21} & a_{22} & 0 & 0 & 0 & 0 & 0 \\ 0 & 0 & a_{33} & a_{34} & 0 & 0 & 0 \\ 0 & 0 & a_{43} & a_{44} & 0 & 0 & 0 \\ 0 & 0 & 0 & 0 & a_{55} & a_{56} & 0 \\ 0 & 0 & 0 & 0 & a_{65} & a_{66} & 0 \\ 0 & 0 & 0 & 0 & 0 & 0 & a_{77} \end{bmatrix} \begin{bmatrix} CN_L \\ CN_H \\ PR_L \\ PR_H \\ GT_{Bypass} \\ GT_{Core} \\ SFC \end{bmatrix}_k + \begin{bmatrix} b_1 \\ b_2 \\ b_3 \\ b_4 \\ b_5 \\ b_6 \\ b_7 \end{bmatrix} W_{ff}\Big|_k \quad \textbf{(6-15)}$$

$$GT_{total}\Big|_k = \begin{bmatrix} 0 & 0 & 0 & 0 & 1 & 1 & 0 \end{bmatrix} \begin{bmatrix} CN_L \\ CN_H \\ PR_L \\ PR_H \\ GT_{Bypass} \\ GT_{Core} \\ SFC \end{bmatrix}_k$$

Different MPC settings can be applied according to the dynamic of output variables (6-15). Different weighting factors control changes control input at each sampling time. As its value gets closer to 0, the change of input value becomes proportional to the error between the control reference and feedback; thus a faster transient response can be obtained, Figure 6-49, and more

transient over-fuelling is applied (Figure 6-50). The smaller weighting factor also creates more difficulty in containing the state variables within the constraints because of more energy being stored in the volume from a larger amount of over-fuelling. The close up plots: Figure 6-51, shows a clearer view of slower transient response and a smaller amount of over-fuelling to the engine when a larger value of weighting factor is chosen. In this case, a slightly smaller weighting factor (0.2) is selected.

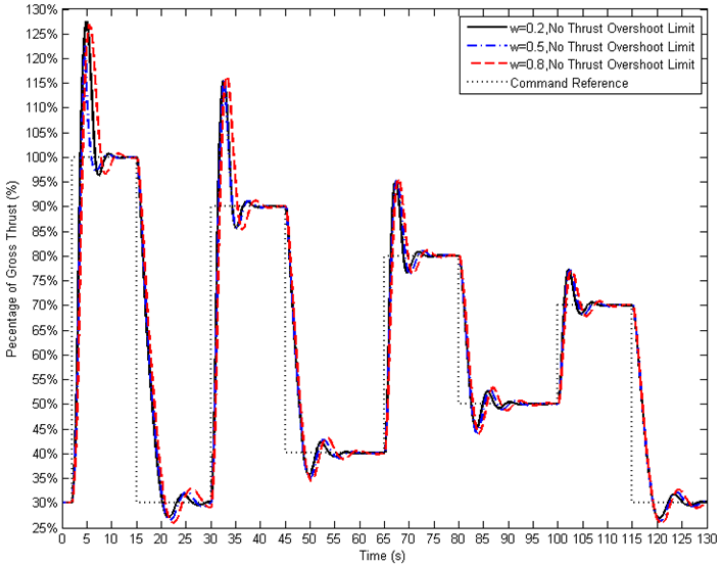

Figure 6-49 The percentage gross thrust to the design point from the control of MPC with different values of weighting factors

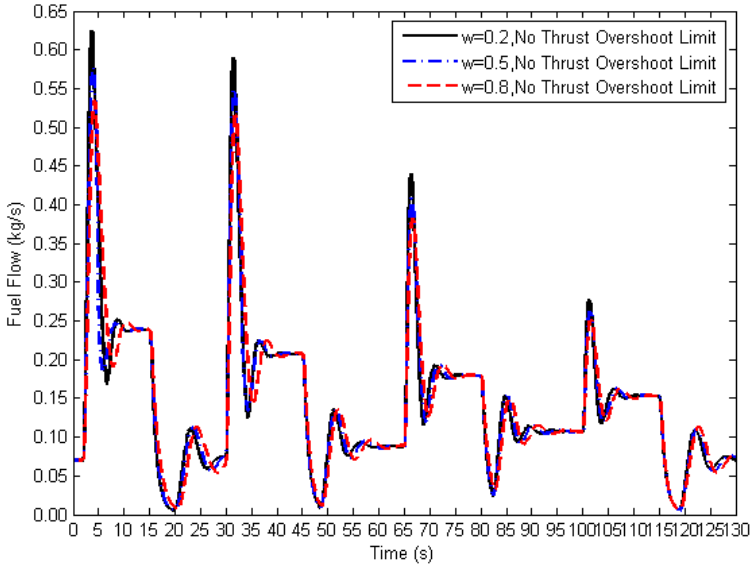

Figure 6-50 Fuel flow given by MPC with different values of weighting factor

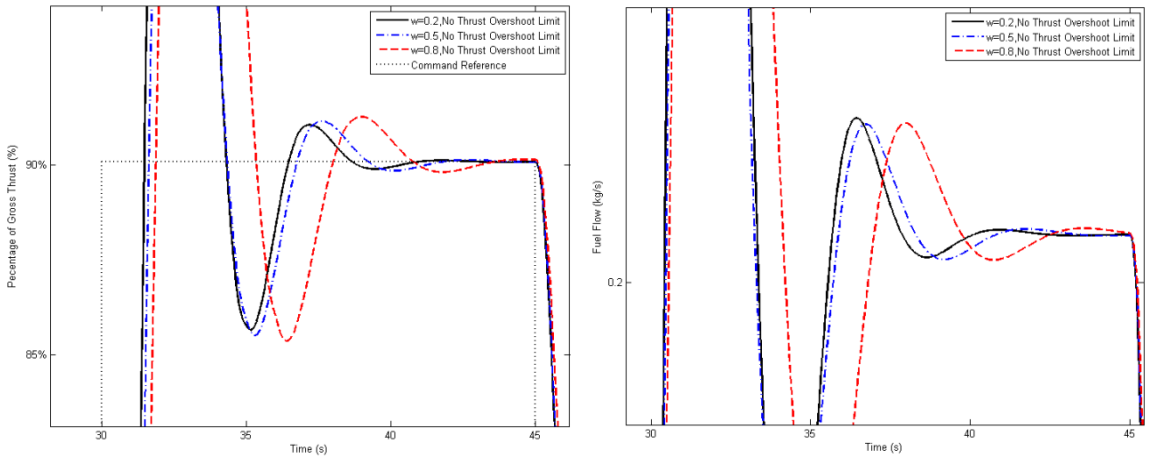

Figure 6-51 Close up of percentage of gross thrust (left), fuel flow (right)

Longer prediction and control horizons allow the controller to have further ability to plan the fuel schedule in order to satisfy the constraints if a smaller weighting factor has been chosen. Figure 6-52 shows the effects on the engine performance by implementing different lengths of horizon. The design of this prediction and control horizon must consider the natural frequency of the parameters from (6-15) in order to maintain the value of these parameters within required limits. Unlike the input constraints, the constraints on the state and output variables are often implemented as “soft” constraints, which means the penalized control actions cannot immediately show their effects on the constrained parameters due to system lag and contradiction to the other constraints. In Figure 6-52, the results given by MPC with 30 and 50 steps of predictions are almost overlapped. In this case, if the length horizon is 50 steps or less, the percentage of overshoot of gross thrust cannot be kept under 5%. Due to input constraints, the change of fuel flow at each sampling time is limited. As a result, a longer horizon allows the MPC to apply earlier control actions in order to change the direction of the vectors. However, the longer horizon has a consequence on the increase of rising or fall time. The increase of horizon length also increases the dimension of all the matrices in (5-25) and reduces the computing speed. In Figure 6-52, one of the horizons is 90 with a sampling time of 0.004s with a total seven states and one output variables in (6-15): the dimension of matrix “F” in (5-8) can be 630×630 for only 0.36s predictions at each sampling time. In this case, a moderate horizon length (70

steps) is chosen, which is not only capable of allowing the transient operation to complete within 5s and constrain the amount of overshoot within 5%, but also saves the computing memory by reducing 140 length (19600 elements) of matrix “F” to 490×490.

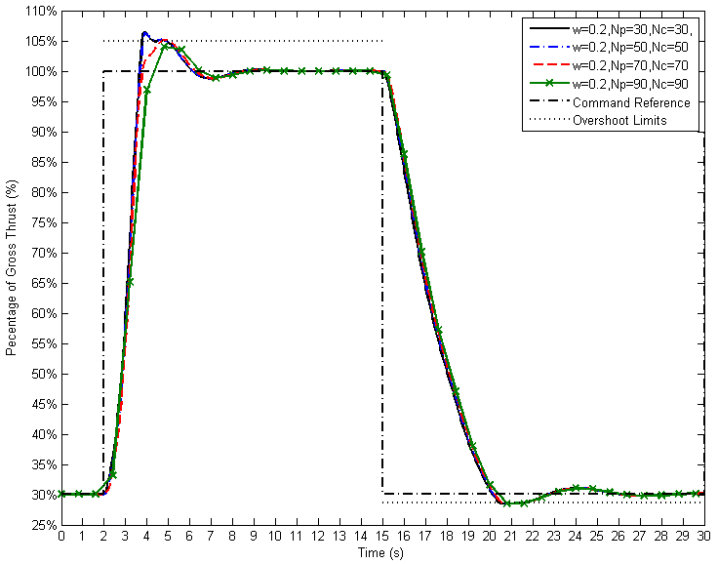

Figure 6-52 Percent total gross thrust to the design point given by MPC with different prediction length

It is important to consider the performance requirements, boundary conditions and the computing efficiency while importing the constraints. Despite the prediction length, additional constraints to the engine variables increase the drain on computing memories since the optimal control solution involves solving the matrix operations in (5-25). Just one additional engine constraint adds at least one row with N_c number of columns to the constraint matrix (M) of (5-23). Furthermore, adding more constraints also increases the possibility of having less control freedom (more active constraints than control variables) or contradiction among the constraints. For example, the lost control freedom can be caused by the confliction between overshoot limit and the limit of fuel flow change while the operating point moves towards the final steady state.

Table 6-9 shows the constraints added to the state variables. The top six constraints are designed for safety concerns and the last two are designed for performance optimization.

$0.01\text{kg/s} \le W_{ff} \le 1.20\text{kg/s}$
$-0.80\text{kg/s} \le \Delta W_{ff} \le 0.80\text{kg/s}$
$55\% \le CN_L \le 105\%$
$71\% \le CN_H \le 112\%$
$PR_{HPC}\big\|_{surge} = f(CN_H) = 9.5625 \cdot CN_H - 2.1096$
$PR_{HPC}\big\|_{idle} = f(CN_H) = 3.0198 \cdot CN_H + 0.0180$
$-5\% \le GTR_{overshoot} \le 5\%$
$SFC \le 0.03$ or 0.02 kg/kNs

Table 6-9 The constraints to the 2-spool engine parameters

In order to prevent compressor surge and combustor flameout, the constraints to the pressure ratio of the high-pressure compressor (HPC-PR) were implemented. The HPC-PR limit was estimated from the compressor map and written as a function of the corrected rotational speed (CN) of the high-pressure shaft, shown in Table 6-9, so that the compressor limit can be estimated online and is varied with the change of operating points. The estimated boundary lines for HPC-PR are shown in Figure 6-54. A fast transient performance can directly drive the pressure ratio towards the boundary lines. As Figure 6-54 shows, the upper limit prevents the compressor driving into surge during acceleration. The lower limit prevents low pressure from reaching the shutdown threshold.

The overshoot limit for gross thrust ratio (output parameter) in Table 6-9 was designed not to exceed the control reference by more than 5%. Removing this limit from the controller, the transient acceleration can be directly driven to the maximum speed limits for both low and high-pressure shafts, shown by Figure 6-53 and Figure 6-54. The maximum value of GTR can reach nearly 130% (30% overshoot) from idle (30%) to 100% thrust, Figure 6-55. For rapid transient operations, the approach time is normally optimized to 3~5s, and the percentage of overshoot is required to be controlled to no more than 5% in order to provide smooth power transition. Therefore, a smaller value of weighting factor for MPC ensures the requirement of transient time, and the control input is limited when the overshoot boundary is being reached. The

impact to the speed of both shafts, as shown by the solid transient line in Figure 6-53, remains a large safety margin to the maximum limits and the speed constraints are inactive.

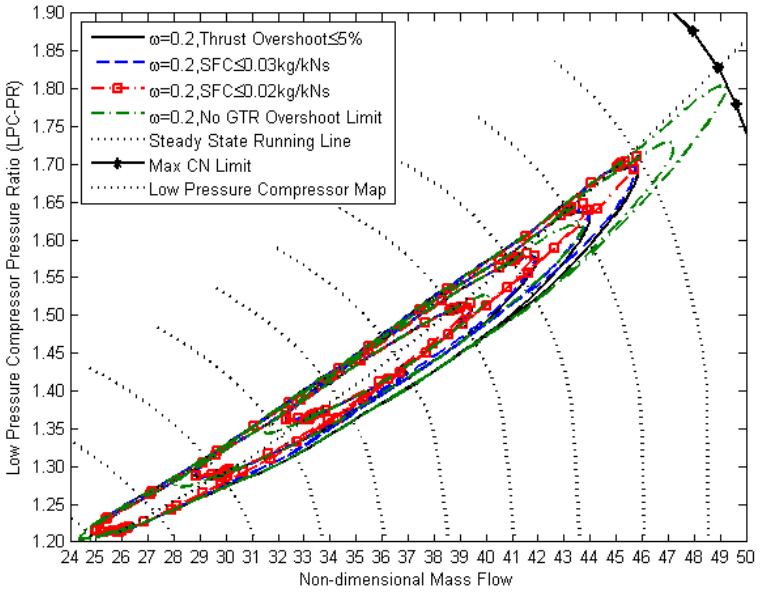

Figure 6-53 Low-pressure compressor transient performance given by the control of MPC with different constraints

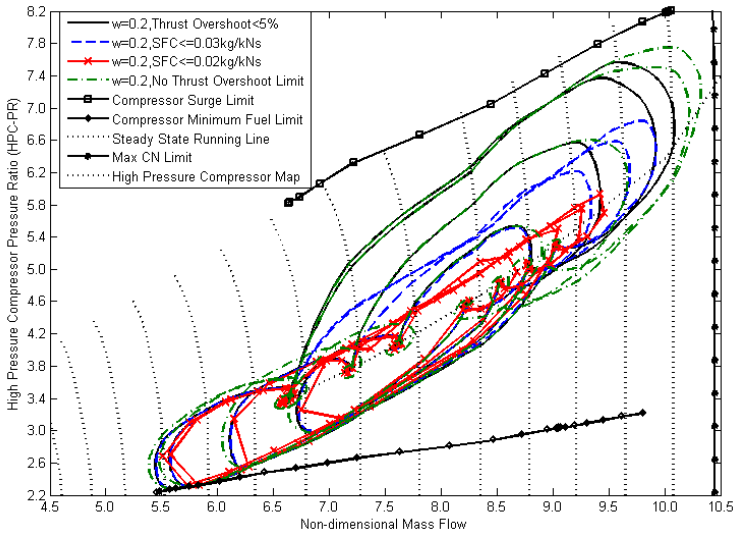

Figure 6-54 High-pressure compressor transient performance given by the control of MPC with different constraints

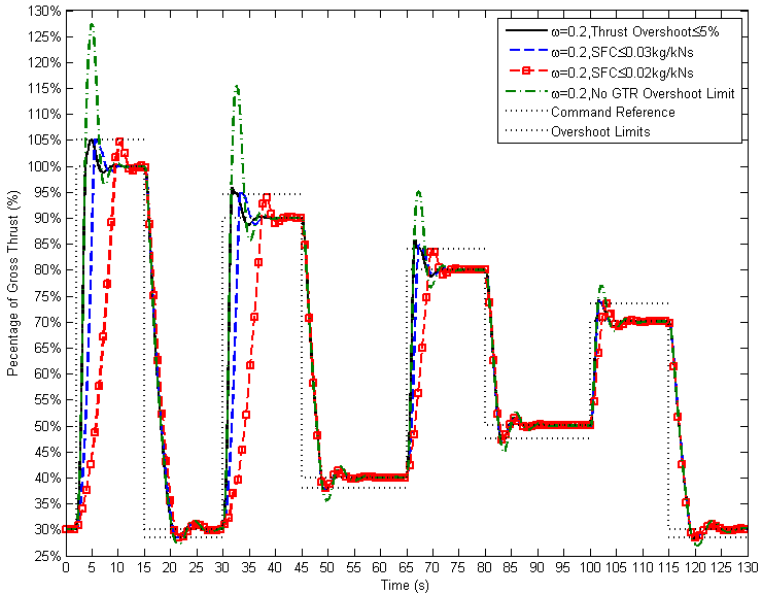

Figure 6-55 The results of gross thrust given by the control of MPC with different parameter constraints

In addition to the transient time optimization, fuel economy can be optimized by constraining the maximum fuel flow, the fuel rate or increasing the control weight to the MPC. However, all of these measures need to introduce fuel or control schedules in order to reach the target of fuel savings for the entire operating range. Figure 6-56 and Figure 6-57 prove that the value of SFC can also be controlled below 0.03kg/N·s by only limiting the maximum value of fuel flow ($W_{ff} \leq 0.32\text{kg/}s$). On the simulation basis, the specific fuel consumption (SFC) can be directly and added to the constraint list in Table 6-9 by taking the ratio from fuel flow to thrust. From the results, the maximum SFC value can be reduced by more than half to the transient operation without limiting the SFC. Figure 6-56 shows that the SFC is successfully kept below the threshold ($\text{SFC} \leq 0.03\text{kg/N} \cdot s$ and $\text{SFC} \leq 0.02\text{kg/N} \cdot s$). Including the SFC constraint allows the system to be more adaptive to the changes in transient operations by giving the authority to the controller to decide the input value and rate of the fuel flow, as shown in Figure 6-57.

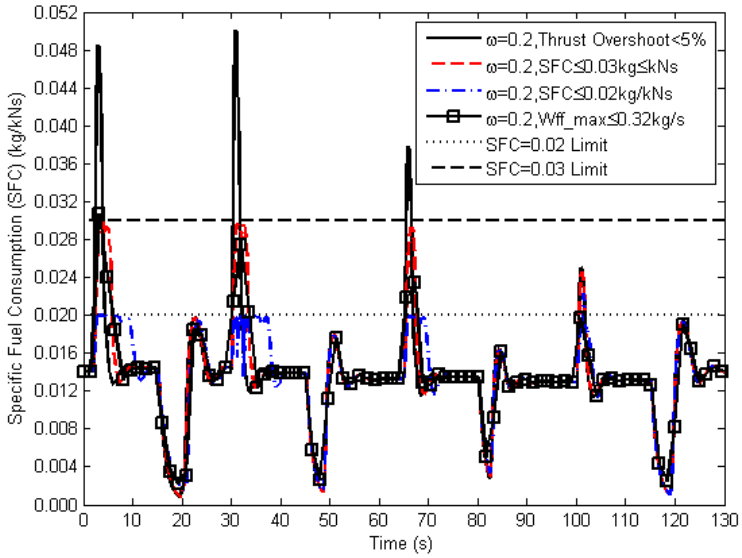

Figure 6-56 SFC from transient performance controlled by MPC with different settings of constraints

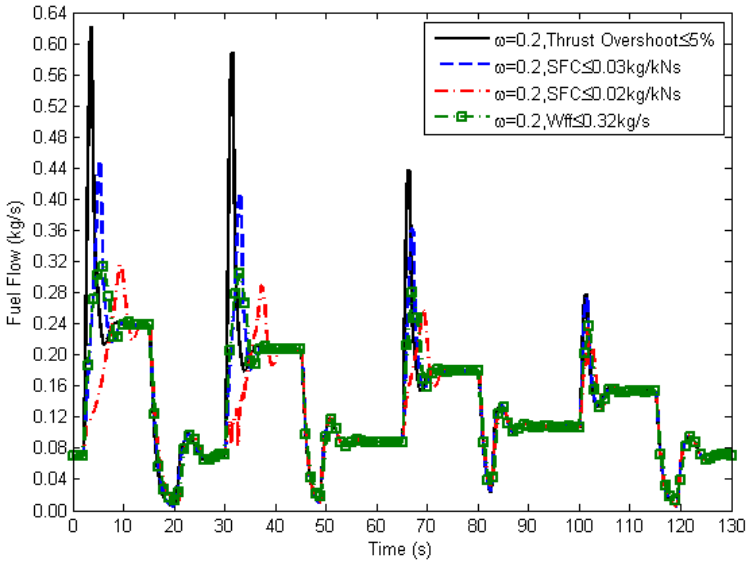

Figure 6-57 Comparison of fuel flow given by MPC with constraints

Table 6-10 shows that the total fuel consumption for the 130s simulation can be saved by 2.63% if the SFC is limited below 0.03kg/N·s, and a further reduction (8.47%) can be achieved if the SFC can be reduced by a further 0.01kg/N·s. Limiting the top value of the fuel input in order to constrain the maximum SFC (0.03kg/N·s), can also reduce a similar percentage of fuel consumption. In Table 6-10, the total fuel consumption has been increased by 7.57% from a higher value of weighting factor ($\omega = 0.8$) in MPC due to slower

dynamic response mainly on decelerations. However, if only the first two transient cycles are considered, 0.55% of fuel can be saved by increasing the weighting factor value. Therefore, adjusting the weighting factor only provides a slight impact on fuel saving and even then, mainly for large transient operations.

$\omega = 0.2$	18.04
$\omega = 0.8$	19.40(+7.57%)
$\omega = 0.2$, no overshoot limit	18.40(+1.99%)
$\omega = 0.2$, $W_{ff} \leq 0.32 kg/s$	17.50(−2.99%)
$\omega = 0.2$, $SFC \leq 0.03$ kg/kNs	17.56(−2.63%)
$\omega = 0.2$, $SFC \leq 0.02$ kg/kNs	16.51(−8.47%)

Table 6-10Total fuel consumption for 130s simulation (kg)

A longer rise time is expected if a smaller value of SFC has been constrained, as shown in Figure 6-55 and more surge margin for HPC in Figure 6-54, and the transient lines are kept closer to the steady state running lines for both LPC and HPC shown by Figure 6-53 and Figure 6-54.

Overall, the engine transient time can be optimized by selecting a smaller value of weighting factor for MPC. The boundary limits, such as shaft speed and compressor surge line, can be added to ensure safe operations. Including additional limits to the engine parameters can improve the quality of transient operations, such as overshoot limit to the output parameters, and an additional performance requirement can be achieved, such as SFC for optimization of fuel consumption.

6.3 Application to Three-spool Turbofan Gas Turbine Engine

The same control design algorithm is also applied to a three-spool high bypass turbo-fan engine. The additional intermediate pressure components increase the complexity of engine configuration. The intermediate pressure system allows the engine to reach a higher total pressure ratio. Higher power can be produced with fewer compressor stages so that a larger bypass ratio (8.5) and higher flow capacity (1179kg/s) can be reached [69]. However, this results in an increased order of estimated functions. In addition, the change of thermal energy in the combustor by change of fuel flow will also require more

time to transmit the thermal-energy from high to low-pressure engine components.

Volumes are not included for consideration at the preliminary design of steady state performance. However, the volume size relates to the physical size of the engine component and so the volume dynamic directly affects the transient performance of the engine. It also brings to different control designs to bear for different volume sizes of the components. In this section, the transient performance of the 3-spool engine with different volume size is investigated.

In addition, the design of a constrained MPC system is also demonstrated to optimise the transient performance for this engine.

The engine modeling was based on the ICV method and the design point shown by Table 6-11 [64,69,70]. The schematic of the three-spool engine is shown in Figure 6-27.

Ambient condition	ISA SLS	[-]
Intake Mach number	0	[-]
Intake mass flow	1179	kg/s
Fan pressure compressor pressure ratio	1.56	[-]
Fan pressure compressor isentropic efficiency	87.4	%
Intermediate pressure compressor pressure ratio	5.19	[-]
Intermediate pressure compressor isentropic efficiency	84.6	%
High-pressure compressor pressure ratio	5.19	[-]
High-pressure compressor isentropic efficiency	85.1	%
Fuel flow	2.8589	kg/s
High-pressure turbine isentropic efficiency	88	%
Intermediate pressure turbine isentropic efficiency	90	%
Low-pressure turbine isentropic efficiency	91	%
Moment of inertia for low-pressure shaft	380	kgm^2
Moment of inertia for intermediate shaft	74.2	kgm^2
Moment of inertia for high-pressure shaft	29.3	kgm^2
Percentage of low-pressure shaft corrected rotational speed at 50 RPS	100	%
Percentage of high-pressure shaft corrected rotational speed at 74.2 RPS	100	%
Percentage of high-pressure shaft corrected rotational speed at 208.3 RPS	100	%
Volume 1	5.80	m3
Volume 2	1.07	m^3
Volume 3	0.17	m^3
Volume 4	0.03	m^3
Volume 5	0.05	m^3
Volume 6	0.91	m^3

Table 6-11 Design point of the three-spool turbofan engine

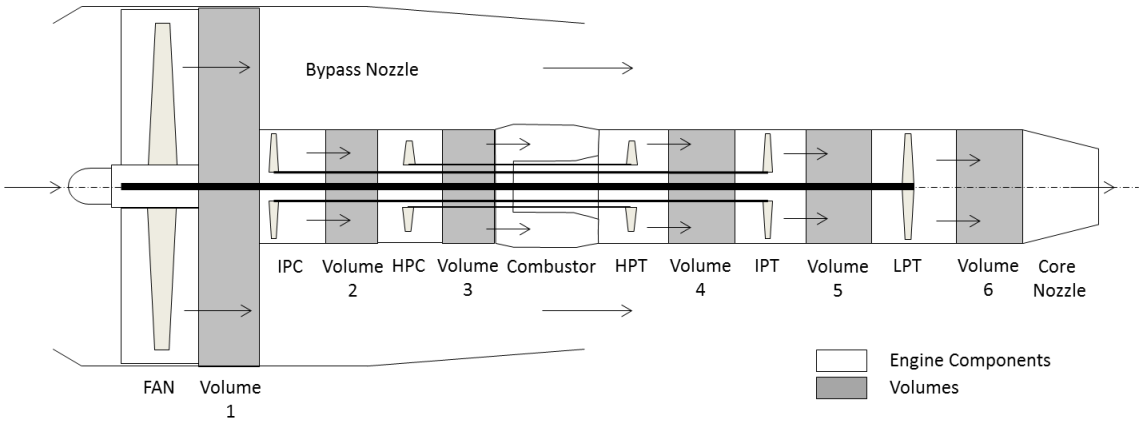

Figure 6-58 The sketch of the three-spool turbofan engine

The value of each volume is defined by the size of the chamber between its upstream volume module and itself. The volumes for the baseline model shown in Table 6-11 are the sizes of the chambers which are measured from the technical drawing [71], and scaled to the real engine size.

6.3.1 Volume Dynamics

The three spool configuration provides an opportunity to investigate the impact of different volume sizes on the overall transient performance and the performance impact on its neighbouring turbomachinery components. An increment of volume size by 0.9m^3 is shown in Table 6-12. The simulation is conducted by a transient acceleration and deceleration between 60% and 80% of PCNL. The transient operation is controlled by a PI controller ($\mathrm{P}=1.7;\mathrm{I}=4.5$) with fuel flow as the control parameter to handle the PCNL, and only one increment of the volume is conducted for each simulation.

	Fan	IPC	HPC	HPT	IPT	LPT
Baseline	5.7989	1.0725	0.1719	0.0262	0.0473	0.9137
Fan	**6.6989**	1.0725	0.1719	0.0262	0.0473	0.9137
IPC	5.7989	**1.9725**	0.1719	0.0262	0.0473	0.9137
HPC	5.7989	1.0725	**1.0719**	0.0262	0.0473	0.9137
HPT	5.7989	1.0725	0.1719	**0.9262**	0.0473	0.9137
IPT	5.7989	1.0725	0.1719	0.0262	**0.9473**	0.9137
LPT	5.7989	1.0725	0.1719	0.0262	0.0473	**1.8137**

Table 6-12 Selection of different volume size for the turbomachinery components

The controller is designed for the baseline model. Any change of volume changes the dynamic response of the engine and results in higher amount of overshoot of overall gross thrust ratio (GTR), Figure 6-59.Increasing the volume reduces the component's sensitivity to the change of pressure. The differentiation of temperature and mass flow are also influenced subsequently. A higher amount of over-fuelling, Figure 6-60, compensates for the longer time constant of the volume dynamics.

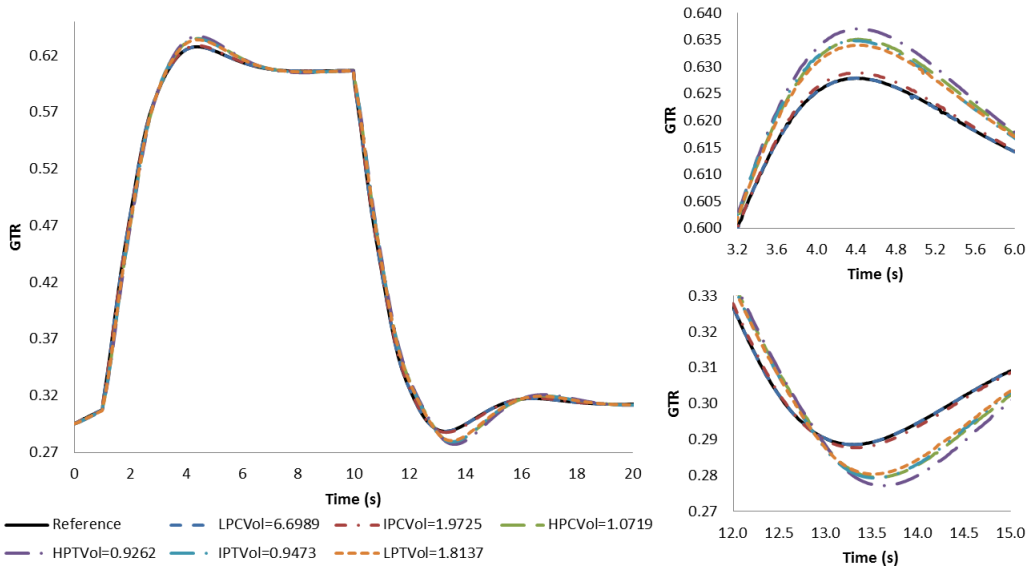

Figure 6-59 Gross thrust ratio from different values of volumes

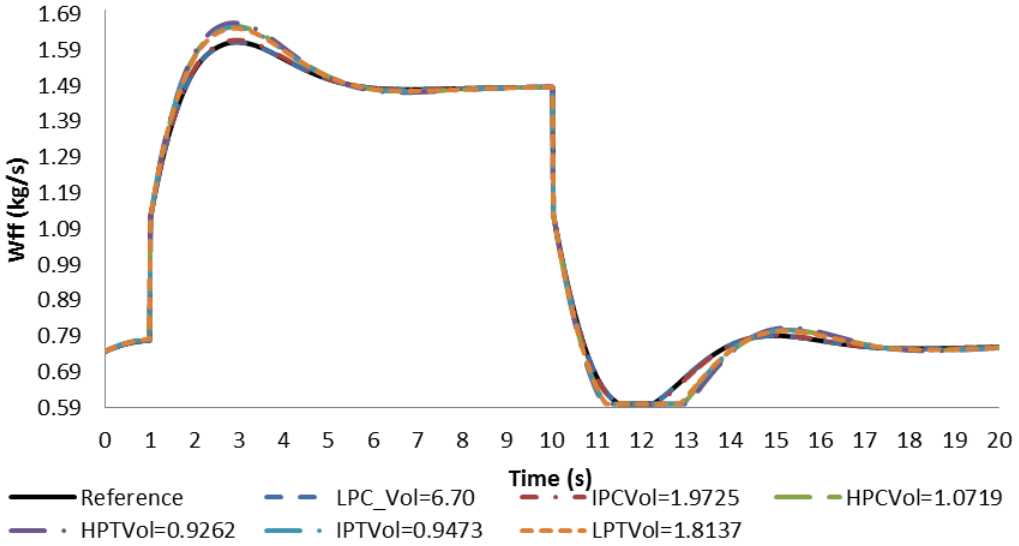

Figure 6-60 Fuel flow for the transient operation between 60% and 100% of PCNL

Increasing the component's volume changes its dynamic characteristics. According to (3-34), change of volume size only affects the dynamic of volume pressure. The volume pressure rate can be written as (6-16) from substitution (3-33).

$$\dot{P}_v = \frac{P_v}{T_v}\left[\frac{\gamma(T_{in}W_{in} - T_v W_{out}) - T_v \dot{m}_v}{m_v}\right] + \frac{RT_v}{V}\dot{m}_v \qquad \textbf{(6-16)}$$

The s-domain of (6-16) in terms of volume mass can be written as:

$$P_v \cdot s = \frac{P_v}{T_v}\left[\frac{\gamma(T_{in}W_{in} - T_v W_{out}) - T_v m_v \cdot s}{m_v}\right] + \frac{RT_v}{V} m_v \cdot s \qquad \textbf{(6-17)}$$

Mass flow is the volume input from upstream and downstream components, thus the approximated transfer function for the volume pressure to the volume mass becomes:

$$\frac{P_v}{m_v} = \frac{RT_v}{2V} \cdot \frac{s}{s + \frac{\gamma(T_v W_{out} - T_{in} W_{in})}{2T_v m_v}} \qquad \textbf{(6-18)}$$

(6-18) shows that the dynamic of volume pressure is a non-linear 1st order time varying system. The variance appears in the time constant and gain of the transfer function by the influence of the volume mass and temperature. The temperature is also the function of volume mass according to (3-33). The mass in (6-18) is not only the input of the volume module; it also creates the nonlinearity to dynamic volume pressure by affecting the time constant. Tuning the volume size only changes the gain of (6-18). The volume acts as a damping factor and increasing the size reduces the response to the volume mass.

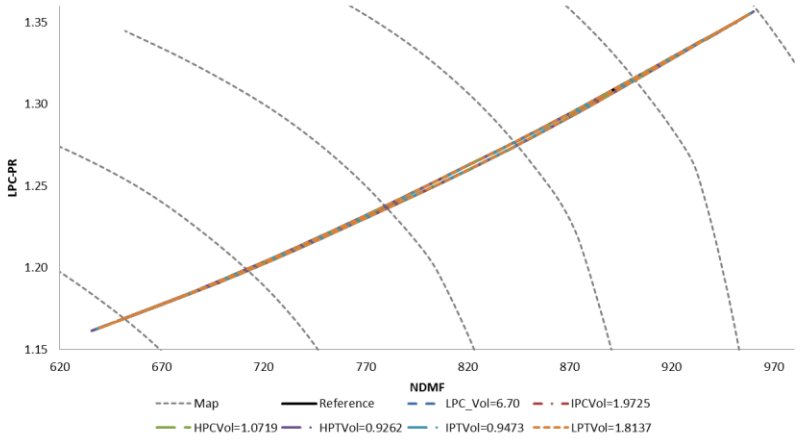

Figure 6-61 LPC transient performance from different volumes of turbomachinery components

Changing volume sizes does not provide significant effects on the transient performance of LPC or fan, Figure 6-61 because its dynamic is determined by the mass flow. The transient line of IPC shows a different characteristic to the transient performance of the baseline model by changing the volumes of compressors and turbines, Figure 6-62.The consequence of an increase in volume size of a compressor is a larger transient performance circumference than the one produced by the baseline model as shown by Figure 6-62.Increasing the compressor volume allows the shaft speed to change faster than the pressure ratio compared with the results from the baseline model. However, changing in fan volume (Vol. 1 in Figure 6-58) only provides a minor effect on the IPC performance as well as on the HPC, Figure 6-63. This is because the bypass ratio is determined by the air flow intake of the IPC. The fan normally contains only one stage in which the maximum pressure ratio is far less than 2.0. The fan dynamic performance is dominated by changes in mass flow and shaft speed. Therefore, the change of fan dynamic characteristic is not significant while tuning the fan volume.

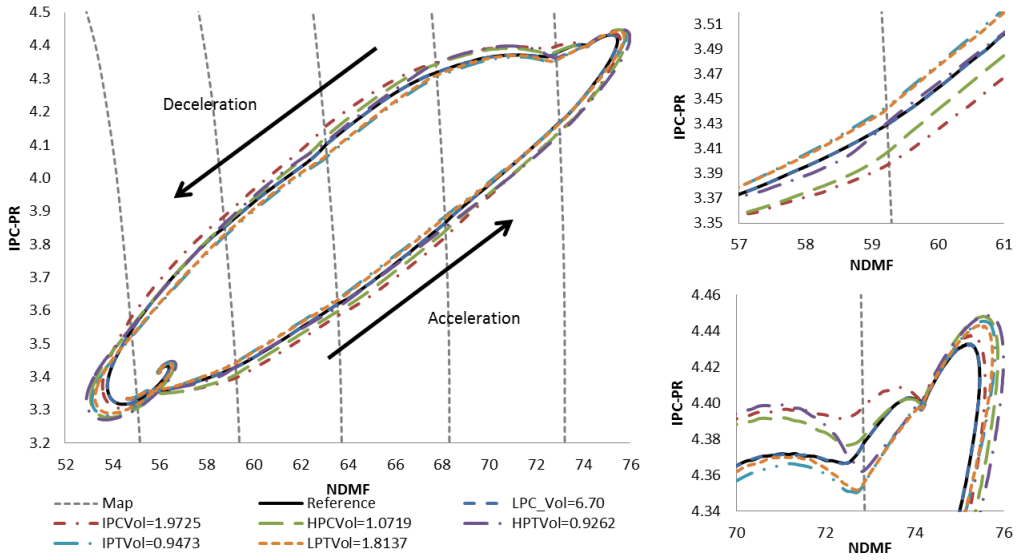

Figure 6-62 IPC transient performance from different volumes of turbomachinery components

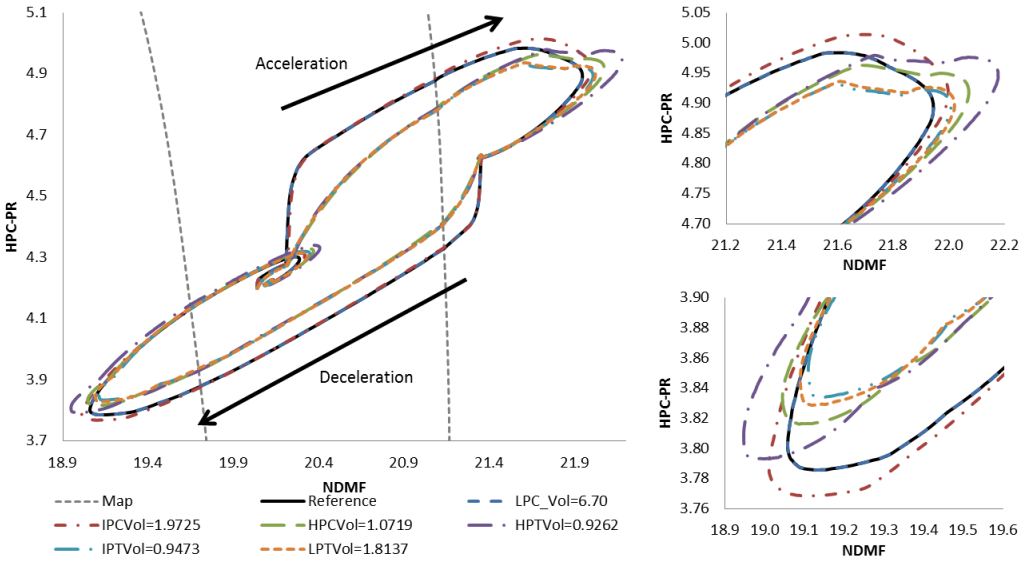

Figure 6-63 HPC transient performance from different volumes of turbomachinery components

According to the computational engine diagram Figure 3-4, the compressor pressure ratio is determined by the ratio between its volume exit pressure and its upstream module exit pressure. Therefore, the dynamic of IPC-PR is mainly determined by its volume size and compressor map due to small pressure changes in the fan during transient operation. However, the dynamic of HPC-PR is affected by both the size of its upstream volume and the volume

of itself. As the results show by Figure 6-63, there is a significant change of transient performance on HPC-PR when its volume has been increased.

The increase of the turbine volumes introduces the lag to the turbine dynamic. Compared to the frequency response Figure D-9, increasing the volume size of HPC and turbines significantly reduces the cut-off frequency for HPC-PR from 77rad/s of baseline model to 5.56rad/s. The cut-off frequency still remains 3.37rad/s for LPC-PR (Figure D-4) and IPC-PR (Figure D-7).

The change of compressor and turbine volumes provides little change to the shaft dynamics, which is shown by the frequency response of LP shaft Figure D-1, IP shaft Figure D-5 and HP shaft Figure D-8. However, the disturbance by changes of volume concentrates the effect to the higher frequency band which provides a minor change of shaft dynamic due to a lower system gain.

The simulation results show that the change of component volumes alters the engine dynamics. The volume mainly controls the pressure gain of its component. According to the results, changing the volumes of components which have no bypass chamber or bleed valve has a significant impact on the overall transient performance. However, the dynamic of fan or IPC has little influence by the alternation because the dynamic is dominated by the influence of mass flow. To improve the transient performance with less amount of steady state overshoot requires adjustment of PID control gains.

6.3.2 Transient Response Optimisation

A smaller value sampling time (0.0005s) is selected due to the high complexity of engine configuration compared to the previous twin-spool engine model. In this case, the 3rd order of functions can be estimated to represent the dynamic of shaft and compressor pressure ratio. The output is the total gross thrust, which is the sum of bypass (GT_{bypass}) and core gross (GT_{core}) thrust. SFC can be included for improvement of engine performance on fuel economy. The only control input is the fuel flow. The total number of state variables is nine and one control input. The reduced discrete state space model is shown by (6-19).

$$\begin{bmatrix} CN_L \\ CN_I \\ CN_H \\ PR_{LPC} \\ -1\cdot PR_{IPC} \\ PR_{HPC} \\ GTR_{bypass} \\ GTR_{core} \\ SFC \end{bmatrix}_{k+1} = A \begin{bmatrix} CN_L \\ CN_I \\ CN_H \\ PR_{LPC} \\ -1\cdot PR_{IPC} \\ PR_{HPC} \\ GTR_{bypass} \\ GTR_{core} \\ SFC \end{bmatrix}_{k} + BW_{ff}\big|_k \qquad \textbf{(6-19)}$$

where:

$$A = \begin{bmatrix} 0.9991 & 0.000963 & 0.0009636 & 0 & 0 & 0 & 0 & 0 & 0 \\ -0.000936 & 0.9873 & -0.00199 & 0 & 0 & 0 & 0 & 0 & 0 \\ 0.0005013 & 0.003903 & 0.9840 & 0 & 0 & 0 & 0 & 0 & 0 \\ 0 & 0 & 0 & 0.9989 & 0.0001543 & 0.0001296 & 0 & 0 & 0 \\ 0 & 0 & 0 & 0.003653 & 0.9875 & 0.01079 & 0 & 0 & 0 \\ 0 & 0 & 0 & 0.003045 & 0.0107 & 0.9837 & 0 & 0 & 0 \\ 0 & 0 & 0 & 0 & 0 & 0 & 0.999 & 0.00747 & 0 \\ 0 & 0 & 0 & 0 & 0 & 0 & -0.004514 & 0.9871 & 0 \\ 0 & 0 & 0 & 0 & 0 & 0 & 0 & 0 & 0.9998 \end{bmatrix};$$

$$B = \begin{bmatrix} 0.000668 \\ 0.005556 \\ 0.005037 \\ 0.000303 \\ 0.005326 \\ 0.006249 \\ 0.000317 \\ 0.004036 \\ 0.008345 \end{bmatrix}$$

From the estimated value of 1st and 4th row of constant matrices A and B (6-19), the low-pressure shaft speed and compressor pressure ratio have weaker linkage to their neighbouring components. In this case, it is optional to include fan speed and pressure ratio to the identified model.

The output discrete state space function is shown by (6-20). Gross thrust ratio (GTR) is the ratio of the engine gross thrust output to gross thrust at design point (DP). Combination of the gross thrust from both nozzles requires conversion from the ratio of their design values ($GT_{bypass\_DP} = 287579\text{kN}$; $GT_{core\_DP} = 338112\text{kN}$) to total gross thrust ratio.

Different engine parameters can be handled by changing the value of elements in matrix “C”.

$$\left[\mathrm{GTR}_{\mathrm{total}}\right]_k = \underbrace{\begin{bmatrix} 0 & 0 & 0 & 0 & 0 & 0 & \dfrac{\mathrm{GT}_{\mathrm{bypass\_DP}}}{\mathrm{GT}_{\mathrm{total\_DP}}} & \dfrac{\mathrm{GT}_{\mathrm{core\_DP}}}{\mathrm{GT}_{\mathrm{total\_DP}}} & 0 \end{bmatrix}}_{\mathrm{C}} \begin{bmatrix} \mathrm{CN}_{\mathrm{L}} \\ \mathrm{CN}_{\mathrm{I}} \\ \mathrm{CN}_{\mathrm{H}} \\ \mathrm{PR}_{\mathrm{LPC}} \\ \mathrm{PR}_{\mathrm{IPC}} \\ \mathrm{PR}_{\mathrm{HPC}} \\ \mathrm{GTR}_{\mathrm{bypass}} \\ \mathrm{GTR}_{\mathrm{core}} \\ \mathrm{SFC} \end{bmatrix}_k \quad \textbf{(6-20)}$$

Unlike the transient performance of LPC and HPC, the transient line of IPC increases below the steady state running line while the engine is accelerating, and vice versa for the deceleration, as shown in Figure 6-62.In this case, the minimum margin of IPC-PR is reduced while the engine is being over-fuel led during acceleration, and the IPC is more likely to be surged (maximum limit) while the engine is being decelerated. The controller will add more fuel to the combustor while the operating point is approaching any minimum boundary and the opposite action occurs while the operating point moves towards to the maximum limit. However, such actions will violate the transient performance and opposite actions are expected for IPC. Due to this IPC feature, the IPC-PR is numerically set to negative in (6-19) as well as to the maximum and minimum pressure ratio limit. The values are multiplied by “-1”, Table 6-13.

An acceleration followed by a deceleration between idle (30%) to 100% of total gross thrust is a simulation. The constraints to engine parameters are shown in Table 6-13. The fuel flow is constrained to a maximum of 200% to the design point fuel flow (at 100% design point fan speed) and to a minimum of 50% of fuel flow (at 46% steady state fan speed). The maximum limit of delta fuel flow is calculated from the fuel flow at idle fan speed to the maximum fuel flow limit; the minimum fuel change is the difference between the fuel value at the 100% fan speed and its minimum fuel limit. The transient performance for LPC shows a slight deviation to the steady state running line, Figure 6-61. Therefore, the constraints to a low-pressure component can be excluded. The

relative corrected value is used for shaft speed (CN). The boundary of CN for intermediate and high-pressure shafts is set to 5% overshoot from its command target speed. The limit of compressor pressure ratio is estimated from the compressor map to the function of relative corrected shaft speed. The gross thrust is the output of (6-20), which it is being handled by the fuel flow and its value is limited to below 3% overshoot of its reference. The limit of SFC can be included in the list, and its value is limited to no higher than 0.009kg/kN·s.

The order of the estimated model has been increased. The length of performance prediction by the MPC should be increased, which should be higher (90 or 110 steps) than the 70 steps used for the two-spool engine. However, considering a larger number of identified states variables, if the prediction length remains the same as the twin-spool, the total dimension of prediction matrix will be630×630 (70×9). Therefore, the prediction length has been reduced to 50 steps thus saving computing memory and time, which reduces the length by 180 columns and rows.

$0.25\,\text{kg/s} \le \text{W}_{\text{ff}} \le 5.72\,\text{kg/s}$
$-2.64\,\text{kg/s} \le \Delta\text{W}_{\text{ff}} \le 4.99\,\text{kg/s}$
$62\% \le \text{CN}_{\text{I}} \le 105\%$
$78\% \le \text{CN}_{\text{H}} \le 105\%$
$\text{PR}_{\text{IPC}}\big\vert_{\max} = \text{f}(\text{CN}_{\text{I}}) = -5.5082 \cdot \text{CN}_{\text{I}} + 1.6569$
$\text{PR}_{\text{IPC}}\big\vert_{\min} = \text{f}(\text{CN}_{\text{I}}) = -9.3962 \cdot \text{CN}_{\text{I}} + 2.0555$
$\text{PR}_{\text{HPC}}\big\vert_{\max} = \text{f}(\text{CN}_{\text{H}}) = 8.1434 \cdot \text{CN}_{\text{H}} - 1.6481$
$\text{PR}_{\text{HPC}}\big\vert_{\min} = \text{f}(\text{CN}_{\text{H}}) = 1.2858 \cdot \text{CN}_{\text{H}} + 0.5819$
$-3\% \le \text{GTR}_{\text{overshoot}} \le 3\%$
$\text{SFC} \le 0.009\,\text{kg/kNs}$

Table 6-13 The constraints to the three-spool engine parameters

Comparing the gross thrust results from the twin-spool engine, Figure 6-52, slightly increasing the value of the weighting factor to the MPC provides a significant impact on the transient performance, as shown in Figure 6-64 due to the larger size of the 3-spool engine configuration. As the result, a larger difference on the fuel inputs occurs for the same transient operation, Figure 6-65. Just a slight change in control weight provides a significant change in the

transient results of other engine parameters, such as the reduction on the compressor transient performance, shown by Figure E-2 and Figure E-3. As the control weights are being increased, the transient lines move closer to the steady state lines for all compressors. This means a slower transient response is expected. The smaller SFC can also result in a slower transient response.

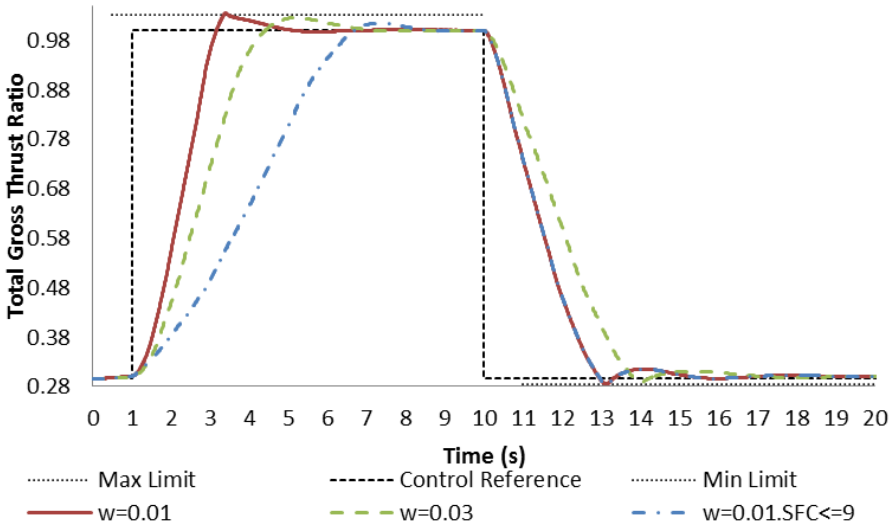

Figure 6-64 Gross thrust ratio of the 3-spool turbofan engine

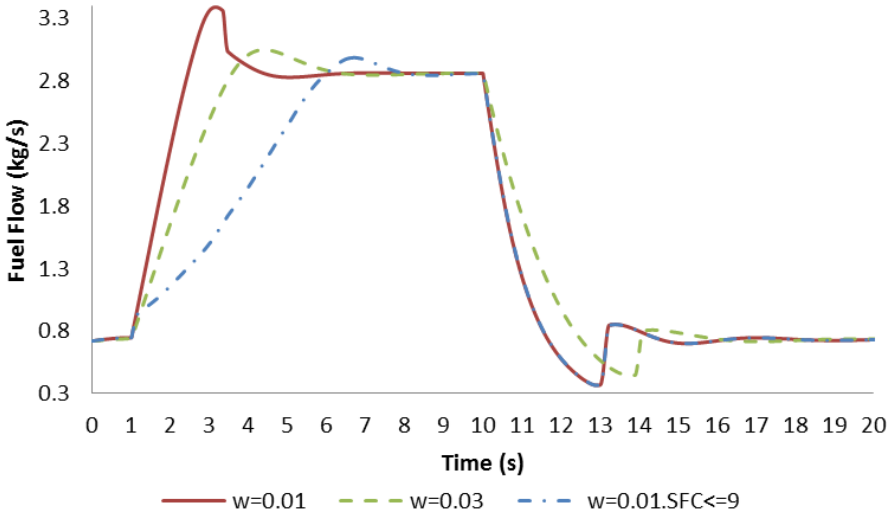

Figure 6-65 Fuel flow to the 3-spool turbofan engine for gross thrust change between idle to 100%

With the implementation of the active SFC constraint ($\mathrm{SFC} \leq 9\mathrm{g/kNs}$), the increment of fuel flow to the engine has been reduced, Figure 6-65, in order to keep the value of SFC below the limit, Figure 6-66. The implementation of SFC constraint is capable of maintaining the fuel consumption below the limited value, Figure 6-66. The reduction to the peak value of specific fuel consumption can also be achieved by increasing the weighting factor to the MPC.

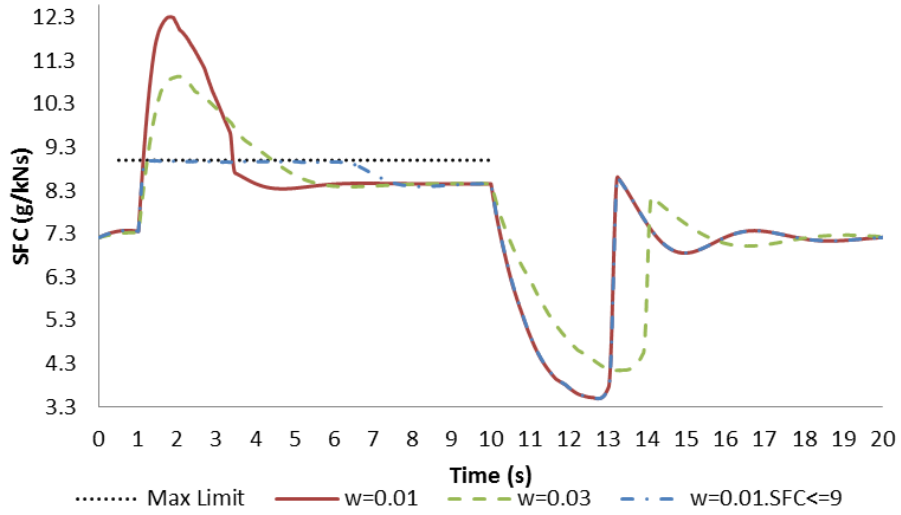

Figure 6-66 SFC for transient operation of the 3-spool engine between idle and 100% gross thrust output

Increasing the weighting factor value to 0.03 reduces the maximum value of SFC and helps fuel saving for acceleration to the performance provided by the weighting factor: 0.01, by approximately 7% for the 10s simulation according to the data from Figure 6-65. However, a slower fuel reduction rate is produced while the engine is decelerating, and results in a final fuel saving of only 0.8%. The implementation of SFC constraint is capable of reducing the fuel consumption by over 10% for the 20s transient simulation.

w=0.01	41.12
w=0.03	40.79 (-0.80%)
w=0.01, SFC ≤0.009 kg/kN·s	36.96 (-10.11%)

Table 6-14 Total fuel consumption of the 3-spool turbo-fan engine for 20s transient simulation (kg)

In summary, the same control design process for single and twin spool gas turbines can be inherited to the design of three spool engine, and the performance objectives can be achieved. However, the more complex engine configuration brings higher frequency gap between the higher and lower pressure components. Therefore, the change value of weighting factor can be more effective to the change of dynamic on relative higher pressure components.

6.3.3 Transient Performance Optimisation of Engine with Different Volume Sizes

From the comparison of the gross thrust results ratio from Figure 6-67 to Figure 6-59, the results given by MPC only show a little reduction on a transient response while the volumes have been increased, and the difference on the transient performance is much less than the change provided by the control from PID controller. This is because the RLS-SV is capable of adjusting the dynamic of identified model to match the performance from the ICV models which have the changed volumes, and provides the updated model to MPC. The MPC is then capable of adjusting its control gains to produce the optimal transient results.

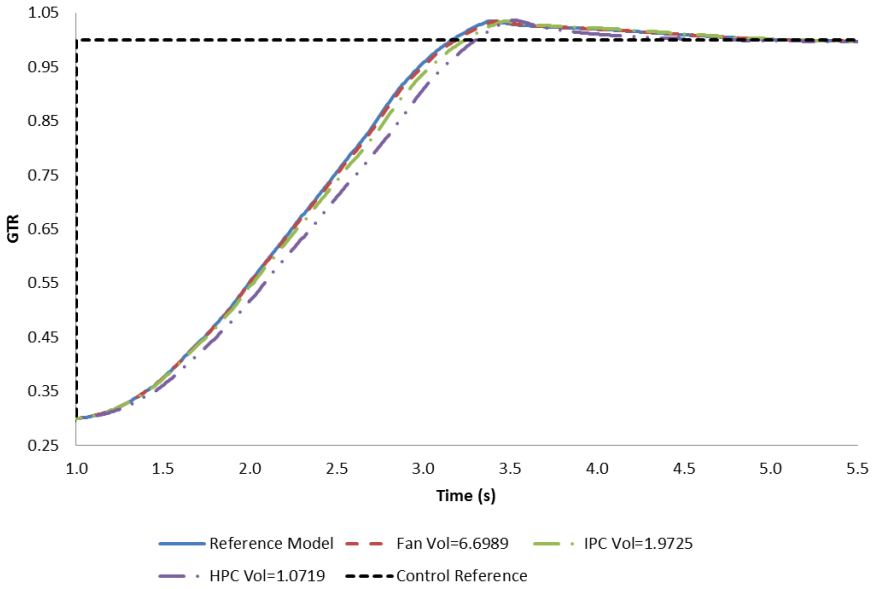

Figure 6-67 Gross thrust ratio given by MPC to the ICV engine model with different value of volumes

Adjusting the volume size changes the engine dynamic characteristics. The classic fuel scheduling method requires revising every item in the table. The PID controller is required to be redesigned to be suitable for the gain of K_p, K_i and K_d in order to achieve the same transient response to the reference model. However, the MPC only requires altering slightly the value of the weighting factor. Since a smaller value of weighting factor is normally set to the MPC. Therefore, as the results show in Figure 6-68, the MPC is still capable of attempting a similar performance for both LPC and HPC as the results from the reference model, although the compressor volumes have been changed.

In summary, the flexible control design provides a significant simplification on the design of transient performance optimisation when the engine volumes have been changed. If the overall engine configuration still remains the same, the transient performance can still be optimised by the same MPC design.

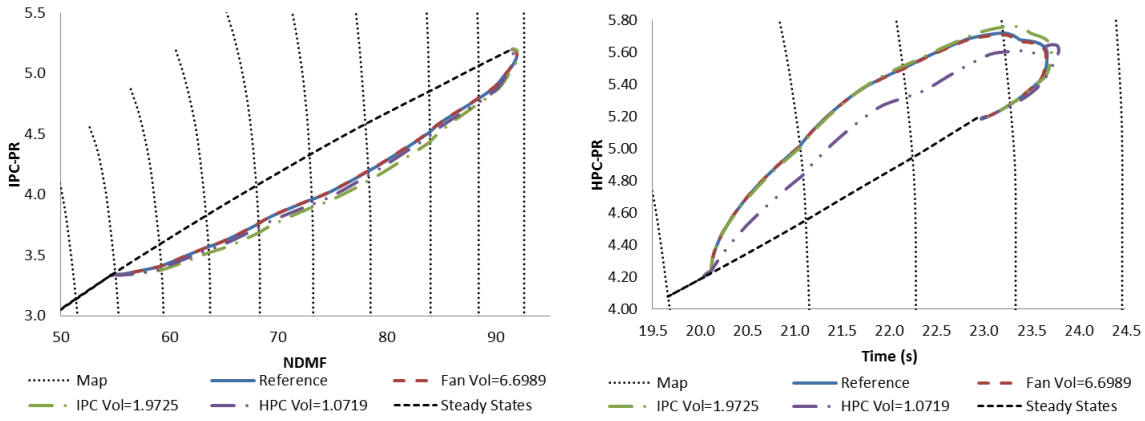

(a) (b)

Figure 6-68 Transient performance of IPC (a) and HPC (b) from the models with different compressor volumes and controlled by MPC

6.4 Summary to Design of the Optimal Engine Transient Performance

In summary to the design control system for optimal transient performance, both of classical fuel schedule and PID controller require look up tables to achieve optimal transient performance for defined operating circumstances. The constrained MPC allows the flexible control decisions to be made according to identified dynamic models from the readings of engine inputs and outputs. The benefit of this algorithm is that the MPC always searches for the optimal options to achieve the minimum number of control actions. The fuel flow can be automatically manipulated by the constrained MPC based on the chosen control target. The control target can be shaft speed, compressor pressure ratio, thrust delivery or any of engine parameters. The optimal transient response will be produced according the control target and satisfaction of the engine constraints.

In addition, this chapter also conducted a research on the behaviours of the model identification techniques for estimating the dynamic models for long period and large number of transient cycles on a twin-spool gas turbine engine. Producing reliable dynamic models require the identification process could produce the identical model estimation results during the same transient operation for any time during operations. This also means the characteristics of the dynamic models must be identical through the same operations. As the result, the recursive least squares method with varying stabilizing factor could produce the most satisfied results.

Furthermore, another research was conducted on a three-spool turbo-fan engine to analyse how different volumes from the inter-component volume techniques affect the controller's behaviour to optimise the transient operations. The research discovered when increase of volume size will reduce the response of pressure change in its corresponding engine component, vise versa. This is applicable to any of turbomachinery component of gas turbine engine. This research also discovered changing the volume size of the components downstream of the combustor will provide more significant impact

on overall engine transient response than the components located upstream of it. This is because the transient operation was handled by engine fuel supply and it primarily change the performance of turbines, then the compressors will catch up through acceleration or deceleration from the shaft.

Finally, for all gas turbine engine configurations, the fastest transient response can be guaranteed by the minimum of control actions from the constrained model predictive controller. The weighting factor is the only variable in the MPC which can be manually tuned to the rate of change of control inputs. A smaller value of weighting factor is suggested to be chosen for guaranteeing a transient time within regulation as mentioned by FAA in section 2.2. The constraints on the compressor pressure ratio can be added to prevent compressor surge and combustor flameout, whilst the constraint on shaft speed prevents over-speed. Adding the fuel flow (input) limit provides saturation on magnitude fuel input. The limited input rate can indirectly control rich and lean mixtures of fuel and air. The additional constraints to the engine parameters introduced by this project can be used for shaping the transient line, such as overshoot limit, or to achieve additional performance requirements, such as fuel consumption.

7 CONCLUSIONS

The transient performance optimisation of gas turbines with an integrated robust control system has been investigated in this project. The model predictive controller (MPC) has been designed and implemented to optimise online the transient time response and fuel consumption of gas turbine engines for their entire operating range. The new system provides an opportunity to increase the control robustness to achieve different performance tasks and to improve adaptability to unforeseen conditions from the classic scheduling control techniques. The new development also simplifies the repetitive work on experiments or simulations for producing the control look-up tables. In addition, the constraints applied to the controller ensure that the MPC is capable of operating the engine efficiently in safety. Furthermore, the control algorithm has been generalised for application to most engine configurations. The control design for performance optimisation has been validated through transient simulations on different engine models.

In this project, a closed loop system was developed for gas turbine engine transient performance control and transient process optimisation, User defines an engine parameter as the system output and specifies a target steady state operating point. The engine constraints can be defined as any of engine parameters for purpose of safe operation and finer performance tuning. Due to a model based control algorithm, the optimal control algorithm cannot directly analyse the readings from the engine module in the closed loop system and produce the optimal control decision so that all of engine output and constrained parameters are required to be represented by dynamic models. A recursive least squares method (RLS-SV) was implemented for identification of dynamic models. This identification process is a self-adaptive method, which reads the values of the defined engine parameters and updates the dynamic models at each time step to produce best fitted estimations to the actual engine performance lines. The MPC manipulates the value of fuel flow as a control input to control engine transient performance. This project introduces the MPC process which is capable of producing optimal engine control solution with

consideration multiple engine parameters as engine performance limitation so that the transient performance could be handled rapidly, efficiently and safely. In this control process, a control value which could produce the fastest transient response is firstly developed from the measurement between current and target operating point. Then, this control input is substituted to dynamic models of constrained parameters in order to ensure no engine limit could be breached within the prediction length. If any of the limits is being breached, the control value will be recalculated until all engine constraint conditions are satisfied. The final control input produced by the MPC is injected to the engine and engine responses to the new fuel flow. The closed loop can be repeated through reading the value of engine parameters, dynamic model identification and producing control inputs and finally providing to the gas turbine engine.

The identification algorithm: recursive least square with varying stabilizing factor (RLS-SV) provides the estimated reduced dynamic model to the MPC due to its having the feature of a model-based control system. The identified model adapts to the change of engine dynamics so that the MPC can adjust its control plans to reach the control target with minimum control actions as well as satisfying the constraints. From the analysis of simulation results, the identification techniques which can be used on estimation of engine dynamic models must be capable of producing the accurate and identical estimation results for the same or repetitive transient operations. Therefore, the RLS with implementation of forgetting factor can only produce the accurate estimation of dynamic models. Due to engine nonlinear performance, the change of dynamic models estimated by RLS must be stabilised. The RLS-SV method produced the most reliable and accurate estimated dynamic model among all identification process which is relative to RLS technique.

The control system has been successfully applied to Turbomatch, and the performance of the control system has been evaluated through simulations on engine models. The engines have been modeled into a component level by the inter-component volume (ICV) method. The more complex engine structure

increases the order of dynamic model as well as the dimension of prediction matrices by the MPC. Consequently, the computing time has been increased.

From the simulation results, due to the non-linear behaviours, the classic linear control method, such as proportional-integral-derivative (PID), is required to design the control gains separately for different accelerations and decelerations in order to satisfy the desired transient time and settling time. The model predictive controller always seeks the fastest transient operation. Defining the input constraint and constraining the engine parameters from dynamic models automatically restricts the rate and amplitude of the control input given by the MPC. As a result, the process of transition between two operating points is no longer important to the MPC system. The defined control reference of the output parameter comprises the control targets, and the engine constraints define the operating range, which has changed the control system to target demand. With a slightly smaller value of weighting factor in the MPC, the optimal control inputs can automatically search for the fastest safe route to reach the target operating point. The constraints to the engine parameters can also be designed to specify the desired transient performance. The simulation results show that the percentage overshoot constraint can be added to improve the performance of output parameters, and better fuel economy can be achieved if the maximum value of specific fuel consumption (SFC) is limited. From the comparisons of simulation results by the output: relative shaft speed (PCN), compressor pressure ratio (CPR) and engine gross thrust ratio (GTR), controlling the output parameter with a higher frequency can also easily satisfy the overshoot requirements of the engine parameters with lower frequencies.

In addition, analysing the simulation results discovered selecting different volume sizes for engine components could produce different transient performance handled the same MPC design. Although the volume sizes are designed during the off-design process and could not be easily changed, this research outcome suggested same change on volume size could produce significant change on transient dynamic behaviour of the engine. In general, increase the volume size could result slower change of the pressure on the

engine components. Slightly change on the volume size if applied on turbine, outcome on the engine performance could be more significant on the engine dynamics than the same change applied on compressors.

Finally, general rules can be followed to design the constrained MPC for obtaining an optimal engine performance on all gas turbine engine configurations. A sufficient horizon length provides the controller with enough time to realize the control efforts on engine parameters in order to achieve the performance requirements, and the computing memory can be kept within an acceptable range. A slightly smaller value of weighting factor for the MPC ensures that transient operations can be completed within the specified time for the entire operating range. Adding appropriate constraints on parameters can maintain the operations within a safe envelope as well as satisfying additional performance requirements such as fuel economy.

8 FUTURE RESEARCH PERSPECTIVES

In this research, an advanced control algorithm: MPC was developed to control the transient performance of gas turbines as well as to obtain the optimal transient performance without the aid of control schedules for the entire operating range. Therefore, the control system was designed based on the optimal control theory with benefits of high level of robustness and adaptability. The research has conducted the simulations in order to examine the new control system on single-, twin- and three-spool gas turbine engines. More simulations on the turboshaft engines or advanced engine configurations such as the intercooled-recuperated engines are required to be performed in order to further validate the applicability of this control method. More detailed research is required to complete a gap in knowledge on what parameters should be selected for dynamic identification. As a result, the MPC can use the identified dynamic model to produce the optimal transient performance of an advanced engine cycle.

Furthermore, the single input and single output (SISO) system with fuel flow as an input variable was investigated in this research. The way to implement the MPC for multi-inputs and multi-outputs (MIMO) system also can be further investigated so that the fuel flow, variable state vanes (VSV) and variable nozzles can be controlled simultaneously. The turboshaft engines with variable power loadings also require control design for a MIMO system. Further research on the capability of MPC and identification algorithm (RLS-SV) to tolerate the noise or disturbance from exogenous inputs is also necessary to be carried out. This investigation measures the applicability of the control system to real engines.

Finally, the computing efficiency of the MPC is required to be further improved such as by using Laguerre functions. The current system is capable of performing online optimisation for the transient performance of gas turbine engines. However, as the length of prediction and control horizon is increased, computing time is also increased. Therefore, the current system is not capable of being applied to the real-time control.

REFERENCES

[1]. Jaw LC., Mattingly JD. Design of Transient and Limit Controllers. Aircraft engine controls: design, system analysis, and health monitoring. American Institute of Aeronautics and Astronautics; 2009. pp. 119–170.

[2]. Kyura N., Oho H. Mechatronics-An Industrial Perspective. IEEE/ASME Transactions on mechatronics. 1996; 1(1): 10–15. Available at: DOI:10.1109/3516.491405

[3]. Bishop RH. Mechatronic Design Approach. The Mechatronics Handbook. CRC Press; 2002.

[4]. Lutambo J., Wang J., Yue H., Dimirovsky G. Aircraft Turbine Engine Control Systems Development: Historical Perspective. Control Conference (CCC), 2015 34th Chinese. IEEE; 2015. pp. 5736–5741. Available at: DOI:10.1109/ChiCC.2015.7260534

[5]. Balakrishnan SR. Control System Development Experience for Aero Gas Turbine Demonstrator Engines. Progress in Nonlinear Dynamics and Chaos. Gas Turbine Research Establishment, DRDO, Bangalore, India; 2013; 1: 15–22.

[6]. Jaw LC., Garg Sanjay. Propulsion Control Technology Development in the United States A Historical Perspective. 2005. Available at: DOI:NASA/TM-2005-213978, E-15299

[7]. Garg S. Fundamentals of Aircraft Turbine Engine Control. Glenn Research Center at Lewis Field; 2010.

[8]. NASA. Transition in Gas Turbine Engine Control System Architecture: Modular, Distributed, Embedded. 45th AIAA/ASME/SAE/ASEE Joint Propulsion Conference & Exhibit. Colorado: NASA; 2009.

[9]. MacIsaac B., Langton R. Gas Generator Fuel Control Systems. Gas Turbine Propulsion Systems. John Wiley & Sons; 2011. pp. 37–88.

[10]. Csank J., May RD., Litt JS., Guo T-H. Control Design for a Generic

Commercial Aircraft Engine. 46th AIAA/ASME/SAE/ASEE Joint Propulsion Conference & Exhibit. 2010;

[11]. Federal Aviation Administration. Part 33 Airworthiness Standards: Aircraft Engines. 2015. p. Sec. 33.73. Available at: http://www.airweb.faa.gov/Regulatory_and_Guidance_Library/rgFAR.nsf/0/227D27BE2CC695DD852565C50060284B?OpenDocument (Accessed: 1 January 2015)

[12]. Walsh PP., Fletcher P. Transient Performance. Gas Turbine Performance. John Wiley & Sons; 2004.

[13]. Evans C., Rees D., Hill D. Frequency-Domain Identification of Gas Turbine Dynamics. IEEE Transactions on Control Systems Technology. IEEE; 1998; 6(5): 651–662. Available at: DOI:10.1109/87.709500

[14]. Evans C., Rees D., Borrell A. Identification of Aircraft Gas Turbine Dynamics Using Frequency-Domain Techniques. Control Engineering Practice. Elsevier; 2000; 8(4): 457–467. Available at: DOI:10.1016/S0967-0661(99)00161-6

[15]. Sun J. Modeling of Aeroengines. Advanced Multivariable Control Systems of Aeroengines. Beihang University Press; 2005. pp. 60–174.

[16]. Sellers J., Daniele C. DYNGEN - a Program for Calculating Steady-State and Transient Performance of Turbojet and Turbofan Engines. 1975.

[17]. Pilidis P. Digital Simulation of Gas Turbine Performance. Mechanical Engineering. 1983.

[18]. Kim S., Pilidis P., Yin J. Gas Turbine Dynamic Simulation Using Simulink. SAE Technical Paper; 2000. Available at: DOI:10.4271/2000-01-3647

[19]. Pilidis P. A5.10 Transient Performance Modelling. Performance, Gas Turbine Theory and Performance. Cranfield University; 2012. pp. 158–162.

[20]. Hunt KJ., Sbarbaro D., Żbikowski R., Gawthrop PJ. Neural Networks for

Control Systems—A Survey. Automatica. Elsevier; 1992; 28(6): 1083–1112.

[21]. Kanelopoulos K., Stamatis A., Mathioudakis K. Incorporating Neural Networks into Gas Turbine Performance Diagnostics. ASME 1997 International Gas Turbine and Aeroengine Congress and Exhibition. American Society of Mechanical Engineers; 1997. pp. V004T15A011–V004T15A011.

[22]. Huang J., Sun J. Adaptive Identification Using Recurrent Neural Network for Nonlinear Systems. Journal of Nanjing University of Aeronautics and Astronautics. 1999; 31(3).

[23]. NLR. About GSP. Gas Turbine Simulation Program. 2015. Available at: http://www.gspteam.com/about.html (Accessed: 1 April 2015)

[24]. GasTurb Main Page. GasTurb. 2015. Available at: http://www.gasturb.de/index.html (Accessed: 1 April 2015)

[25]. Richter H. Chapter 4 Engine Control by Robust State Feedback. Advanced Control of Turbofan Engines. Springer Science & Business Media; 2011.

[26]. Janikovič J. Gas Turbine Transient Performance Modeling for Engine Flight Flight Path Cycle Analysis. Cranfield; 2010.

[27]. Richter H. Gain Scheduling and Adaptation. Advanced Control of Turbofan Engines. Springer New York; 2011. pp. 92–110. Available at: DOI:10.1007/978-1-4614-1171-0

[28]. Isermann R., Baur U., Bamberger W., Kneppo P., Siebert H. Comparison of Six On-Line Identification and Parameter Estimation Methods. Automatica. 1974; 10: 81–103. Available at: DOI:10.1016/0005-1098(74)90012-0

[29]. Chapter 16 Estimation of Model Parameters. 2014. Available at: http://home.hit.no/~hansha/documents/control/theory/parameters_estimati

on.pdf (Accessed: 1 January 2014)

[30]. Wellstead P.E.E., Zarrop M.B. Recursive Esimation. Self-Tuning Systems: Control and Signal Processing. John Wiley & Sons, Inc.; 1991. pp. 71–114.

[31]. Yang, J. N., Pan, S. and Lin S. Least-Squares Estimation with Unknown Excitations for Damage Identification of Structures. Journal of Engineering Mechanics. 2007; 133(1): 12–21. Available at: DOI:10.1061/(ASCE)0733-9399(2007)133:1(12)

[32]. Vahidi, A., Stefanopoulou, A. and Peng H. Recursive Least Squares with Forgetting for Online Estimation of Vehicle Mass and Road Grade: Theory and Experiments. Vehicle System Dynamics. 2005; 43(1): 31–55. Available at: DOI:10.1080/00423110412331290446

[33]. Wilson E., Lages C., Mah R. On-line Gyro-based, Mass-Property Identification for Thruster-Controlled Spacecraft Using Recursive Least Squares. The 2002 45th Midwest Symposium on Circuits and Systems, 2002. MWSCAS-2002. (2002). 2002; 2: 334–337. Available at: DOI:10.1109/MWSCAS.2002.1186866

[34]. Torres MP., Sosa G., Amezquita-Brooks L., Liceaga-Castro E., Zambrano-Robledo PDC. Identification of the Fuel-thrust Dynamics of a Gas Turbo Engine. Proceedings of the IEEE Conference on Decision and Control. 2013; : 4535–4540. Available at: DOI:10.1109/CDC.2013.6760588

[35]. Arkov V., Evans C., Fleming PJ., Hill DC., Norton JP., Pratt I., et al. System Identification Strategies Applied to Aircraft Gas Turbine Engines. Annual Reviews in Control. 2000; 24: 67–81. Available at: DOI:10.1016/S1367-5788(00)90015-4

[36]. Paleologu C., Benesty J., Ciochiňa S. A Robust Variable Forgetting Factor Recursive Least-squares Algorithm for System Identification. IEEE Signal Processing Letters. 2008; 15(3): 597–600. Available at:

DOI:10.1109/LSP.2008.2001559

[37]. MATLAB. Linear Parameter-Varying Models. MathWorks. 2015. Available at: http://uk.mathworks.com/help/control/ug/linear-parameter-varying-models.html (Accessed: 1 March 2015)

[38]. Balas GJ. Linear, Parameter-Varying Control and its Application to a Turbofan Engine. International Journal of Robust and Nonlinear Control. Wiley Online Library; 2002; 12(9): 763–796. Available at: DOI:10.1002/rnc.704

[39]. Abbott J. State-Space Control Systems. Utah Telerobotics, University of Utah. 2015. Available at: http://www.telerobotics.utah.edu/index.php/StateSpaceControl (Accessed: 1 March 2015)

[40]. Samar R., Postlethwaite I. Multivariable Controller Design for a High Performance Aero-Engine. Control, 1994. Control'94. International Conference on. IET; 1994. pp. 1312–1317. Available at: DOI:10.1049/cp:19940326

[41]. Kolmanovsky I V., Jaw LC., Merrill W., Tran Van H. Robust Control and Limit Protection in Aircraft Gas Turbine Engines. Control Applications (CCA), 2012 IEEE International Conference on. IEEE; 2012. pp. 812–819. Available at: DOI:10.1109/CCA.2012.6402640

[42]. Wang H-S., Yung C-F., Chang F-R. Mixed H2 and H Infinity Control Problems. H∞ Control for Nonlinear Descriptor Systems. Springer; 2002. pp. 123–133.

[43]. Pilidis P., Maccallum NRL. A General Program for the Prediction of the Transient performance of Gas Turbines. ASME 1985 International Gas Turbine Conference and Exhibit. American Society of Mechanical Engineers; 1985. pp. V001T03A053–V001T03A053. Available at: DOI:10.1115/85-GT-209

[44]. Rahman NU., Whidborne JF. Real-Time Transient Three Spool Turbofan

Engine Simulation: A Hybrid Approach. Journal of Engineering for Gas Turbines and Power. 2009; 131(5): 051602. Available at: DOI:10.1115/1.3079611

[45]. Walsh, Philip P.; Fletcher P. Chapter 2: The Operational Envelope. Gas Turbine Performance. 2nd edn. Blackwell Science Ltd; 2004.

[46]. Cohen H., Rogers GFC., Saravanamuttoo HIH., Saravanamutto HIH (r). Gas Turbine Theory. Longman Scientific & Technical Harlow (England); 1987;

[47]. Pilidis P. Gas Turbine Theory and Performance. Cranfield University. 2012.

[48]. Marco Mucino. CCGT Performance Simulation and Diagnostics for Operations Optimisation and Risk Management. Propulsion Engineering Centre, Cranfield University; 2007.

[49]. Bücker D., Span R., Wagner W. Thermodynamic Property Models for Moist Air and Combustion Gases. Journal of Engineering for Gas Turbines and Power. 2003; 125(1): 374. Available at: DOI:10.1115/1.1520154

[50]. Jaw, Link C; Mattingly JD. Engine Modeling and Simulation. Aircraft Engine Controls : Design, System Analysis, and Health Monitoring. American Institute of Aeronautics and Astronautics; 2009. pp. 37–68.

[51]. Li YG., L. MacCallum NR., Pilidis P. Pressure Waves in Volume Effect in Gas-Turbine Transient-Performance Models. Journal of Propulsion and Power. 2001; 17(3): 706–710. Available at: DOI:10.2514/2.5799

[52]. Kulikov GG., Thompson HA. Off-line Models. Dynamic Modelling of Gas Turbines: Identification, Simulation, Condition Monitoring and Optimal Control. 1st edn. Springer-Verlag London; 2004. pp. 27–46. Available at: DOI:10.1007/978-1-4471-3796-2

[53]. Juang J-N. Identification Process. Applied system identification. Prentice

Hall; 1994. pp. 3–10.

[54]. Richter H. Engine Models and Simulation Tools. Advanced Control of Turbofan Engines. 1st edn. Springer-Verlag New York; 2011. pp. 19–34. Available at: DOI:10.1007/978-1-4614-1171-0

[55]. Isermann, Rolf; Münchhof M. Least Squares Parameter Estimation for Dynamic Processes. Identification of Dynamic Systems: An Introduction with Applications. Springer-Verlag Berlin Heidelberg; 2011. pp. 223–290. Available at: DOI:10.1007/978-3-540-78879-9

[56]. Juang J-N. System Realization Theory. Applied System Identification. Prentice Hall; 1994. pp. 121–174.

[57]. Wellstead, P. E.; Zarrop MB. Using Recursive Estimators. Self-tuning Systems: Control and Signal Processing. John Wiley & Sons, Inc.; 1991. pp. 117–164.

[58]. Malik MB. State-Space Recursive Least-Squares: Part I. Signal processing. Elsevier; 2004; 84(9): 1709–1718. Available at: DOI:10.1016/j.sigpro.2004.05.022

[59]. Milek JJ., Kraus FJ. Stabilized Least Squares Estimators for Time Variant Processes. Proceedings of the 1st IFAC Symposium on Design Methods of Control Systems. 1991. pp. 1803–1804 vol.2. Available at: DOI:10.1109/CDC.1989.70466

[60]. Milek JJ., Kraus FJ. Stabilized Least Squares Estimators: Convergence and Error Propagation Properties. Proceedings of the 30th IEEE Conference. 1991. pp. 3086–3087 vol.3. Available at: DOI:10.1109/CDC.1991.261118

[61]. Astrom KJ. PID Control. PID Controllers: Theory, Design and Tuning. Instrument Society of America; 1995. pp. 59–119.

[62]. Stefan Jahn. Integration Methods. 2015. Available at: http://qucs.sourceforge.net/tech/node24.html (Accessed: 1 January 2015)

[63]. Wang L. Discrete-Time MPC with Constraints. Model Predictive Control System Design and Implementation Using MATLAB. Springer; 2009. pp. 2–78. Available at: DOI:10.1007/978-1-84882-331-0

[64]. Daly M., Gunston B. Jane's Aero Engines. Jane's Information Group. 2007;

[65]. Dr D Auger. ROLLS-ROYCE AVON The World's Most Widely-manufactured Gas Turbine : a History of its Development. 1955; : 900.

[66]. Ziegler JG., Nichols NB. Optimum Settings for Automatic Controllers. trans. ASME. 1942; 64(11).

[67]. Zhong J. PID Controller Tuning: A Short Tutorial. Mechanical Engineering, Purdue University. 2006;

[68]. Lawson CL., Hanson RJ. Solving Least Squares Problems. SIAM; 1974.

[69]. Yin J. Performance Simulation of TRENT 900 High Bypass Turbofan Engine. 1998.

[70]. EASA. EASA Type-Certificate Data Sheet: RB211 Trent 900 Series Engines. 2013; E.012(06).

[71]. Gunston B. Rolls-Royce, Trent Series. In: Gunston B (ed.) Jane's Aero Engines. 2001. p. 438.

APPENDICES

Appendix A Flow Diagram of Constant Mass Flow Method

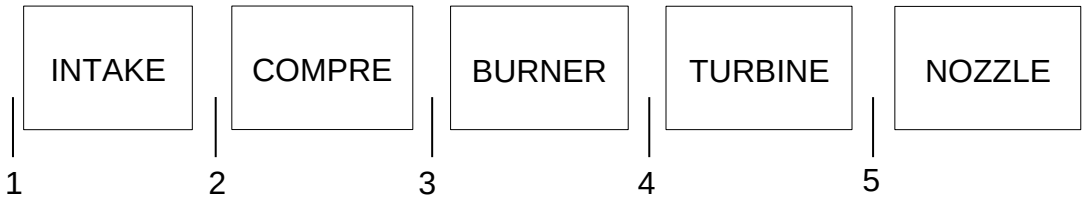

Figure A-1 Stations and station number of a single spool gas turbine

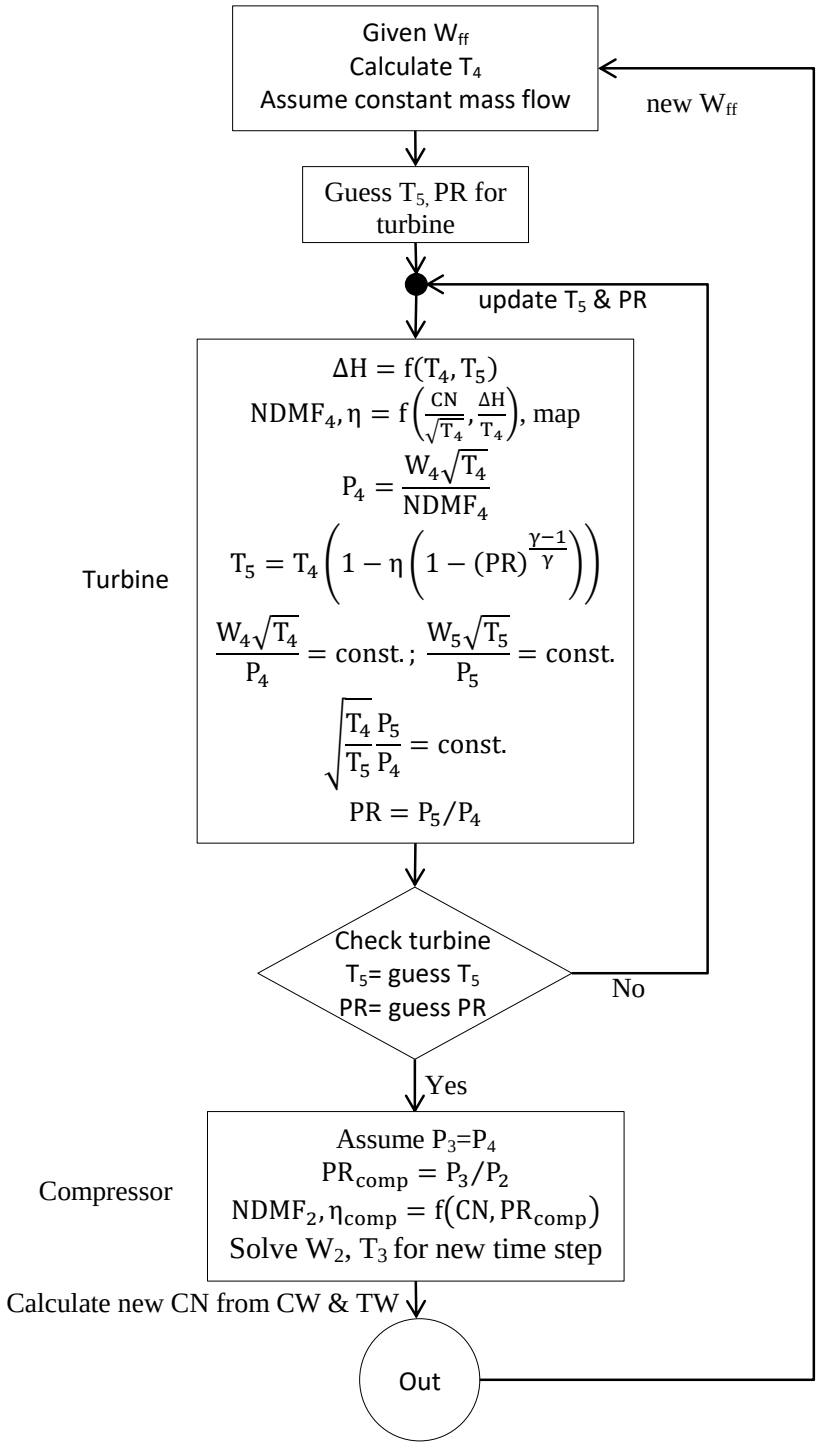

Figure A-2 Flow diagram of constant mass flow method

Appendix B Gas Turbine Model

B.1 Flow Diagram for Performance Calculation of Combustor

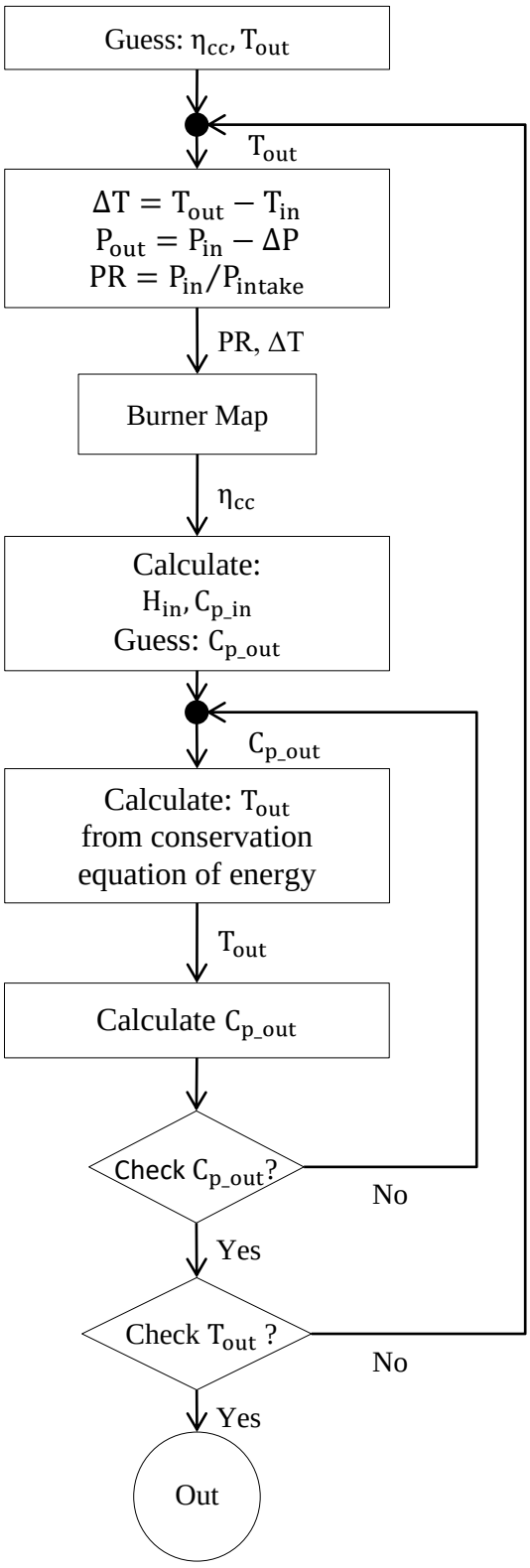

B.2 Flow Diagram for Performance Calculation of Turbine

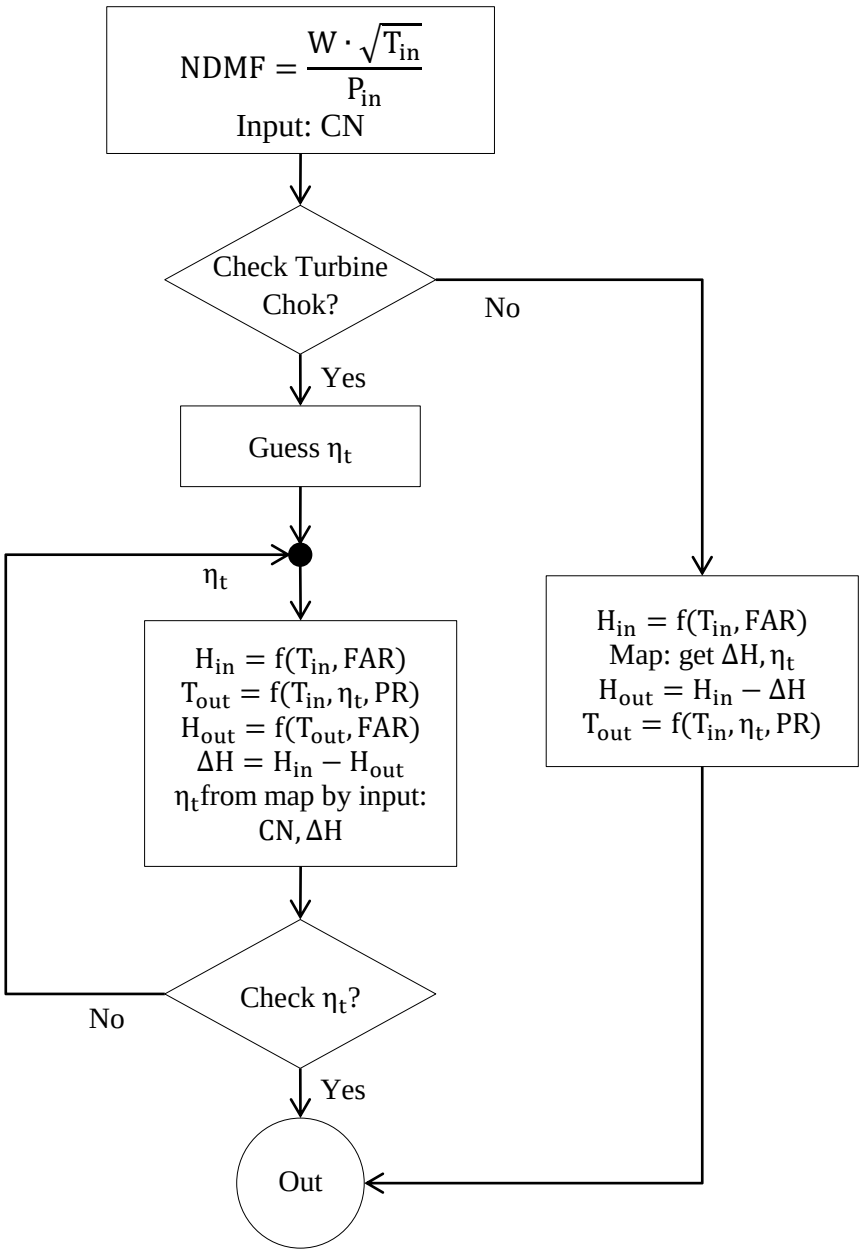

B.3 Flow Diagram for Performance Calculation of Nozzle

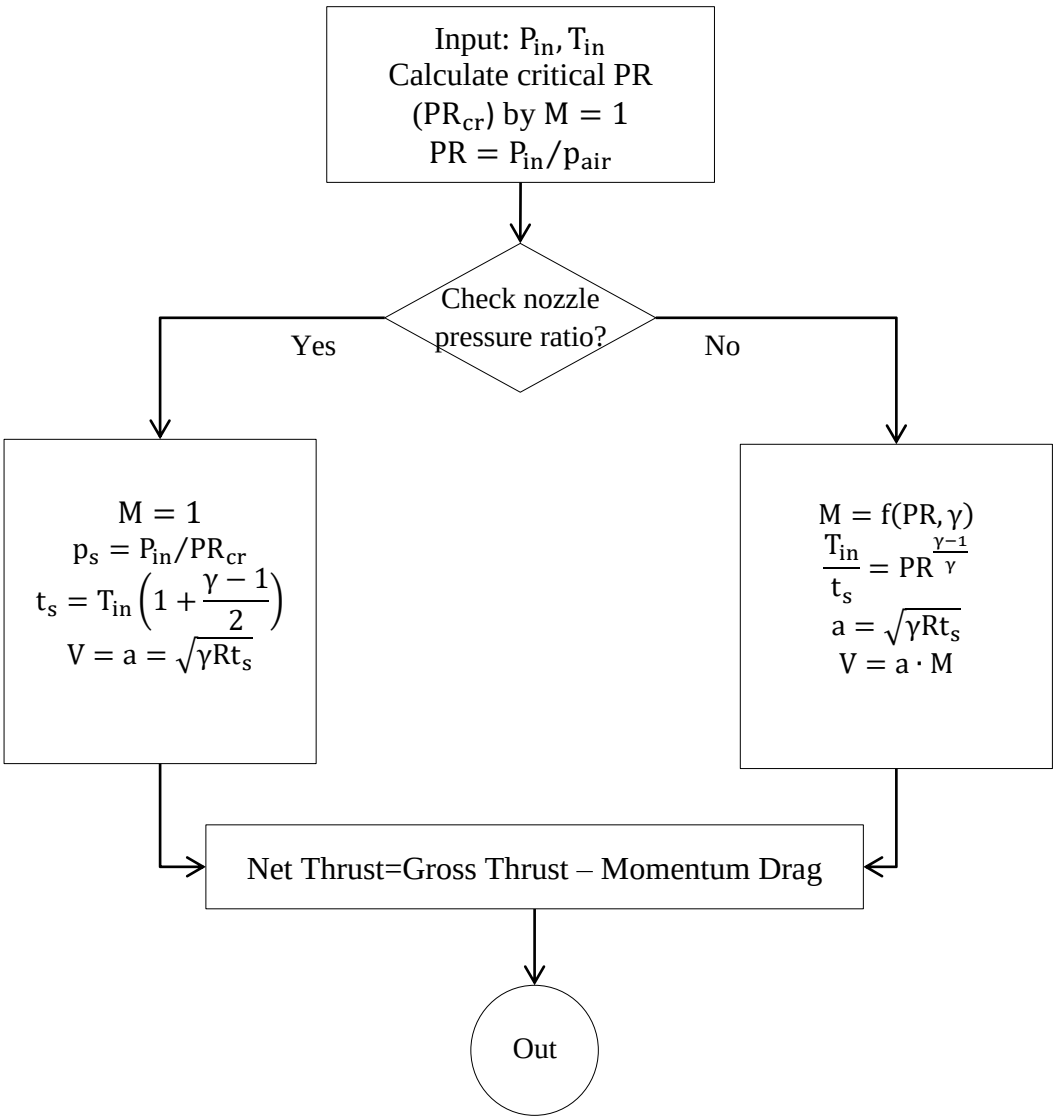

Appendix C Simulation of Transient Acceleration on GSP

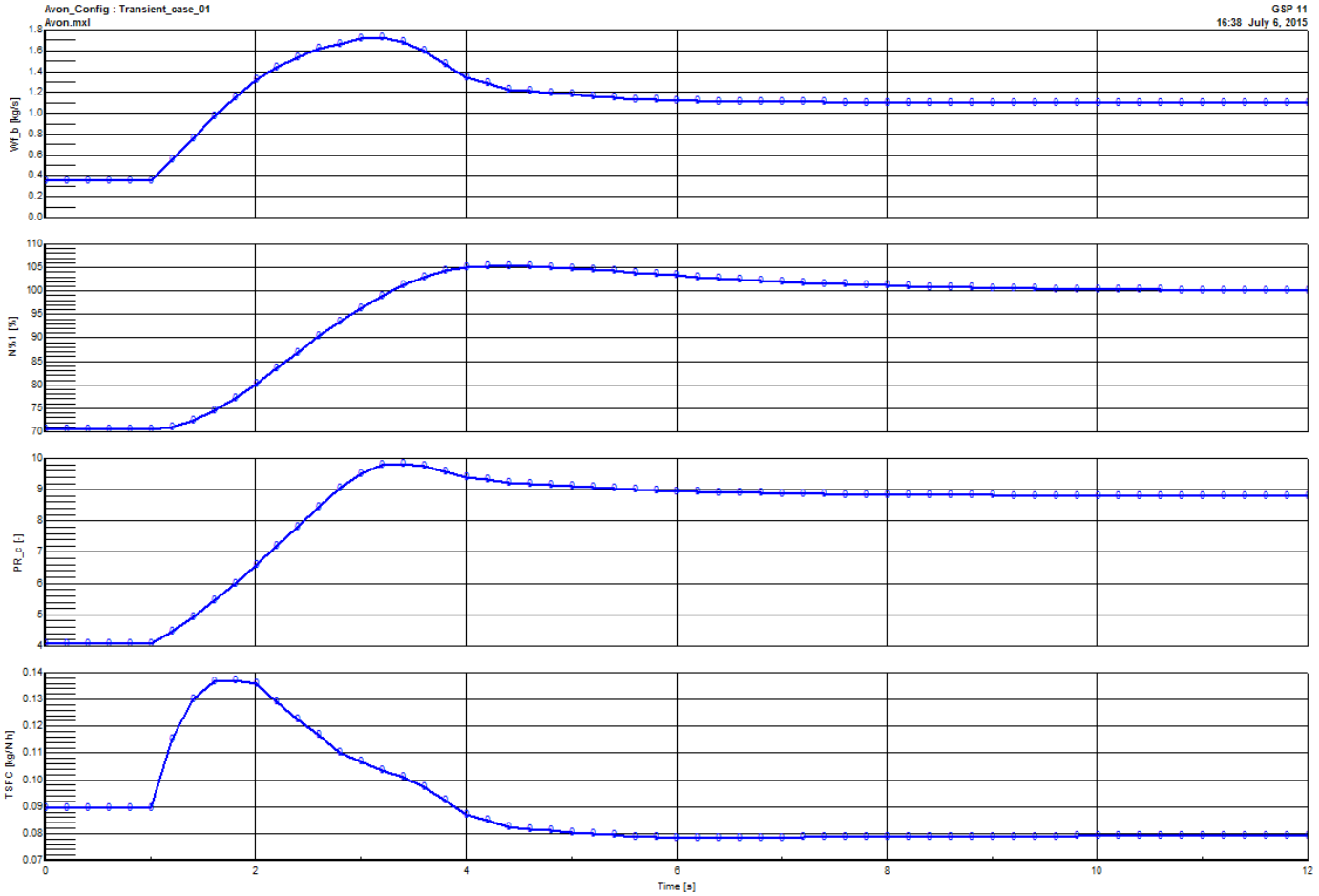

Appendix D Frequency Response of the Three-Spool Turbofan Engine

D.1 Frequency Response of Low Pressure Shaft and Compressor

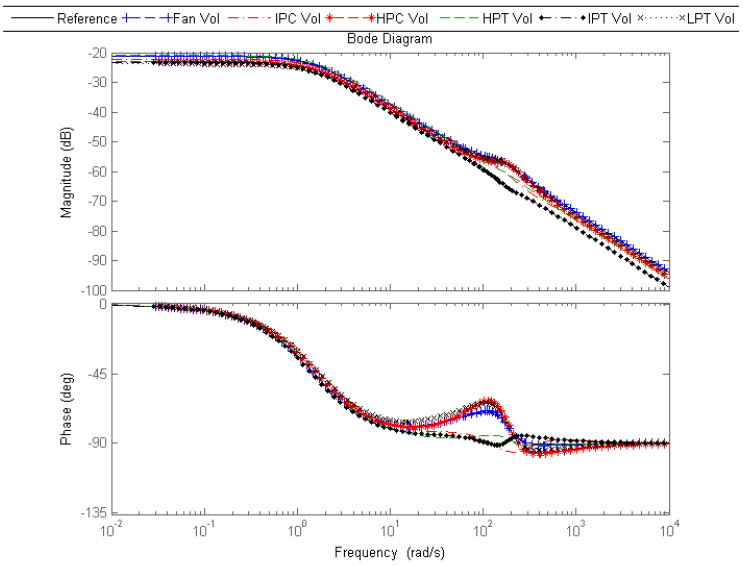

Figure D-1 Frequency response of the low pressure shaft with different design volumes for transient between 60% and 80% PCNL

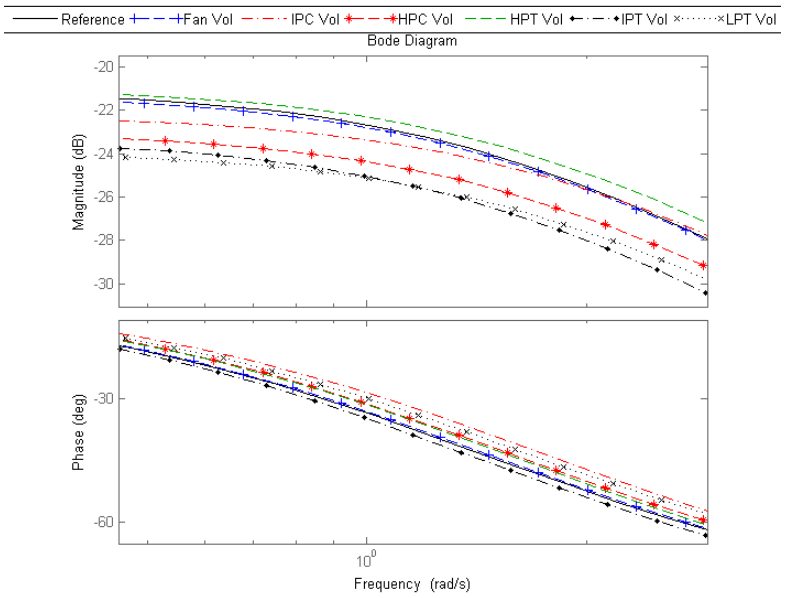

Figure D-2 Cut-off frequency of the low pressure shaft with different design volumes (close up of Figure D-1)

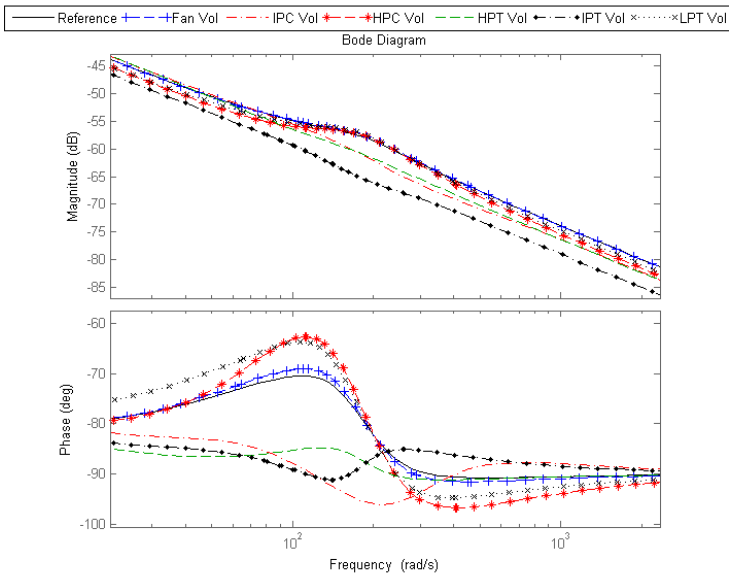

Figure D-3 Close up from Figure D-1 for low pressure shaft

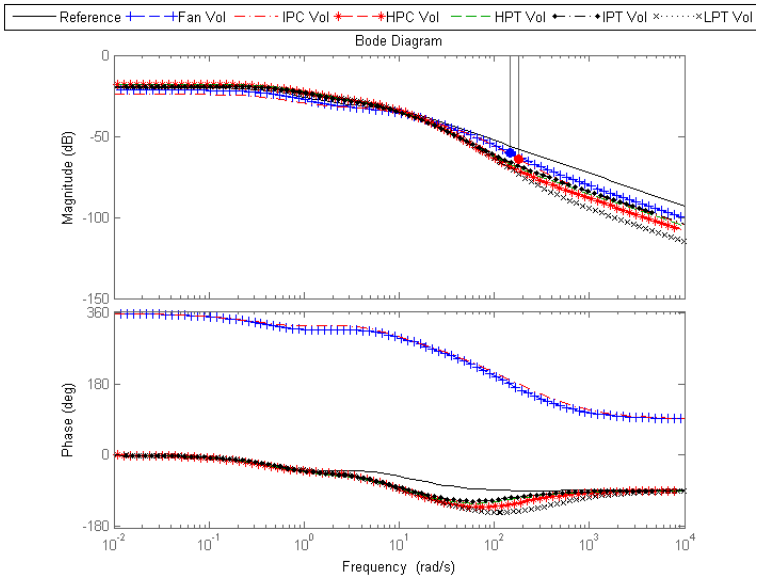

Figure D-4 Frequency response of the LPC-PR with different design volumes for transient between 60% and 80% PCNL

D.2 Frequency Response of Intermediate Pressure Shaft and Compressor

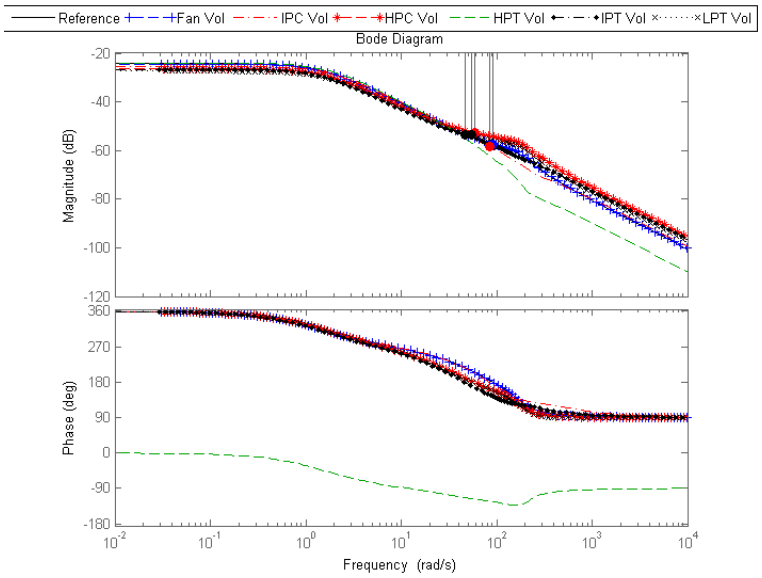

Figure D-5 Frequency response of the intermediate pressure shaft with different design volumes for transient between 60% and 80% PCNL

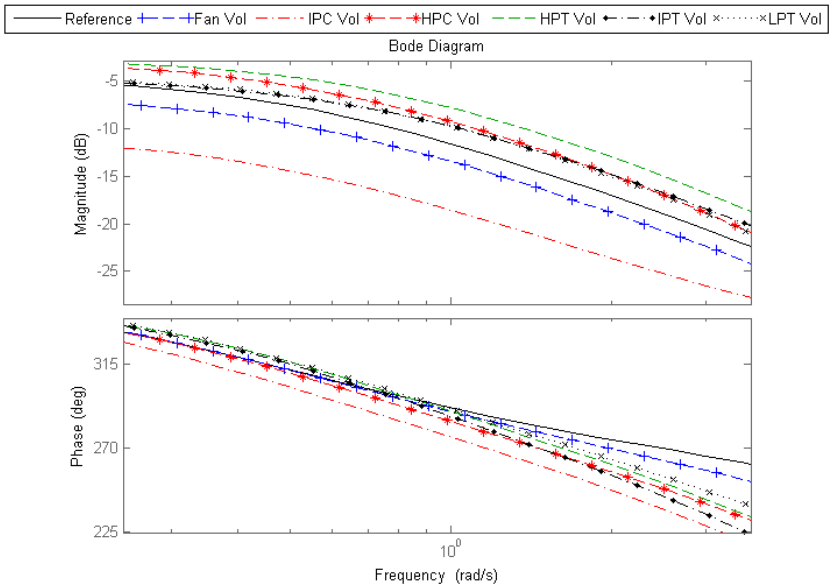

Figure D-6 Cut-off frequency of the intermediate pressure shaft with different design volumes (close up of Figure D-5)

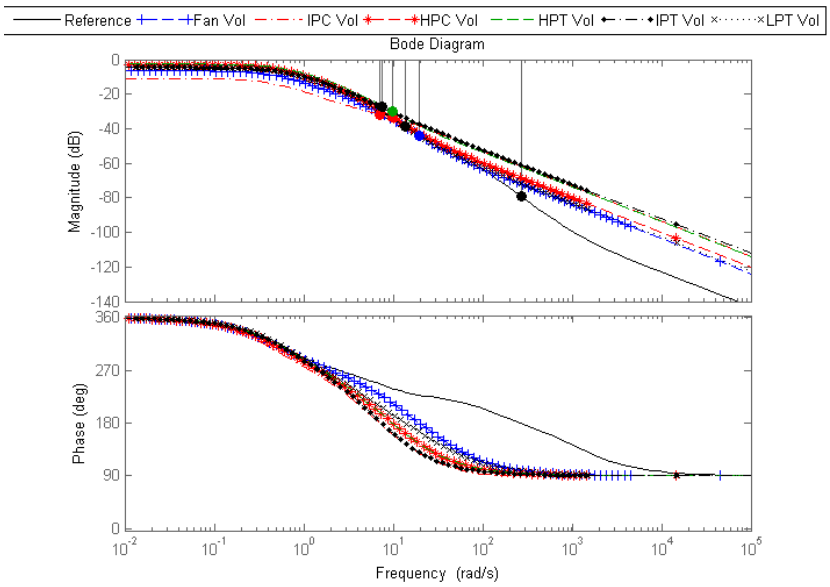

Figure D-7 Frequency response of IPC-PR with different design volumes for transient between 60% and 80% PCNL

D.3 Frequency Response of High Pressure Shaft and Compressor

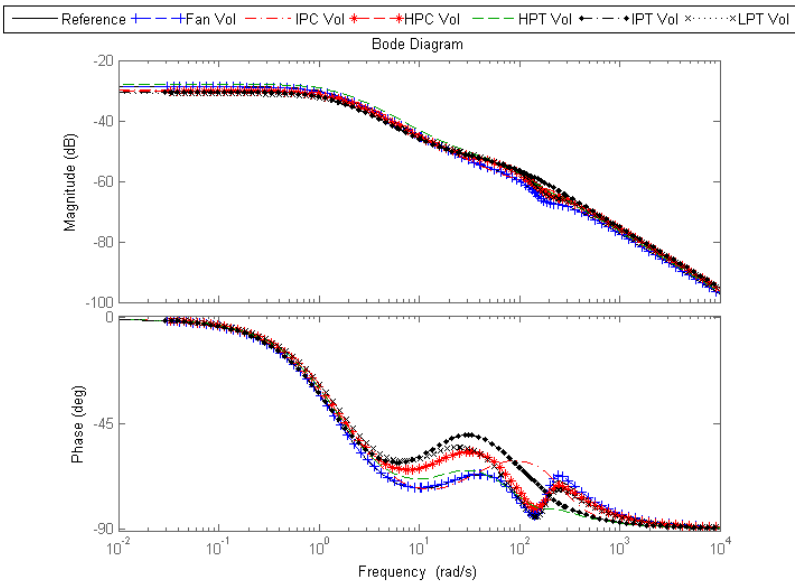

Figure D-8 Frequency response of the high pressure shaft with different design volumes for transient between 60% and 80% PCNL

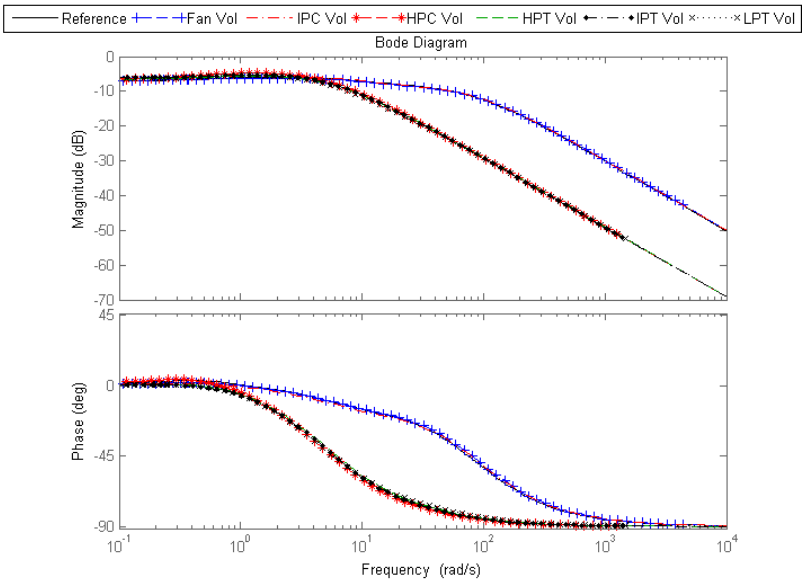

Figure D-9 Frequency response of HPC-PR with different design volumes for transient between 60% and 80% PCNL

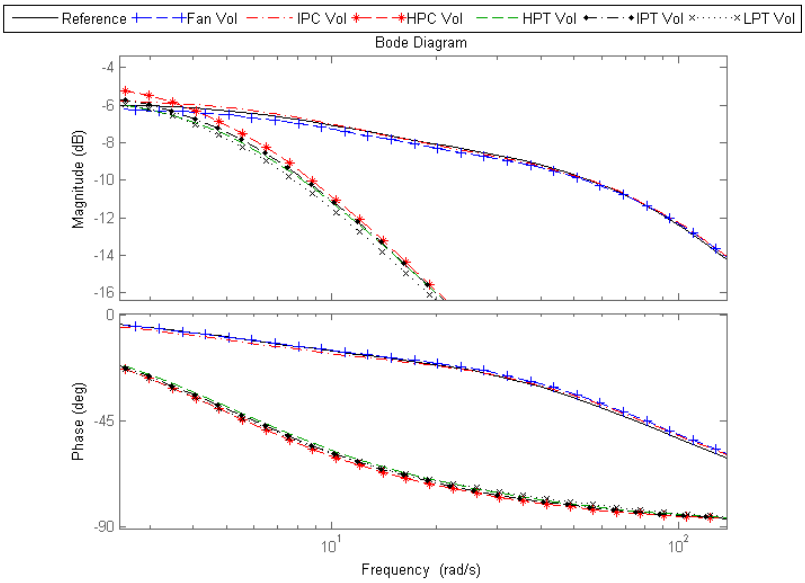

Figure D-10 Cut-off frequency of the HPC-PR with different design volumes (close up of Figure D-9)

Appendix E Transient Performance of the Three-Spool Turbofan Engine

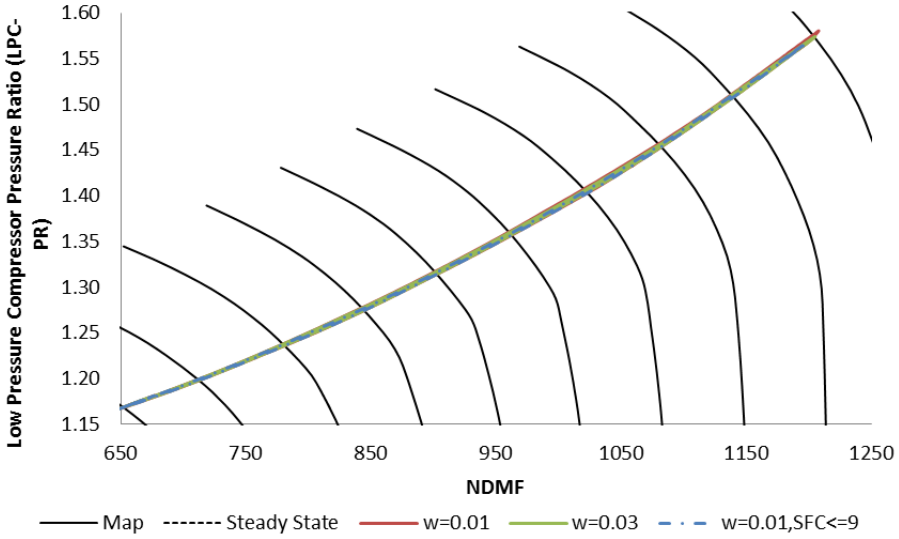

Figure E-1 Fan transient performance of three-spool turbofan engine by the control of MPC with different values of weighting factor as well as the SFC constraint

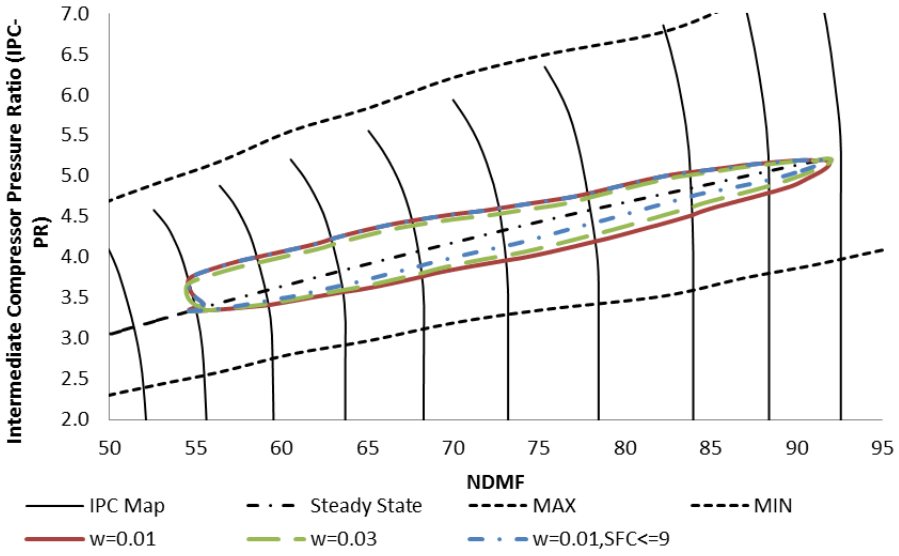

Figure E-2 LPC transient performance of three-spool turbofan engine by the control of MPC with different values of weighting factor as well as the SFC constraint

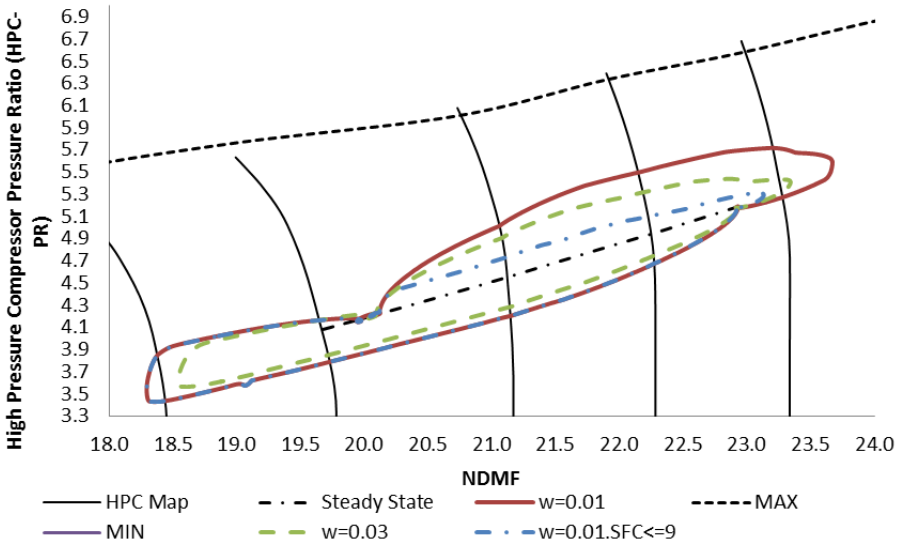

Figure E-3 HPC transient performance of three-spool turbofan engine by the control of MPC with different values of weighting factor as well as the SFC constraint